ADIPOSE-DERIVED PROGENITOR CELL ALTERATIONS TO THE TUMOR MICROENVIRONMENT PROMOTE TUMORIGENESIS

A Dissertation

Presented to the Faculty of the Graduate School

of Cornell University

In Partial Fulfillment of the Requirements for the Degree of

Doctor of Philosophy

by

Emily Millar Brooks

August 2012

ADIPOSE-DERIVED STEM CELL ALTERATIONS TO THE TUMOR MICROENVIRONMENT PROMOTE TUMORIGENESIS

Emily Millar Brooks, Ph. D.

Cornell University 2012

Rather than simply focusing on the malignant cancer cells, the role of the tumor microenvironment as a whole is increasingly being studied. As this amalgamation of malignantly transformed cells, host tissue cells, growth factors, cytokines, and extracellular matrix (ECM) proteins forms the tumor, the interactions between these heterotypic components contribute to tumorigenesis. As the origin of the various components of what has not been fully elucidated, the work presented here focuses on a likely contributor – the breast tumor stroma. A cell type of interest in the tumor stroma is the myofibroblast, which is largely responsible for the excessive ECM accumulated within tumors. Adipose-derived stem/progenitor cells (ASCs) are adult mesenchymal stem cells present within adipose tissue, a main component of the mammary tissue surrounding breast tumors, which are utilized for regenerative tissue-engineering approaches. These multipotent cells have been shown to play a critical role in wound healing, which has similarities to the stromal reaction seen in tumors and therefore may contribute to the tumor stroma by undergoing myofibroblastic differentiation.

Within the tumor microenvironment chemical cues in the form of secreted molecules from tumor cells as well as altered ECM composition and stiffness are mechanisms through which ASC function may be altered. Here the ability of ASCs to be altered by tumor conditioned media (TCM) as well as enhanced stiffness has been studied. The results indicate that ASCs cultured in TCM take on an altered tumor-associated (TA) phenotype which entails increased proliferation and pro-angiogenic potential as well as the ability to alter the tumor ECM composition, by differentiating into myofibroblasts. Through a positive feedback loop system, the increased ECM stiffness of tumors also signals ASCs to proliferate

and become more pro-angiogenic. These resultant changes within the TA-ASC ECM propagate pro-tumorigenic signals. In essence, ASCs receiving tumor-derived chemical and mechanical cues alter the tumor stroma to produce the malignant microenvironment. With this knowledge, the regenerative potential of ASCs should be mindfully harnessed to ensure that their pro-tumorigenic capacities do not induce undesirable effects.

BIOGRAPHICAL SKETCH

Emily M. Brooks, originally Emily M. Chandler, was born in Raleigh, NC the younger of two sisters and raised in the mountains of Western North Carolina. Her accelerated abilities in the fields of mathematics and science encouraged her to attend North Carolina School of Science and Math for the final two years of her secondary education. Following her graduation, she moved back to the town of her birth to become a legacy at North Carolina State University (NCSU), the daughter of 2 NCSU graduates. There she acquired her B. S. in Biomedical Engineering, a major combining the fields of study she most enjoyed. As an undergraduate she completed research projects in Dr. Peter Mente's Lab at NCSU evaluating the cellular changes that occur within cartilage follow injury as well as in Dr. Stephen Rao's Lab at the Medical College of Wisconsin looking at the parts of the brain that are utilized during specific tasks. Her undergraduate research experiences assured her of her desire to pursue a graduate degree.

In the Fall of 2006, she relocated to Ithaca, NY to attend Cornell University in pursuit of a Ph.D. in Biomedical Engineering. The invaluable guidance of Claudia Fischbach-Teschl during her graduate studies has enabled Emily to prospered as both a researcher and a mentor. During this time Emily was married to Daniel J. Brooks and gave birth to their daughter, Annabelle Caroline. In addition to her personal endeavors, she has received both local and national recognition for her scientific work, receiving a National Science Foundation (NSF) Graduate Research Fellowship in 2008, 2nd place poster honors from the Cornell Stem Cell Club in 2008, a Student Travel Achievement Recognition from the Society for Biomaterials in 2009, and a CLIMB BME NSF GK-12 Graduate Fellowship in 2010. Additionally, Emily's mentorship to M.Eng., undergraduate, and high-school students has further encouraged their pursuit of careers in the sciences. She has been the first author on 4 manuscripts published in peer-reviewed journals with 2 more submitted or in preparation. Emily plans to continue her research in the field of oncology with more focus on therapeutic approaches and a goal to improve the life of those afflicted with this disease.

This work is dedicated to my family for the nurturing support that enabled me to achieve my dreams, to my loving husband for proving me a shoulder to cry on and never-ending encouragement, my friends for cheering me on through the hard times, and my daughter for providing me an eye to the future.

ACKNOWLEDGMENTS

Although my name may appear as the author on this work, the studies presented within would not have been possible without the guidance and hard work of a lot of other individuals. The most influential assistance I received, without whom this work would not be possible, is my advisor and committee chair, Prof. Claudia Fischbach-Teschl. Without her continued encouragement, I would not be where I am today which makes me eternally grateful. Many other professors here at Cornell played vital roles in my dissertation project. My committee members, Profs. Lawrence Bonassar and Tracy Stokol, provided valuable feedback on experimental design. Collaborations were essential to my ability to complete this work, and without Profs. Brian Kirby and Delphine Gourdon my photo-crosslinked alginate scaffold and fibronectin conformation work, respectively, would not have been possible. Furthermore, my selection as a NSF GK-12 Fellow in the CLIMB program by Shivaun Archer, Ph.D. and Prof. Chris Schaffer provided me the experience to work with Ann Phinney-Foreman and be inspired to pursue career options in teaching.

An essential key to the collection of these data was the dedication of the many undergraduate, graduate, and visiting scientists with whom I had the pleasure to work. Of greatest importance, is another graduate student Bo Ri Seo who was both critical in the completion of the *in vivo* work, but also as a support within the lab. Although not all the names of the students with whom I have worked have appeared on my papers, they have all impacted my work and I would like to thank them for their contributions: Ana Martin-Ryals (traction force microscopy and 3-D alginate beading experiments), Caroline Berglund (photocrosslinking experiments), Christina Cossell (media conditioning), Christine Yoon (staining, Western blotting, and much more), David Tims (measurement of collagen gel stiffness), Jason Lee (alginate cultures), Kerstin Hoger (migration and conditioning experiments), Matthew Saunders (FRET analysis), Maya Madhavan (matrix experiments), Tomasz Rutkowski (alginate beading experiments), and William Polacheck (photocrosslinking experiments). Additionally, I would like to thank all members of the Fischbach Lab including the post-doctoral researchers (Caroline Coffey, David Infanger, Maureen Lynch, and Scott Verbridge) for all the helpful discussions and insights that

contributed to this body of work.

I would also like to thank my sources of stipend and research funds: NIH/NCI RC1CA146065, R21 CA161532, the Cornell Center on the Microenvironment and Metastasis through Award Number NCI U54 CA143876, NSF Graduate Research Fellowship, Cornell CLIMB BME NSF GK-12 program: DGE 0841291, and Cornell University. Finally, I would like to acknowledge my husband, Daniel Brooks for always stepping in and helping when needed.

TABLE OF CONTENTS

LIST OF FIGURES

LIST OF ABBREVIATIONS

2-D	two-dimensional
3-D	three-dimensional
ANOVA	analysis of variance
α-MEM	minimum essential medium (α-modification)
α-SMA	alpha smooth muscle actin
APC	adipose-derived progenitor cell
ASC	adipose-derived stem cell
BCA	bicinchoninic acid
bFGF	basic fibroblast growth factor
BrdU	bromodeoxyuridine
CAF	cancer-associated fibroblast
CAM	cell adhesion molecule
DAB	3,3´-diaminobenzidine
DAPI	4',6-diamidino-2-phenylindole
DMTA	dynamic mechanical thermal analysis
ECM	extracellular matrix
EGF	epidermal growth factor
ELISA	enzyme-linked immunosorbent assay
ER	estrogen-receptors
FA	focal adhesions
(p)FAK	(phosphorylated) focal adhesion kinase
FL	fibril linearity
Fn	fibronectin
Fn-DA	donor/acceptor labeled fibronectin
FRET	fluorescence resonance energy transfer
GdnHCl	guanidine hydrochloride
GPDH	glycerol-3-phosphate dehydrogenase
HER2	human epidermal growth factor receptor 2
HIF	hypoxia-inducible factor
HUVEC	human umbilical vein endothelial cell
IL-8	interleukin-8
NADH	oxidized form of nicotinamide adenine dinucleotide
RGD	Arg-Gly-Asp amino acid sequence
RT-PCT	reverse transcription polymerase chain reaction
PBS	phosphate buffered saline
PBS-X	phosphate buffered saline containing 0.05% triton-X
PDGF	platelet-derived growth factor
PMSF	phenylmethanesulfonylfluoride
PPARγ	peroxisome proliferator-activated receptor gamma
PR	progesterone-receptors
PVDF	polyvinylidene fluoride
SCID	severe combined immunodeficiency (mice)
SHG	second harmonic generation
TBST	Phosphate buffered saline with 0.05% Tween-20
TCM	tumor-conditioned medium
TFM	traction force microscopy

TGF-β	transforming growth factor beta
un-Fn	unlabeled fibronectin
UV	ultraviolet
VEGF	vascular endothelial growth factor

CHAPTER 1

INTRODUCTION

1.1 Breast Cancer

When making a comprehensive assessment of the disease, the American Cancer Society (ACS) estimates that one-half of all men and one-third of all women within the United States will be afflicted by at least one type of cancer during their lives (1). These cancers form when individual cells within complex multicellular organisms go rogue and begin multiplying in an unregulated manner. The defining characteristics of cancer are continually evolving but, most recently the main hallmarks are considered to be: promotion of proliferation, evasion of growth suppression and apoptosis, replicative immortality, angiogenic switch, invasion, avoidance of immune destruction, and reprogrammed cell metabolism (2). Although much research focuses on the genetic aberrations in cancer cells that lead to these changes, it is increasingly apparent that perturbed tissue homeostasis may enable this malignant transformation, and thus this area of study deserves more research.

The term cancer refers to a broad group of more than 100 diseases afflicting many of the tissues of the body, and is more specifically described by the originating tissue of the initial cell undergoing uncontrolled growth. For example, when a rogue cell within the mammary epithelial tissue proliferates to form a lump or mass, a breast tumor is formed. Breast cancer is a specific form of cancer that afflicts a substantial number of women, making it a leading cause of cancer-related deaths (1). These tumors can range in malignancy from benign (non metastatic) to invasive carcinoma where the cells aggressively invade local and distant organs. The ACS estimates that nearly a quarter-million people were diagnosed with invasive breast cancer in 2011, and of those diagnoses, 95% were in women 40 years of age or older (1). With improved diagnostic techniques enabling earlier detection and superior treatments, survival rates have greatly improved over the last half-century and a large portion of these afflicted women will survive at least 5 years beyond diagnosis (3). Improvements are still necessary to further understand this disease

because 39,510 Americans are predicted to succumb to breast cancer in 2012 (3).

Breast tumors are often first detected as a hard lump within the compliant breast tissue. Generally, these hard tissue masses do not cause pain which is why they are often first detected by manual palpation rather than through other symptomatic means. In order to enable earlier detection, women younger than 40 are recommended to have a clinical breast exam (CBE) every 3 years in addition to the suggested monthly self breast exam (1). It is also suggested that after reaching 40 years of age women have a CBE and mammogram performed on a yearly basis as their risk for breast cancer development increases. Additionally, women who are at higher risk for developing breast cancer should undergo increased screening as early stage diagnosis provides for improved survival (4).

Through investigation, our understanding of breast cancer has greatly improved. Risk factors for disease development, including mutations in BRCA1/BRCA2, were first identified in the early 1990s (5, 6). With the identification of breast cancer gene-expression signatures such as expression of estrogen-receptors (ER), progesterone-receptors (PR) and human epidermal growth factor receptor 2 (HER2), molecular diagnosis is possible leading to improved therapies for targeted implementation (7). In fact, much research has been spent isolating what changes occur within cancer cells on a genetic level that enable tumors to grow while bypassing the robust cell machinery designed to inhibit this type of behavior. As an example, trastuzumab an antibody drug target of HER2 has been shown to significantly enhance survival of patients with HER2-postitive breast tumors (8). As is true for any battle, having a better understanding of your enemy allows for the best counterattack. In the case of tumors, a lot of progress has been made in understanding the genetic aberrations that lead to the development of this disease as well as variances within tumors which provide for better or worse prognosis. Although these approaches focus on the ability to identify and target the cancer cells, a greater appreciation has been gained in more recent years for the role of the entire tumor microenvironment in the process of tumor growth or tumorigenesis (9). In particular, a correlation has been shown between enhanced mammographic density, a measure of tissue density and thus stiffness, and the incidence of breast cancer (10). This may indicate that alterations to the tissue prior to transformation of malignant cells may even contribute to tumor initiation.

One cell type of great interest to these changes in the extracellular matrix (ECM) is the myofibroblast, as further discussed in the following section.

1.2 Activated Fibroblasts/Myofibroblasts

The role of the stromal compartment within tumors is quickly receiving more attention as both a prognostic tool and a chemotherapeutic drug target (11, 12). The tumor stroma is the connective scaffolding around and within tumors made up of mesenchymal cells, ECM, vasculature, and supporting cells (13). A large cellular component of the stroma is the carcinoma-associated fibroblasts (CAFs). When fibroblasts assume an increased proliferative and ECM depositing phenotype, these cells are termed 'activated' fibroblasts or myofibroblasts (13). Markers specific to the activated fibroblasts within tumors include: alpha-smooth muscle actin (αSMA) and fibroblast-specific protein 1 (FSP1) (13). These cells are increasingly being recognized for the multimodal role they play in tumorigenesis, namely that CAFs are responsible for promoting tumor growth (14), fostering vasculature development (15), and mediating the inflammatory response (16) in addition to altering the ECM (13).

Fibroblasts secrete a large portion of the proteins within the ECM, including the fibrillar proteins collagen I and fibronectin (Fn) (both further discussed in section 1.6), which are found in increased densities within tumors (17). The process through which these ECM components accumulate at excessive levels in the tumor storma is termed desmoplasia. CAFs play a prominent role in this defining characteristic of the tumor stroma (2). Altered ECM composition and arrangement, largely due to these myofibroblasts, may contribute to the overall stiffening of the tumor microenvironment. One signaling molecule involved in this process is transforming growth factor beta (TGF-β) as increasing TGF-β levels in tumors has been correlated with tumor desmoplasia (18). Although TGF-β can generate signaling through a tumor suppressing pathway, its signaling ability is broad and can also lead to the activation of CAFs, or their differentiation into myofibroblasts (19) which causes cells to take on a more contractile phenotype (20). In addition to TGF-β, basic fibroblast growth factor (bFGF) and platelet-derived growth

factor (PDGF) have been shown to contribute to the proliferative (21) and ECM depositing (22) characteristics of activated fibroblasts, respectively. Fibroblasts can also assume an activated phenotype due to alternative (non-growth factor) signals as is possible in response to reactive oxygen species, ECM signaling (23), and cell-cell junctions (24). Although it is not clear whether CAFs act more as cancer initiators or propagators (25), these cells represent a promising therapeutic target (26) due to their regulatory role in cancer progression. Whether CAFs arise from local fibroblasts which become activated or from the differentiation of stem cells remains unclear, however, as CAFs are a principle source of vascular endothelial growth factor (VEGF) within the tumor microenvironment (15), these cells intimately contribute to angiogenesis, a hallmark of cancer, further discussed in the next section.

1.3 Angiogenesis

Paramount to tissue survival is the ability to receive nutrients and oxygen while disposing of unwanted cellular waste. These processes are accomplished in the body by the blood supply carried by the vasculature. When a new tissue forms, as is true during tumor formation, new blood vessels must be recruited to perform these functions. During development, the formation of new microvasculature networks is referred to as neovascularization; however, the term angiogenesis is used to describe the process when new vessel sprouts are formed from existent vascular beds.

In a tissue like malignant tumors, where cells proliferate profusely, the recruitment of vasculature to support growth may not be able to occur at a sufficient rate, in which case hypoxia and necrosis may occur. Hypoxia arises when oxygen levels are inadequate to maintain cell metabolism. Cell death is a result of prolonged hypoxia and depletion of nutrients, which results in the necrosis of tissues as is often seen in the core of aggressively growing tumors. As a survival mechanism, cells secrete growth factors and cytokines that will promote the process of angiogenesis when encountering a nutrient-poor environment. This occurs through various signaling means. Of note, lack of oxygen leads to changes in hypoxia-inducible factor (HIF), which has direct and indirect proangiogenic transcriptional targets (27).

In 1971, Judah Folkman suggested that combating the process of tumor angiogenesis could be a promising therapeutic approach by starving tumors (28). A variety of pro-angiogenic growth factors and cytokines have been identified since this initialization of this field of study, including: VEGF, bFGF, PDGF, TGF-β, angiopoietins, and interleukin 8 (IL-8) (29, 30). In 2004, the FDA approved the use of Avastin (bevacizumab), an inhibitory antibody against VEGF, for the treatment of colorectal cancers, which was later expanded to include other cancers. However, after minimal benefits were indicated for the treatment of breast cancer the FDA recalled its accelerated approval (31). Many other anti-VEGF treatments have been approved as anti-cancer therapeutics citing increased survival, although the survival rates are merely increased a few months indicating the need for different approaches (29). Combinatorial approaches targeting additional molecular and cellular mediators of angiogenesis or other microenvironmental changes may be necessary in order to produce substantial changes in patient outcomes.

1.4 The Tumor Microenvironment

The build-up of genetic alterations in a cell may enable it to go rogue by avoiding the normal anti-cancer pathways; however, tumors are not insular as cancer cells alone cannot produce a sizable tumor. In fact, supportive cells (e.g. CAFs) may largely orchestrate and even initiate tumor formation through diverse signaling mechanisms not yet fully understood. There is a diverse population of heterotypic cells within the tumor tissue and its stroma, including immune cells, fibroblasts, as well as the cells that make up the vasculature. The tumor microenvironment is considered to be the normal cells, molecules, and blood vessels which work in concert to provide tumor cells the structure and nutrients necessary for growth (Figure 1.1). The intricate interplay between all of these cell types and how this contributes to tumorigenesis has increasingly been investigated in recent years.

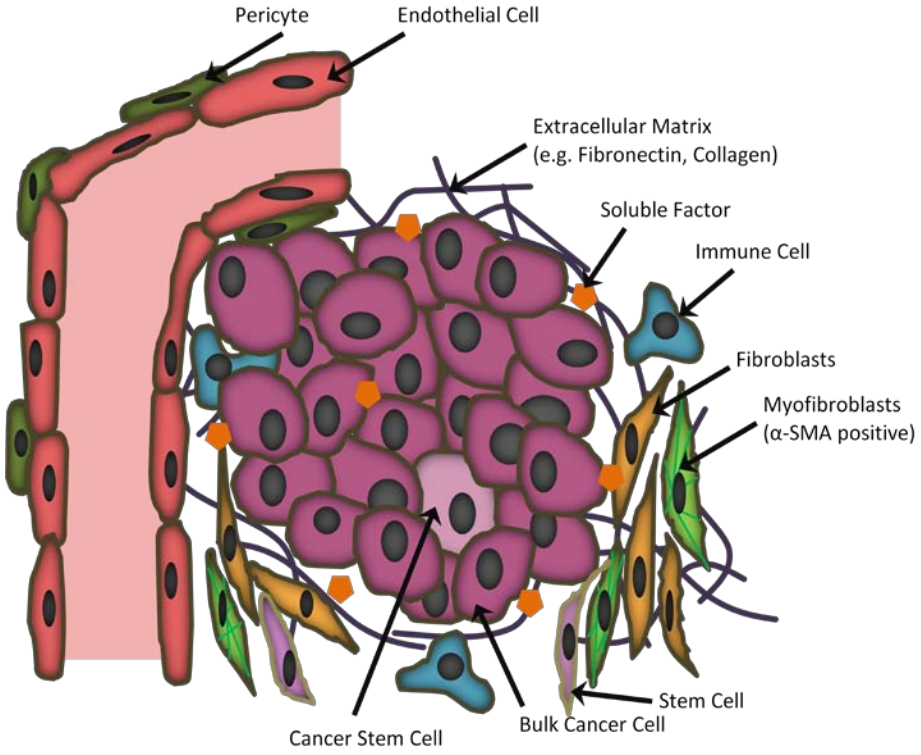

Figure 1.1 The Tumor Microenvironment

Within the local space surrounding a tumor (or the tumor microenvironment) a diverse population of cell types is found. Interactions between the varying cell types via direct contact, soluble factor signals, or through the extracellular matrix are the armamentarium enabling tumor development. Understanding the heterotypic cell population present and the types of interactions that take place within the local microenvironment will provide better insight into the workings of a tumor.

Within the tumor microenvironment various types of communication are utilized to transmit signals between the aforementioned cell types (Figure 1.2). These include direct cell-cell communication through junctions which bridge the cytoskeleton of neighboring cells. Indeed, this type of interaction has been shown to promote tumorigenesis as direct contact between tumor cells and their neighboring stormal fibroblasts has been shown to promote breast cancer cell growth (32). Additionally, cell communication is fostered through secreted signals including growth factors and cytokines which can bind to cell receptors

and signal in an autocrine or paracrine fashion. An ever-growing number of soluble signals are investigated for their role in tumorigeneis, including TGF-β (33) and VEGF (29), which have already been discussed. While cells can signal to each other through these more direct means, signals are often transmitted through the ECM as well. This signaling matrix is constantly remodeled during various processes including tumorigenesis (34). Additionally, through a more recently recognized means of communication, aptly named mechanotransduction (more thoroughly discussed in section 1.7), cells are also able to interpret mechanical signals within their microenvironment. These mechanoreceptors transmit signals to intracellular pathways which lead to an ever-growing number of altered cell behaviors (35).

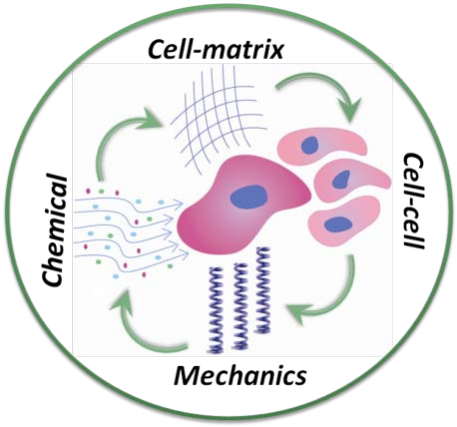

Figure 1.2 Microenvironmental Cell Interactions

Cells are able to send and receive signals via various means. These include direct cell-cell and cell-ECM contacts as well as via chemical and mechanical cue transmission. Cells receive these signals via various types of receptors which transmit the signal through an intracellular cascade, leading to changes in various cell behaviors. Adapted (36) with permission.

Direct cell-cell communication

Cells are able to bind to their surroundings via a broad class of glycoproteins referred to as cell adhesion molecules (CAMs). The heterotypic cells within the tumor microenvironment are able to

interact through direct cell-cell interactions enabled by CAMs. The specific CAMs involved in cell-cell adhesions are cadherins which are often designated with a prefix indicative of the tissue in which they generally found. For example, epithelial cadherin (E-cadherin) is found on epithelial cells and plays a role in cancer. CDH1, which is the gene that codes for E-cadherin, is often mutated in various types of epithelial cancers and is an indicator of poor prognosis in breast cancer (37), likely causing decreased cell-cell junctions and thus promoting tumor cell proliferation, invasion, and metastasis (38). Furthermore, direct cell-cell interactions via an atypical cadherin, cadherin-23, between fibroblasts and tumor cells enhances tumor growth (39).

Chemical-mediated cell communication

Soluble factor signaling occurs through the secretion of molecules from one cell which can then either bind to receptors on the same cell, neighboring cells, or distant cells. Upon binding to a cell surface receptor, conformational changes in the receptor activate an intracellular signaling cascade that ultimately alters cell behavior. Two tumor microenvironmental processes that at least in part rely on changes in soluble factor signaling are angiogenesis and fibroblast activation, as discussed in the previous sections. In both of these examples, the tumor-derived growth factors signal surrounding cells to behave in a specified manner which then contributes to the overall growth and maturation of tumors. While many soluble factors key to tumorigenesis have been discovered, only limited success has occurred to date in using this information for the treatment of various cancers (40).

Cell-ECM communication

CAMs are also involved in the ability of cells to bind to their ECM. The most common type of CAM used to bind the ECM is the integrin. ECM proteins (discussed further in section 1.6) like collagen, fibronectin, laminin, and vitronectin all contain cell adhesion sites which are amino acid sequences that fit into the binding site of integrins, in the same way the growth factors have binding sites to receptors on the

cell surface. Tumor desmoplasia caused by CAFs alters the ECM composition within tumors leading to changes in cell-ECM signaling (41). Critical cell processes within tumors include proliferation, differentiation, and migration which are all influenced by the binding of cells to the ECM (42). As these processes are key to tumor progression, an improved understanding of ECM-tumor interactions will likely lead to better cancer therapeutics. In fact, integrin engagement (43) and expression (44) is known to vary in tumors and targeting of specific integrin subunits involved in these cell-ECM interactions has been shown to reduce prostate cancer cell survival and metastasis (45).

Mechanical signal communication

Cells are bombarded with an array of mechanical signals including fluid shear, stress from adhesion to other cells, and adherence to an ECM of varied tissue strain which cells transduce into biochemical signals (46). The ability of cells to interpret these mechanical signals is more thoroughly discussed in section 1.7. Within tumors, however, these mechanical cues are often altered as compared to host tissue. Particularly in the breast, where tumors are of greater stiffness than surrounding host adipose tissue (47), this means of cellular communication can lead to changes in various cell functions. As tissue stiffness is known to vary throughout the body, these mechanical cues have been investigated for their role in proliferation as well as adhesion and motility (35, 48). Stiffness has also been shown to lead to additional phenotypic changes, including: altered differentiation (49), angiogenesis (50), and cell malignancy (51). These processes are key to tumorigenesis, and thus tumors can utilize signals resulting from altered tissue mechanics to promote their own growth, such as stiffness. The combinatorial effect of these signaling modalities (cell-cell, cell-ECM, chemical, and mechanical communication) produces a microenvironment facilitating tumorigenesis; however, the effect of all these signals on the function of surrounding host tissue cells remains unclear.

1.5 Stem Cells and Cancer

The exact source of the various cell types that make up the tumor microenvironment is not fully understood. One likely population contributing to produce these cells is adult stem cells which can be of various origins (e.g. mesenchymal or hematopoietic). Stem cells are defined by their ability to both self-renew and differentiate into cells of specialized function (52). Many tissues within the body contain a fractional population of stem cells; however, there are a few large tissue sources of mesenchymal stem cells including the bone marrow and adipose tissue (53). The mammary microenvironment (Figure 1.3), or the host tissue surrounding breast tumors, is largely composed of adipose tissue which contains an abundant population of mesenchymal stem cells, termed adipose-derived stem cells (ASCs) (52). These mesenchymal stem cells possess the capacity to differentiate toward many lineages including adipocytes, chondrocytes, myocytes and osteocytes and can be easily acquired from the lipoaspirate resulting from elective lipoplasty procedures (52).

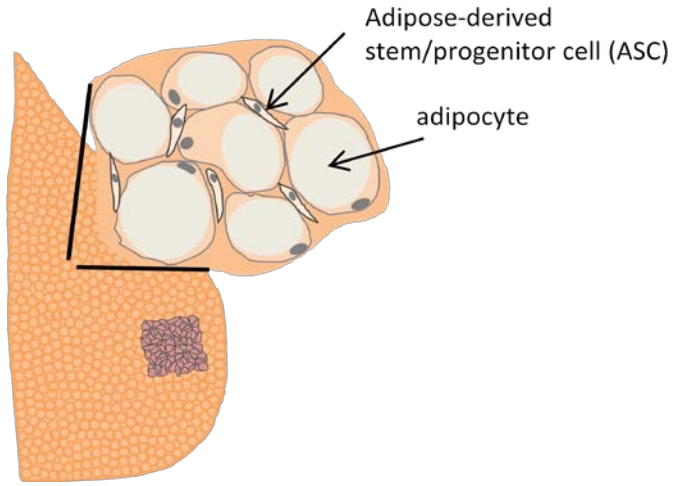

Figure 1.3 Mammary microenvironment

Tumors found within the breast are surrounded by mammary tissue which is largely composed of adipose tissue. This loose connective tissue contains mature adipocytes (or fat cells) as well as undifferentiated stem/progenitor cells.

Initially, bone-marrow derived stem cells (BMSCs) received a lot of attention for the role that these cells play in tumorigenesis. Although BMSCs have been shown to minimally contribute to the vascular endothelium of human tumors (54, 55), their role in other facets of tumor growth may be more significant. Specifically, BMSCs are known to secrete chemokines that enhance tumor aggressiveness by promoting metastasis (56). Additionally, the presence of BMSCs in tumor models has been shown to cause chemotherapeutic resistance, further highlighting the pro-tumorigenic capacity of these cells (57). While the complete role that BMSCs may play in the initiation and progression of tumors is not clear, in the context of breast tumors, ASCs represent a population of stem cells with similar differentiation capacities that are in closer proximity to the incipient tumor. ASCs, like BMSCs, can be recruited via the vasculature to distant tissues.

Unlike some types of adult stem cells with multilineage potential, ASC acquisition is easier as more individuals elect for liposuction procedures as opposed to bone marrow extraction. The ease of ASC accessibility makes them very attractive for tissue engineering and regenerative therapy approaches. In fact, adipose tissue containing ASCs improves the repair of breast tissue after tumor resection (58). This regeneration may be due to the adipogenic differentiation and pro-angiogenic character of ASCs (59). However, while ASCs have been shown to aid in cosmetic breast augmentations, the appearance of cysts and microcalcifications at these regeneration sites (60) may indicate the need for more thorough investigation into the role of ASCs in these processes.

Some more recent studies have shown that ASCs likely play a pro-tumorigenic role within the tumor microenvironment. In particular, ASC pro-angiogenic and pro-inflammatory cytokine secretions are a means by which these cells can promote tumor growth (61). ASCs have been shown to promote tumor growth in lung and brain cancer models (62). Additionally, a specific pro-inflammatory cytokine secreted by ASCs, interleukin 6 (IL-6), has been shown to enhance breast cancer cell migration and invasion (63). As the rate at which ASCs are being studied for regenerative tissue engineering purposes increases, a more complete understanding of the role that ASCs play in tumorigenesis should be evaluated to ensure their usage at the site of regeneration does not lead to tumor development.

1.6 The Extracellular Matrix

The portion of tissues external to a cell, or the extracellular compartment, is comprised of a matrix providing support and structure to the cellular component of tissue. In addition to the fibrous proteins, proteoglycans, and adhesive glycoproteins that create the ECM scaffold mesh on which cells can bind and grow, additional signaling molecules including cytokines and growth factors are resident within the ECM (64). By binding to, rearranging, and applying force to the ECM cells are able to utilize this ever-changing matrix as a signaling depository. The main structural proteins within the ECM include collagen, fibronectin (Fn), elastin, and laminin, to which cells are able to bind at specific adhesion sites (64).

The ECM proteins are structured to contain various domains that contribute to overall structure and function, providing sites for adhesion to other proteins, cells, or growth factors with the ECM (65). As collagen is the most abundant protein within the human body (66), it is also the most abundant protein with the ECM. Although collagen types I-XXVIII have been identified to date (67), collagen I and IV are the main constituents of the tumor stroma (68) and basement membrane (69), respectively and thus play critical roles in tumorigenesis. Collagens fibrils are quarter-staggered assemblies of homo- or heterotrimeric molecules of α chains such as α1 and α2 which combine in a 2:1 ratio in collagen I (67). Alternatively, collagen IV produces a mesh network when 3 α chains combine to form a trimeric molecule that binds in an end-to-end fashion forming the network (67). Cells bind to collagen I and IV by using integrins $\alpha_1\beta_1$ and $\alpha_2\beta_1$ integrins (70, 71). The role of collagen in tumorigenesis is increasingly studied as increased amounts of collagen I within the tumor stoma and its reorganization are known to enhance tumor aggressiveness (68). Additionally, breakdown of the collagen IV component of the basement membrane, which acts as a barrier, enables malignant cell invasion (72). Furthermore, the crosslinking of collagen by lysyl oxidase (LOX) augments tumor progression (73).

Although changes in collagen contribute to tumorigenesis, Fn is an additional fibrillar protein which undergoes changes within the tumor ECM and even controls the deposition and reorganization of the collagen I matrix (74, 75). Fn contains three types of repeating globular modules which contain cell

adhesion sites, such as the arginine-glycine-aspartic acid (RGD) site as well as protein binding sites (76). Cell adhesion to Fn is largely mediated by the $\alpha_5\beta_1$ integrin through the combination of the RGD and synergy sequence sites (76). The content of Fn in the tumor ECM is amplified over normal epithelial ECM and these changes promote tumor malignancy (77). The larger than normal quantities found in the tumor ECM raises questions regarding the role of this ECM protein in tumorigenesis and its organization within the microenvironment. Targeting of the Fn within tumors may prove to be a therapeutic option, as binding of tumor cells to the Fn component of the ECM has been shown to enhance tumor malignancy by enabling tumor cell resistance to apoptosis when treated with chemotherapeutic treatments (78).

In addition to the structural proteins, proteoglycans which are made of glycosaminoglycans (GAGs) play a critical role in the ECM. As GAGs are clusters of carbohydrate chains often attached to a protein backbone they are highly hydrophilic molecules and, their presence in the ECM promotes the incorporation of water and the ability of tissues to withstand compressive forces (79). Enhanced levels of GAGs were first noted thirty years ago (80), and more recent work has shown chondroitin sulfate, a particular type of GAG, to play a role in tumorigenesis, specifically through the promotion of breast cancer metastasis (81). As changes in the tumor ECM composition and arrangement have been shown to largely regulate critical processes in tumorigenesis, further investigation is necessary to fully illuminate the cellular components causing these changes and the ideal pathways to target for anticancer therapeutics.

1.7 Mechanotransduction

The ability of a cell to translate a mechanical signal into a chemical signal transmitted within the cell that can lead to altered cell dynamics is termed mechanotransduction (46). A great deal of progress has been made to date to understand the process of mechanotransduction; although, work is ongoing to understand more thoroughly the mechanoreceptors and subsequent signaling cascades through which cells are able to sense their surroundings. Mechanotransduction is carried out through cell surface receptors,

stretch-activated ion channels, focal adhesion (FA) complexes, and cell-cell junctions (46).

Within FAs, the best characterized of adhesion complexes, cells engage a specific type of transmembrane receptor, namely integrins. These heterodimer complexes are composed of one α and one β subunit which, through a combination of eight β and eighteen α subunits, form twenty-four distinct integrins (82). Different integrins are engaged at differing cell adhesion sites on ECM proteins. For example, the $\alpha_v\beta_3$ integrin is used by cells to bind to vitronectin, an adhesion protein abundant within serum and the ECM. Specific amino acid sequences like RGD (Fn) and DGEA (collagen) found within ECM proteins enable this integrin engagement.

As integrins bind to the ECM, conformational changes in the intracellular domain of the receptor occur that lead to the recruitment of various intracellular proteins to FAs, causing the propagation of a signaling cascade (Figure 1.4). Talin (both 1 and 2) as well as kindlin (2 and 3), which bind the β subunit of integrins and link to the actin cytoskeleton, are critical for the activation of integrins, enabling high-affinity ECM binding (83). While the head of talin links integrins to actin, the tail domain is able to bind vinculin which then initiates the integrin clustering at FAs and, by binding to actin as well, further reinforces the connection between integrins and the cytoskeleton (84). Crosslinking of actin which can be done by α-actinin produces the actin-rich cytoskeletal fibers (64). Additional proteins recruited to FAs include tensin, paxillin, and focal adhesion kinase (FAK). Tensin, similar to talin and kindlin, is able to bind both actin and the β integrin subunit (64). Paxillin is able to interact with both the β integrin subunit and protein tyrosine kinases, including FAK, to create a signaling bridge (85). Phosphorylation of FAK at FAs leads to the propagation of intracellular signals through the Rho-ROCK pathway (64).

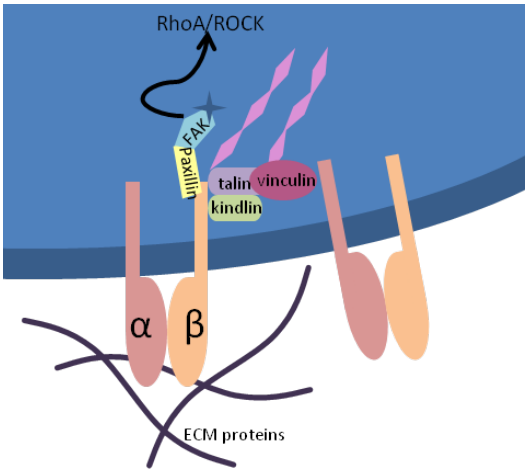

Figure 1.4 Focal Adhesions

Cells bind to their ECM proteins using integrins which are heterodimers made of an α and β subunit. Once these integrins engage a protein adhesion site, intracellular molecules are recruited which, create a bridge with the actin cytoskeleton and further promote the recruitment of other integrins and trigger intracellular signaling cascades.

Signaling within mechanotransduction pathways is increasingly relevant to tumor biology. Enhanced stiffness created within the tumor microenvironment by changes in both the ECM as well as cytoskeletal tension can then signal cells through various mechanisms including the Rho-ROCK pathway to produce a positive feedback loop promoting tumor cell malignancy and proliferation (46). Additionally, as FAK expression is also enhanced within tumors which, promotes proliferation, inhibitors to these pathways represent promising therapeutic targets (86). While augmented tissue stiffness impacts tumor cell behavior, altered mechanotransduction within the stromal cell compartment of tumors likely also contributes to tumor progression (50, 87).

1.8 Research Objectives

There exists a need for a better understanding of the role that surrounding host tissue stromal cells play in the organization of the tumor ECM, how this impacts tumor stiffness, and the resultant changes in tumor growth. As the mammary microenvironment, the host tissue surrounding breast tumors, is largely composed of adipose tissue which is abundant in ASCs, evaluation of the role these cells play in altering the tumor ECM is critical. A major cellular contributor to these ECM alterations is CAFs, or myofibroblasts. The ability of ASCs to become myofibroblasts in order to contribute to tumorigenesis is unclear. Tumors which produce an altered physicochemical environment as compared to normal mammary tissue, interface with host tissue and contribute to tumor progression by signaling surrounding cells through these altered physicochemical cues within the tumor microenvironment(88). Here, the ability of ASCs to assume a myofibroblast phenotype and cause changes in the tumor ECM as a result of tumor-derived physicochemical cues have been studied.

In this work analyzing the ability of altered tissue mechanics and chemical signals (Figure 1.5) to influence ASC pro-tumorigenic behaviors a myriad of physical science oncology approaches have been implemented. To model the progenitor cellular component of the host tissue both 3T3-L1 (ATCC) mouse preadipocytes, a well-characterized cell line modeling adipogenesis (89) as well as human primary adipose-derived stem cells (isolated by Lonza based on stem cell marker expression analyzed via flow-cytometry) were used. Mammary tumor-derived chemical cues were collected in tumor-conditioned media (TCM) from highly malignant human breast cancer cells (MDA-MB231, ATCC). Comparisons with additional normal and malignant cells were made to measure how tumor aggressiveness impacted these chemical cues. Assessment of the effect of ECM stiffening as seen in tumors on ASC behavior was measured with hydrogels (e.g. alginate, polyacrylamide, collagen) of varying stiffness.

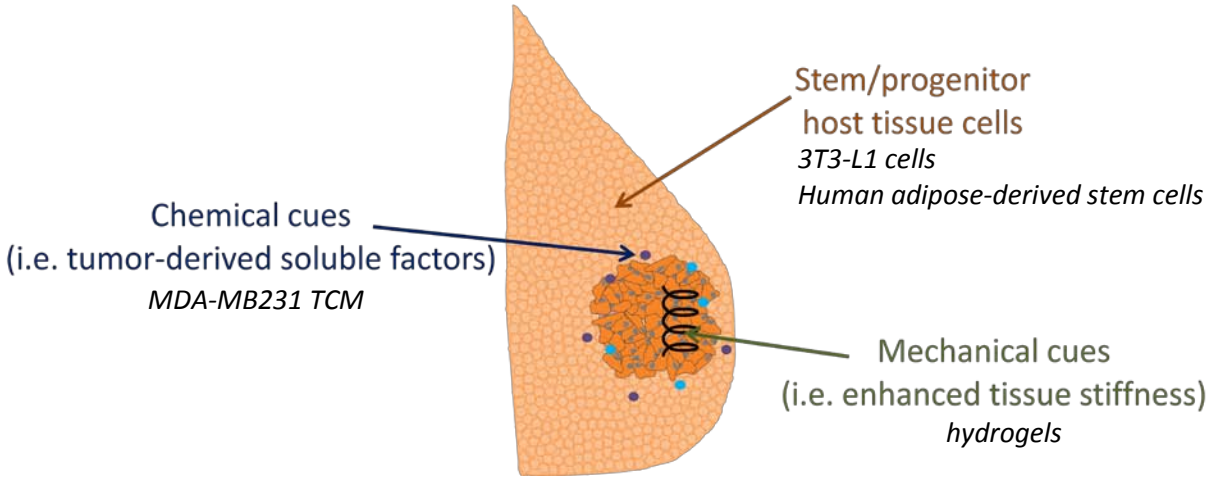

Figure 1.5 Modeling Tumor-derived Cues

The physicochemical microenvironment of a breast tumor varies from that of the normal host mammary tissue within which these tumors originate. The local tissue contains a population of stem cells, ASCs, which may be signaled by the tumor via physicochemical cues the chemical portion of which is released into tumor-conditioned media (TCM). Additionally, the enhanced tumor tissue stiffness, which is often responsible for the initial tumor diagnosis, may also cause changes in ASC behavior.

I propose that ASCs encountering the breast tumor microenvironment experience differential mechanical and chemical stimuli, altering their behavior to promote tumor ECM stiffening and angiogenesis, and thus contribute to increased mammary tumor malignancy. In order to address this hypothesis, I have investigated the following sub-hypotheses:

1. **ASCs alter the composition of the tumor ECM**
2. **Enhanced tissue stiffness, as seen in tumors, alters ASC functions**
3. **Tumor-derived physicochemical cues promote ASCs to differentiate into myofibroblasts, and thus enhance tumorigenesis**

The ever-growing utilization of ASCs for regenerative purposes warrants investigation of the ability of these cells to be altered by mechanical and chemical cues which vary throughout the body, and particularly at the site of tumor growth. With an improved understanding of ASC behavior in response to varied physicochemical signals, implementation of ASCs for regenerative purposes will be markedly improved by harnessing their potential while adjusting for any off-target capacities. Furthermore, as we further understand the roles ASCs play in tumorigenesis, we can better target any pro-tumorigenic capacity of these cells while properly harnessing their capacity at the site of tumor excision.

1) ASCs alter the composition of the tumor ECM

Alterations to the ECM of ASCs were studied as a function of exposure to tumor-derived soluble factors. The ECM protein Fn was specifically evaluated as this protein is found at higher concentrations within tumor tissue (90) and Fn complexity enables this protein to become stiffer through conformational changes (91). Additionally, TGF-β, a growth factor readily produced by tumor cells has been shown to increase Fn expression and incorporation into the ECM (92). To investigate the role of tumor-derived chemical cues, and specifically TGF-β, on ASC organization and deposition of Fn within the tumor ECM, the matrix produced by ASCs in response to soluble cues collected from breast cancer cells was studied (Chapter 2). A well-characterized murine preadipocyte cell line (3T3-L1) was used to represent ASC function. Specifically, 3T3-L1 cell-derived matrices were analyzed for Fn composition and conformation in response to TCM from MDA-MB231 cells. Through inhibition and supplementation studies, TGF-β was studied for its role in signaling ASCs in the tumor microenvironment to alter the Fn ECM.

2) Enhanced tissue stiffness, as seen in tumors, alters ASC functions

The ability of ASC behavior to be altered with mechanical cues was tested by implementing a novel alginate photocrosslinking system which produced artificial ECMs of varying stiffness while maintaining the density of cell adhesion sites throughout the matrix. This system enabled isolation of the

effect that altered ECM stiffness, as seen at the site of tumors, has on ASC behavior. To address this question, 3T3-L1 cells were seeded within alginate gels of stiffness similar to that of normal to malignant breast tissue and evaluated for their ability to proliferate, differentiate, and produce pro-angiogenic secretions (Chapters 3 and Figure 4.8).

3) Tumor-derived physicochemical cues promote ASCs to differentiate into myofibroblasts, and thus enhance tumorigenesis

To further delve into the altered ASC phenotypic changes that occur due to physicochemical tumor-derived cues, the function of ASCs in response to both TCM and altered tissue stiffness was measured (Chapter 4). Utilizing a comprehensive approach, both 3T3-L1 cells and ASCs were evaluated for their ability to proliferate, differentiate, and alter VEGF-induced pro-angiogenic endothelial cell behavior as a function of chemical cues and mechanical from breast cancer cells. Furthermore, the ability of these cells to undergo myofibroblastic differentiation (become α-SMA positive) and alter the local mechanics due to the TCM was measured. Their altered behavior due to the amalgamation of both chemical and mechanical tumor-derived cues was additionally assessed. An *in vivo* model was finally implemented to evaluate the cumulative contribution of myofibroblastic differentiation of ASCs to breast tumorigenesis.

CHAPTER 2

ADIPOSE PROGENITOR CELLS INCREASE FINBRONECTIN MATRIX STRAIN AND UNFOLDING IN BREAST TUMORS

Published in *Physical Biology* (93)

2.1 Contributors

Co-authors to this work made the following contributions: Matthew Saunders, an M. Eng. Student in the Gourdon lab, imaged and analyzed the FRET data presented in this chapter. Christine J. Yoon, an undergraduate student in the Fischbach lab, biochemically analyzed the ECMs. The work was completed as a collaborative project between the labs of Delphine Gourdon and Claudia Fischbach who both contributed greatly to the preparation of the manuscript presenting this work.

2.2 Abstract

Increased stiffness represents a hallmark of breast cancer that has been attributed to altered physicochemical properties of the extracellular matrix (ECM). However, the role of fibronectin (Fn) in modulating the composition and mechanical properties of the tumor-associated ECM remains unclear. We have utilized a combination of biochemical and physical science tools to evaluate whether paracrine signaling between breast cancer cells and adipose progenitor cells regulates Fn matrix assembly and stiffness enhancement in the tumor stroma. In particular, we utilized fluorescence resonance energy transfer (FRET) imaging to map the molecular conformation and stiffness of Fn that has been assembled by 3T3-L1 preadipocytes in response to conditioned media from MDA-MB231 breast cancer cells. Our results reveal that soluble factors secreted by tumor cells promote Fn expression, unfolding, and stiffening by adipose progenitor cells and that transforming growth factor-β (TGFβ) serves as a soluble cue underlying these changes. *In vivo* experiments using orthotopic co-transplantation of primary human

adipose-derived stem cells and MDA-MB231 into SCID mice support the pathological relevance of our results. Insights gained by these studies advance our understanding of the role of Fn in mammary tumorigenesis and may ultimately lead to improved anti-cancer therapies.

2.3 Introduction

Increased stiffness represents a hallmark of solid tumors, which is largely attributed to altered physicochemical properties of the extracellular matrix (ECM) (94). In particular, breast tumors are stiffer than their surrounding host tissue (51, 95), and accumulating experimental evidence indicates that this reduction in tissue compliance originates from altered ECM composition and crosslinking. More specifically, collagen is known to be up-regulated and more densely crosslinked within breast tumors as compared to healthy mammary tissue (73, 96). This variation advances tumorigenesis in an integrin-dependent manner (51, 73) and likely occurs not only by modulating the behavior of tumor cells, but also by altering mechanotransduction of stromal cells (50, 87). In addition to collagen, the tumor-associated ECM contains other fibrillar components whose role in promoting stiffness is less clear. In particular, fibronectin (Fn), which is critical for collagen turnover (74), is also up-regulated in mammary tumors and enhances tumor cell malignancy (78, 97). However, the specific characteristics of Fn underlying these variations remain to be elucidated.

Fn is a large (450-500 kD) dimeric glycoprotein consisting of three types of repeating globular modules (denoted FnI, FnII, and FnIII) (98) and plays an important role during embryonic development and regeneration of normal tissues (99). It contains numerous *surface-exposed* binding sites for cell receptors (in particular an Arg–Gly–Asp [RGD] loop which binds multiple integrins) and other matrix proteins (e.g., collagen, fibrin), including itself (100). Fn also has a number of *cryptic* binding sites, which remain buried when the protein is in its globular form (101). These cryptic sites, however, may be exposed when Fn undergoes conformational changes. In fact, Smith *et al*. have used fluorescence resonance energy transfer (FRET) imaging to map Fn molecular conformation, demonstrating that a broad

range of Fn conformations coexist within the fibers. The authors attributed this variety of Fn conformations to the presence of cells, which, by exerting tension on surrounding fibers (Rho-mediated cellular contractility), led to the loss of both quaternary and tertiary structures of around half of the Fn molecules forming the highly dynamic (strained) fibrillar network (102). Similarly, Klotzsch *et al.* demonstrated that stretching of Fn fibers not only induced partial unfolding of Fn modules (leading to the exposure of cryptic binding sites), but also increased the stiffness of the resulting strained fibers in a non-linear (albeit reversible) fashion (91). Despite these connections between Fn matrix organization and stiffness, the specific characteristics of Fn fibrils in the tumor microenvironment remain to be identified.

The ECM, which mediates increased tumor stiffness, is predominantly assembled by stromal cells (13), and adipose-derived stem cells (ASCs) represent a subpopulation of these cells in breast tumors. More specifically, mammary tumors are surrounded by adipose tissue, which in addition to differentiated adipocytes, contains an abundant population of ASCs (103). While adipocytes assemble a basement membrane that promotes mammary tumor progression through collagen IV (104), ASCs deposit an ECM that is rich in Fn (105). However, it is not clear whether ASC-mediated alterations of the Fn matrix contribute to increased tumor stiffness. We therefore investigated the capability of tumor-derived soluble factors to modulate Fn expression and conformation by ASCs. In particular, we focused on elucidating the effect of transforming growth factor β (TGFβ), due to its central role in tumorigenesis (19), Fn incorporation into the ECM (92), and cell contractility (20).

Utilizing a combination of biochemical assays and FRET imaging to monitor the expression and conformation of ASC-deposited Fn matrices, we provide experimental evidence that tumor-derived soluble cues promote Fn matrix assembly and enhanced stiffness. We further show that these differences involve TGFβ and may play a role during tumorigenesis *in vivo*. Collectively, our findings implicate Fn matrix assembly by stromal cells as an important contributor to increased tumor stiffness that may be explored towards more efficacious anti-cancer therapies.

2.4 Methods

In vivo studies

Experimental animal procedures were performed according to protocols reviewed and approved by the Cornell University Institutional Animal Care and Use Committee. Specifically, primary human adipose derived stem cells (ASCs) were obtained from commercial sources (Lonza) and were cultured in manufacturer supplied growth medium (ADSC-GM, Lonza). ASCs were injected into the cleared mammary fat pad of 3 week old female SCID mice (Charles River Labs) either alone or in combination with MDA-MB231 breast cancer cells (1×10^6 cells of each type in 20 µL of DMEM/ Ham's F-12 (Gibco), 10 % FBS (Tissue Culture Biologicals), 1 % antibiotic (penicillin/streptomycin, Invitrogen)). Injection of only MDA-MB231 cells served as an additional control. Tumors were harvested 5 weeks after implantation, fixed in neutral buffered formalin (EMD), paraffin embedded, and sectioned. Using standard immunohistochemistry, sections were stained for nuclei and Fn with a primary antibody raised against Fn (Sigma-Aldrich), an Alexa Fluor 488-labelled secondary antibody, and 4',6-diamidino-2-phenylindole (DAPI) (both from Invitrogen). Samples were mounted with ProLong Gold Antifade Reagent (Invitrogen) and were imaged on a Zeiss Observer Z.1 microscope with an AxioCam MRm camera. Blinded researchers made conclusions regarding the fibril formation. Fn staining intensity was evaluated via image analysis of 5-7 randomly selected areas in each of 4 specimens per condition using ImageJ (NIH).

Cell culture and media conditioning

3T3-L1 preadipocytes and MDA-MB231 breast cancer cells (both from ATCC) were routinely cultured in MEM (α-modification [αMEM], Sigma-Aldrich) containing 10% FBS and 1% antibiotic. For all experiments, 3T3-L1 cells were used at passage eight or lower. To obtain tumor conditioned media (TCM), subconfluent cultures of MDA-MB231 were washed with PBS (Invitrogen) and incubated with αMEM, 1% FBS, 1% antibiotic. After 24 hours, media were collected and normalized to cell number in

order to ensure equal concentrations of tumor cell-derived soluble factors in all experiments. To this end, cells were trypsinized and counted using a Beckman Coulter Z2 Particle Analyzer, and media volumes were adjusted with αMEM, 1% FBS, 1% antibiotic. The normalized media were concentrated 10-fold using Amicon Ultrafree 15 centrifugal filter units (3000 MWCO, Millipore). Prior to cell culture, this medium was diluted to a 2-fold concentration with αMEM, 1% FBS, 1% antibiotic. Control media were obtained by incubation of αMEM, 1% FBS, 1% antibiotic in the absence of cells for 24 hours and similar processing. TGFβ concentrations in the different media were quantified with a Quantikine TGFβ1 ELISA (R&D Systems) according to manufacturer's instructions.

Immunostaining, Western Blotting, and Real-Time RT PCR

To analyze changes of Fn matrix assembly on the protein and mRNA level 3T3-L1 cells were seeded and allowed to adhere overnight. Subsequently, media was replaced with either control or TCM for 3 days with a media change after 2 days. For immunostaining of cell- and matrix-associated Fn, cultures grown on coverslips were fixed, permeabilized with PBS containing 0.05% Triton-X (VWR), and incubated with a primary antibody raised against Fn (Sigma-Aldrich), an Alexa Fluor 488-labelled secondary antibody, and DAPI (both from Invitrogen). Samples were mounted with ProLong Gold Antifade Reagent (Invitrogen) and randomly selected areas were imaged on a Zeiss Observer Z.1 microscope using an AxioCam MRm camera (with equal exposure times between conditions). Researchers who made conclusions regarding fibril formation were blinded to the conditions. For Western Blot analysis, lysates of cells and decellularized matrices (obtained by detergent extraction according to (106)) were prepared with RIPA buffer containing protease inhibitor cocktail (both from Sigma-Aldrich). Protein concentrations were determined with a BCA kit (Pierce), and 2 µg of protein were loaded in gels (12% Ready Gel Precast Gels, BioRad), resolved by SDS-PAGE, and transferred to PVDF membranes (Biorad). Membranes were probed for Fn (rabbit anti-Fn) and β-actin (mouse anti- β-actin) as a loading control (both from Sigma-Aldrich) and subjected to ECL detection (Amersham Biosciences).

Densitometry was performed using Adobe Photoshop CS4 (multiplying the mean pixel intensity by the band size measured in pixels) and normalized to β-actin.

For Real-Time RT PCR, total RNA was extracted using TRIzol® (Invitrogen) according to the manufacturer's protocol. RNA (1 μg total) was reverse-transcribed using High Capacity cDNA Reverse Transcription Kits with random hexamers (Applied Biosystems). Real-time RT PCR was performed in triplicate (25 ng template) using SYBR green detection (Quanta) on an Applied Biosystems 7500 System. Primer sequences for mouse Fn (fwd: 5'cggagagagtgcccctacta3', rev: 5'cgatattggtgaatcgcaga3') and GAPDH (fwd: 5'tgtgatgggtgtgaaccacgag3', rev: 5'tgggagttgctgttgaagtcgc3') were used (107) (synthesized by IDT Technologies), and relative quantification was performed using the ΔΔCt method as previously described (108).

FRET labeling of Fn

Fn used for FRET analysis was doubly labeled using a previously described two-step process (109). In the first step, human plasma Fn (Swiss Red Cross, SRK) was denatured in 4 M guanidine hydrochloride (GdnHCl, Sigma-Aldrich) to expose four free cysteine residues located on $FnIII_7$ and $FnIII_{15}$ (Figure 2.1A). Subsequently, a 10-fold excess of the acceptor label (A), Alexa 546 maleimide (Molecular Probes), was added. After incubation for 1 hour at room temperature, the reacted Fn solution was dialyzed in a Slide-a-lyzer dialysis cassette (10,000 MWCO; Pierce Biotechnology) to remove unbound fluorophores and GdnHCl. This procedure was performed in 0.1 M sodium bicarbonate in PBS (pH 8.6), which served as the labeling buffer for the subsequent reaction. In the second step, the donor label (D), Alexa 488 succinimidyl ester, was non-specifically conjugated to lysine residues by using a 60-fold excess of Alexa 488 as directed by the standard amine-labeling protocol of the manufacturer (Molecular Probes). The D/A-labeled Fn (Fn-DA) was then purified by size-exclusion chromatography using a PD-10 gel filtration column (GE Healthcare). The labeling ratio of donors to acceptors per Fn dimer was determined using published extinction coefficients for the dyes and Fn. The batch of Fn-DA

used in the described experiments resulted in approximately 10 donors and 4 acceptors per molecule.

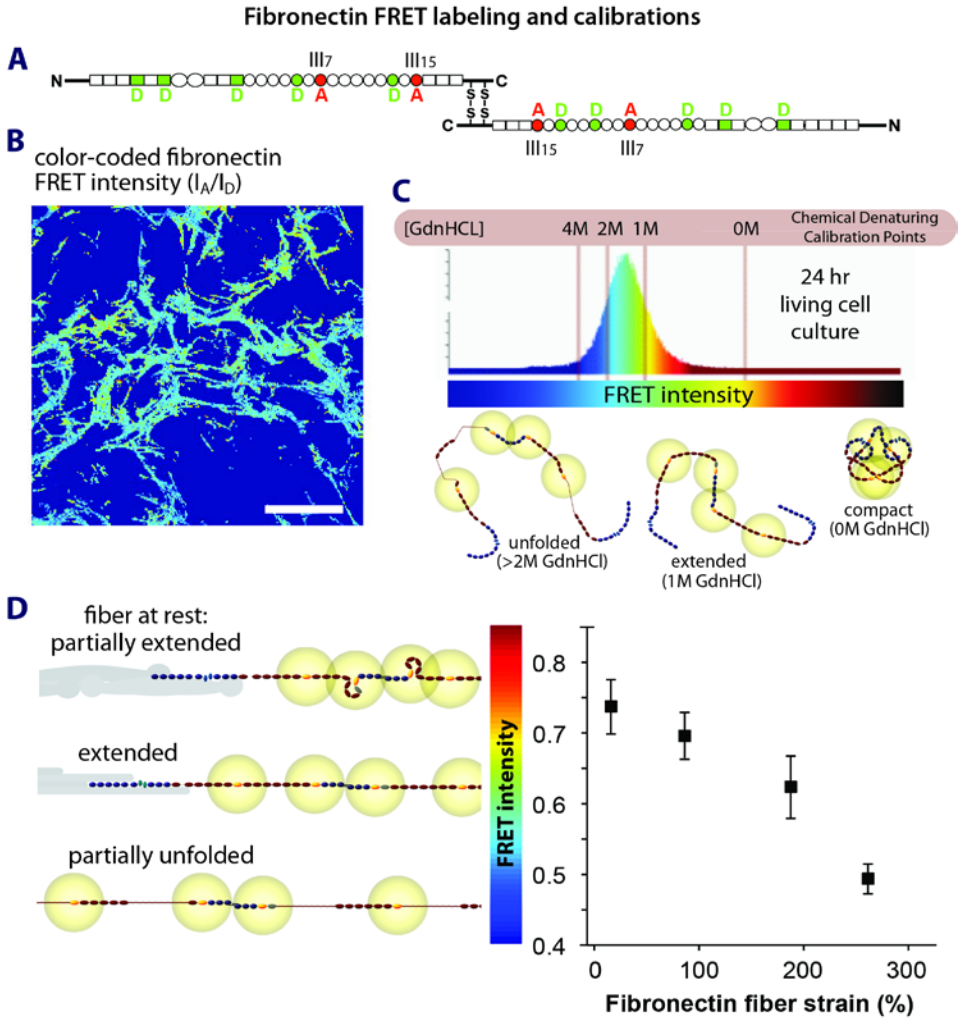

Figure 2.1 FRET-Fn intensity correlates with Fn conformation and strain

(A) Labeling scheme of Fn for FRET analysis: acceptor fluorophores were conjugated to each of the four cysteines located on modules III_7 and III_{15} and donor fluorophores to random lysines. (B) Representative image of a confocal z-stack that was color-coded to better visualize FRET intensities (i.e., acceptor intensity divided by the donor intensity [I_A/I_D]) resulting from heterogeneous strain within the Fn matrix. Blue indicates low FRET and fiber unfolding while green-yellow indicates higher FRET and intact secondary/tertiary structure of the fibers (scale bar = 50 μm). (C) Histogram of the FRET intensities derived from analysis of the field of view shown in B, including chemical denaturation data acquired by

denaturing Fn-DA with different concentrations of GdnHCl and corresponding Fn conformations *in solution*. Correlation of FRET intensity with likely conformations adopted by Fn *in fibers* and resulting Fn fiber strains. (D) A plot of the average FRET intensity ($I_A/I_D \pm SD$) versus strain applied to manually-deposited Fn fibers that were extended up to 260% strain is shown.

Preparation of culture substrates for FRET analysis

3T3-L1 cells were cultured in control or TCM for 3 days with a media change on the second day. For studies involving modulation of TGFβ signaling, 2 ng/mL recombinant human TGFβ1 and 0.5 μg/mL anti-human LAP (neutralizing TGFβ1 antibody) (both from R&D) were added to control media and TCM 30 minutes before administration to cultures, respectively. These concentrations were based on manufacturer descriptions of activity and the TGFβ concentrations measured in the TCM via ELISA. After this preconditioning period, the cells were trypsinized, counted, and resuspended in αMEM, 1% FBS, 1% antibiotic at a concentration of 100,000 cells/mL. Subsequently, 200 μL of this cell suspension was seeded onto Lab-Tek™ glass chamber slides (Thermo Scientific) that were previously coated with unlabeled Fn ([un-Fn], 50 μg/mL in PBS) to promote cell adhesion. Additionally, 200 μL of 100 μg/mL human plasma Fn (only 8% Fn-DA with an excess of 92% un-Fn to prevent intermolecular energy transfer between adjacent proteins in fibers (109)) in αMEM, 1% FBS, 1% antibiotic was added per well to enable FRET analysis of Fn deposition. Following 24 hours of culture (i.e., a time period during which cells incorporate labeled Fn into matrix fibrils (109)), cultures were fixed with neutral buffered formalin (EMD) and imaged.

FRET analysis

Donor and acceptor peak intensities resulting from cell-mediated deposition of FRET-labeled Fn were analyzed by confocal microscopy and subsequent image processing. Z-stack images were acquired through the entire thickness of the matrix at 6-8 representative locations per well with a z-step of 1.125

μm using a Zeiss Meta 710 Confocal Microscope with a 40x water immersion lens and imaging parameters that prevented photobleaching. However, only images captured >2.25 μm above the glass were utilized for analysis of FRET intensities to exclude artifacts mediated this interface. A 20% laser output was used as optimized by calibration testing with a 600 V voltage gain for both the donor and acceptor channels with ranges of 514-526 nm and 566-578 nm, respectively. Matrix thickness of 6-8 sections per condition was determined as the distance between the slices when the matrix first came into focus and when the matrix first began to go out of focus. Thickness values reported as the average change relative to control conditions for at least 2 independent experiments. Image processing of the acceptor and donor images was performed as previously described (102). Briefly, MATLAB (MathWorks, Inc.) was used to determine the FRET for each pixel of a FRET image, to calculate the mean and standard deviation of the FRET intensities, and to compile FRET intensity data at each representative location for histogram plotting. To assess the spread in the FRET intensity between conditions, the mean of the standard deviation of the FRET intensities within each image of a stack was averaged for all locations within an experiment.

Correlation of FRET intensities with Fn conformations and strains

Because the utilized FRET labeling approach relies on multiple fluorophores present on each Fn-DA molecule, and because the labeling with donors is random, our technique cannot measure absolute distances between fluorophores but rather determines population averages. The ratio of the acceptor to the donor peak intensity (FRET intensity) was, therefore, calibrated (1) to known conformations of soluble Fn in solution, and (2) to known strains of deposited Fn fibers. For (1), a 0.1 mg/ml Fn solution (5% Fn-DA, 95% un-Fn) was denatured in different concentrations of guanidine hydrochloride (GdnHCl) and the FRET intensity was measured. In physiological buffer, soluble Fn exists in a pretzel-like shape (compact conformation), held together by ionic interactions (110) (Figure 2.1). Previous studies using circular dichroism have shown that Fn's quaternary structure is disrupted in 1M GdnHCl (extended conformation)

and that further increase in GdnHCl concentration results in partial unfolding of its tertiary and secondary structure (unfolded conformation), which is essentially complete in 4M GdnHCl (102). In practice, the FRET intensity of the 1M GdnHCl denaturation point using monomeric Fn-DA (to prevent additional FRET caused by crossover of the Fn dimer arms) was used as the onset for partial Fn unfolding as previously described (102). For (2), manually pulled Fn fibers were deposited on silicone sheets and strained on a custom-made, one-dimensional strain device as previously described (111). Briefly, 0.25 mm-thick silicone sheets (Specialty Manufacturing) were cut into a dog-bone shape and cleaned by sonication in 2% PCC-54 (Sigma-Aldrich) and then 70% ethanol. A 0.5 mg/ml Fn solution (5% Fn-DA, 95% un-Fn) was deposited as a small drop on the silicone sheet. Fibers were extruded from the drop with a sharp tip and deposited onto the silicone sheet. Afterwards, the sample was washed with 2% (w/v) BSA in PBS, and soon thereafter immersed in PBS buffer for further studies. Fiber strain was calculated from the macroscopic strain of the silicone sheet and correlated with FRET determined as described above (102).

Analysis of cell numbers, cell morphology, and pore size of the Fn matrices

Cell numbers and cell morphology were analyzed by fixing samples utilized for FRET analysis with neutral buffered formalin, staining them with DAPI and Alexa Fluor 568-phalloidin (both from Invitrogen), and conducting image analysis using ImageJ (NIH). To this end, ten representative images of each well were taken and the average number of nuclei per field of view (FOV) was assessed. To quantify cell morphology, the spreading of each cell was measured in 8 representative images per sample (4 samples per condition). Pore size was analyzed by measuring the average size of the empty space within reconstructed z-stack images of the donor channel using ImageJ.

Statistical analysis

Statistical analysis was performed using Prism 5 (GraphPad Software). Student's T-tests were

used to determine statistical significance between conditions and a p-value less than 0.05 was considered statistically significant. The spread of FRET intensity between the four conditions was analyzed by one-way analysis of variance (ANOVA) followed by the Tukey method to make *post hoc* pair wise comparisons with $\alpha = 0.05$. Biochemical and FRET experimental results are shown for one representative study after similar results were replicated in separate experiments. Matrix thickness and spread of FRET intensity relative to control conditions are reported as the average changes calculated from at least 2 independent experiments. Unless otherwise noted, values are reported as the mean with error bars to indicate standard deviations.

2.5 Results

Adipose progenitor cells contribute to increased Fn in tumors in vivo

Fn expression increases in the tumor microenvironment and promotes malignancy (78, 97); however, the cellular origin of Fn up-regulation remains unclear. To evaluate whether ASCs contribute to Fn deposition in mammary tumors, human MDA-MB231 breast cancer cells were xenografted either alone or in combination with primary human ASCs into the cleared mammary fat pad of SCID mice. Quantification of Fn in the explanted tissues by image analysis of immunohistochemically stained cross-sections revealed that tumors containing ASCs exhibited a 1.4-fold denser and more fibrillar Fn matrix as compared to tumors generated using MDA-MB231 cells alone (Figure 2.2). Additionally, injection of ASCs only did not increase the Fn concentration at the implantation site likely due to their differentiation into adipocytes, a cell type that forms a basement membrane rather than an ECM rich in Fn (112). These results not only suggest that ASCs enhance Fn deposition and remodeling in the mammary tumor microenvironment, but also that tumor-derived factors are capable of altering the phenotype of ASCs which contributes to these changes.

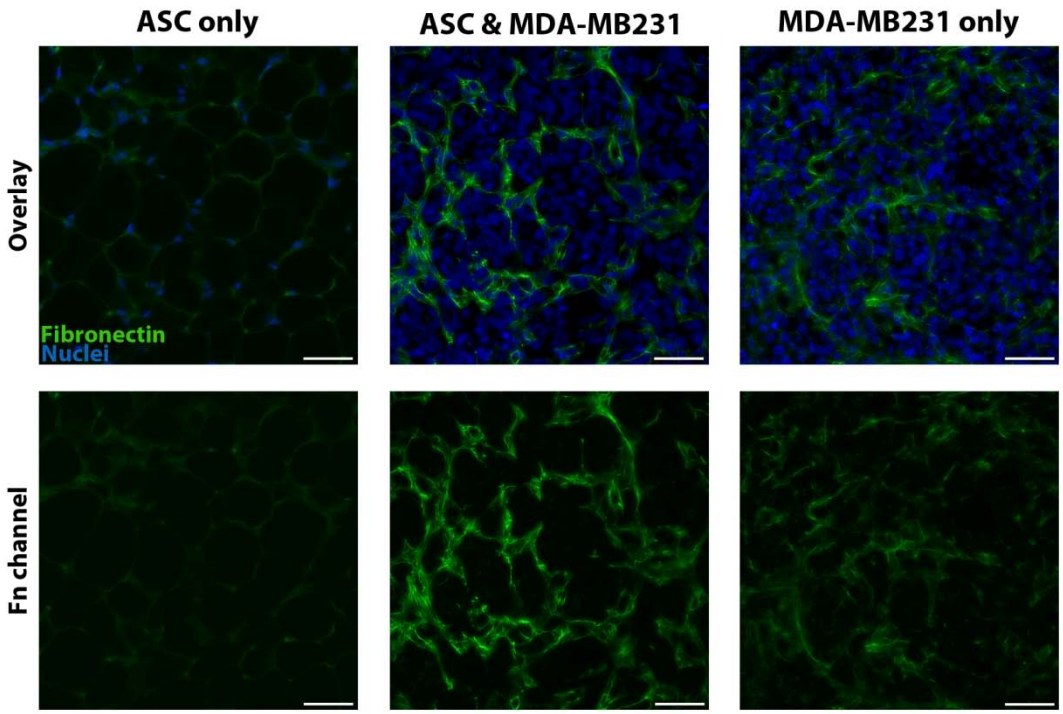

Figure 2.2 Fibronectin (Fn) deposition by ASCs in vivo

Co-implantation of human MDA-MB231 and primary human ASCs into the cleared mammary fat pad of SCID mice yielded tumors with a denser and more fibrillar Fn matrix as compared to implantation of MDA-MB231 cells alone. Additionally, co-implantation with MDA-MB231 cells promoted Fn matrix assembly by ASCs as compared to injection of ASCs alone (scale bars = 50 μm).

Tumor-derived soluble factors regulate Fn matrix formation by adipose progenitor cells

To evaluate Fn matrix deposition and remodeling by adipose progenitor cells in the presence of mammary tumor cells, we conducted *in vitro* studies utilizing two well-characterized cell lines: 3T3-L1 preadipocytes as a model of ASCs and MDA-MB231 breast cancer cells as representative of aggressive disease. First, we broadly assessed the effect of breast cancer-derived soluble factors on Fn matrix formation via biochemical assays. To this end, 3T3-L1s were incubated for 3 days in either control media or media conditioned by MDA-MB231 cells (TCM), and we subsequently evaluated Fn transcription and protein levels. Immunofluorescence analysis indicated that cultures maintained in TCM produced a

denser and more fibrillar Fn matrix relative to cells that were fed with control media (Figure 2.3A). Western Blot analysis of both total cell lysates and matrices prepared by detergent extraction showed increased Fn levels in TCM-incubated cultures, further supporting our microscopic observations (Figure 2.3 B,C). We further analyzed Fn gene expression in 3T3-L1 cells via real-time RT PCR, which revealed up-regulated Fn expression in the presence of tumor-derived soluble factors (Figure 2.3D). Together, these results suggest that ASCs in the breast cancer microenvironment exhibit enhanced Fn transcription and Fn matrix assembly.

FRET-imaging allows monitoring of Fn unfolding and stiffness by adipose progenitor cells

Cells assemble their Fn matrix not only by incorporating endogenously derived Fn, but also by polymerizing soluble Fn from exogenous sources (113). This characteristic allowed us to monitor the deposition of FRET-labeled Fn into newly developed fibrils in order to determine the conformation and stiffness of the 3T3-L1-derived Fn matrices. For these studies, dual labeled Fn (Fn-DA) was prepared by labeling each of the four cysteines located on Fn modules III_7 and III_{15} with acceptor fluorophores and random lysines with donor fluorophores (Figure 2.1A). When cells adhere and apply traction forces to their matrix (114), incorporated Fn-DA is exposed to dynamic levels of strain that can be monitored by analyzing the average increase of donor-acceptor distances. More specifically, cell-mediated stress leads to increased separation of donors and acceptors via Fn unfolding and, hence, decreased FRET intensity (i.e., acceptor intensity divided by the donor intensity [IA/ID]) in certain regions of the matrix [blue fibrils], while other regions are strained less as indicated by higher FRET [green-yellow fibrils] (Figure 2.1B).

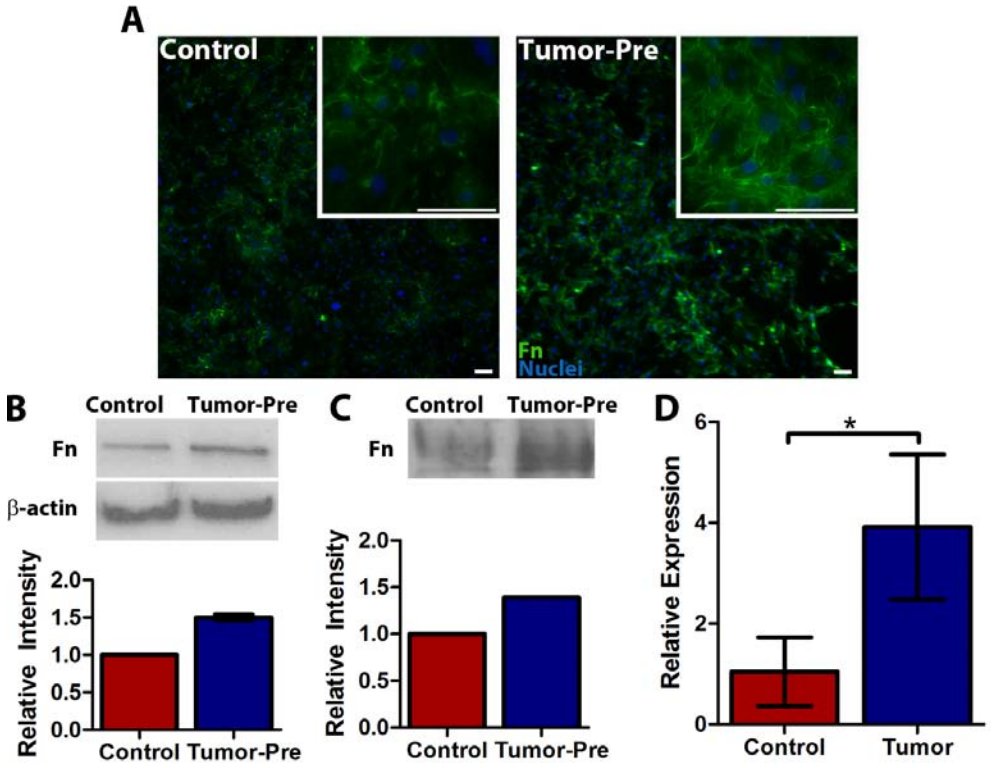

Figure 2.3 Biochemical analysis of Fn matrix assembly

Immunofluorescence revealed that 3T3-L1 preadipocytes exhibit increased Fn matrix assembly when cultured in the presence of MDA-MB231-conditioned media (Tumor-Pre) as compared to the same cells maintained in control media (Control). (A) Insets depict representative areas of matrices shown in the overview images (scale bars = 100 μm). Western Blot analysis of 3T3-L1 cultures (B) or detergent extracted matrices (C) followed by densitometry confirmed that 3T3-L1 cells that were exposed to tumor-conditioned media (Tumor-Pre) deposited increased amounts of Fn as compared to cells maintained in control medium (Control). (D) 3T3-L1 cells significantly up-regulated Fn expression when exposed to tumor-conditioned media relative to control conditions as measured by Real-Time RT PCR. (n=3, *$p < 0.05$ from Control).

Tumor-derived soluble factors regulate Fn matrix thickness

We measured the thickness of the Fn-DA matrices produced by 3T3-L1 cells in response to tumor-secreted soluble factors using z-stack confocal microscopy analysis. 3T3-L1 cells were pre-conditioned in either control media or MDA-MB231-conditioned media for 3 days (i.e., a time period similar to the biochemical studies described above). Subsequently, FRET analysis was performed in fresh serum-reduced media (i.e., following re-seeding and throughout 24 hours of culture) with defined concentrations of Fn (8% dual-labeled Fn-DA). Our results indicate that the Fn matrix assembled by tumor-conditioned 3T3-L1 cells was significantly thicker than that produced by cells in control media (Figure 2.4A). Quantification of DAPI-stained nuclei confirmed similar cell numbers in all conditions, suggesting that the detected differences in matrix thickness were due to changes in Fn matrix assembly rather than cell proliferation (Figure 2.4B). Additionally, neither the morphology of the cells nor the pore size of the matrices differed between conditions suggesting that the detected change in thickness was due to increased Fn deposition rather than incorporation of cells (Figure 2.4 C,D). These measurements confirmed our biochemical results, and collectively provide strong evidence that soluble factors from the tumor increase Fn deposition by adipose progenitor cells.

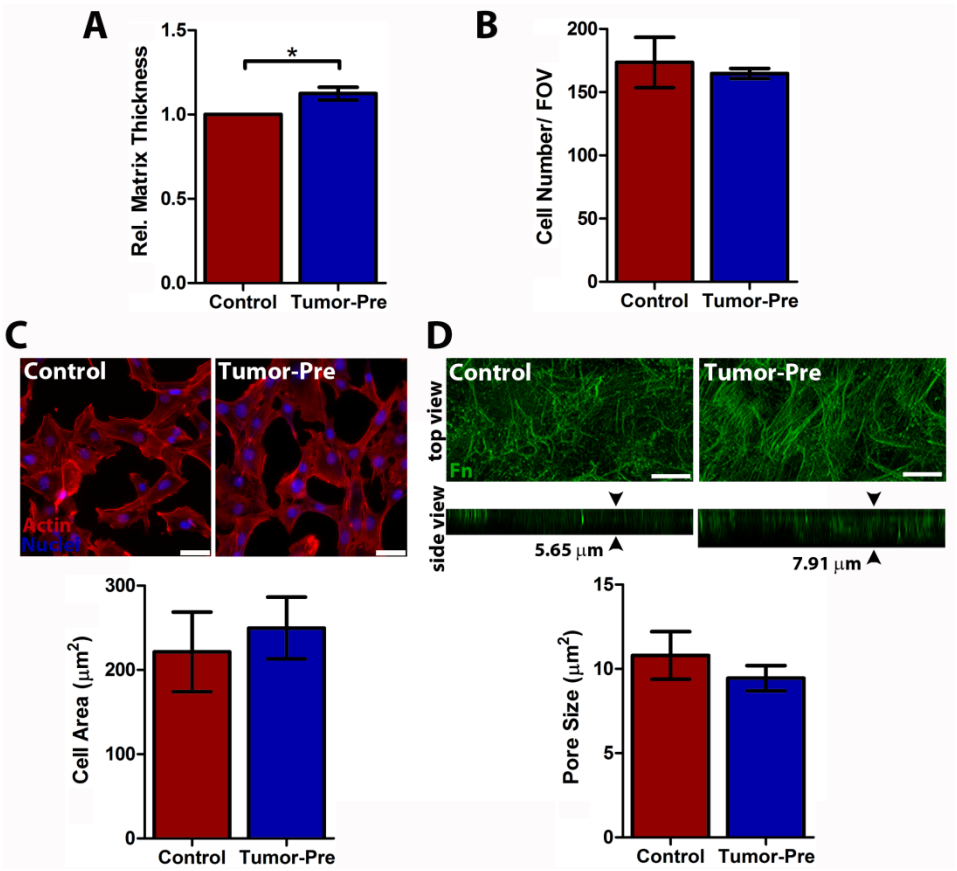

Figure 2.4 Fn matrix thickness

3T3-L1 preadipocytes assemble thicker matrices when pre-conditioned in the presence of tumor-derived soluble factors (Tumor-Pre) relative to the same cells that were maintained under control conditions (Control). (A) Matrix thickness was quantified by confocal analysis of z-stack images that were obtained following incubation of the differently pre-conditioned cells with FRET-labeled Fn for 24 hours. * $p < 0.05$ for 8 independent experiments. (B) Quantification of cell number via image analysis of DAPI stained cells demonstrated equal cell densities in both conditions indicating that differences in matrix thickness were not due to altered cell proliferation (n=10, $p = 0.26$). (C) Quantification of cell spreading via image analysis of cells stained with phalloidin and DAPI, demonstrates that cell morphology is similar in control and tumor-preconditioned 3T3-L1 cells (scale bars = 50 μm, n = 7 or 4, $p = 0.45$). (D) Control and tumor-preconditioned cells assembled Fn matrices of similar pore size as tested using image analysis of 3-D reconstructed confocal image stacks (scale bars = 20 μm, n = 8, $p = 0.16$).

Tumor-derived soluble factors regulate Fn matrix unfolding and stiffness

To determine if the presence of tumor-derived soluble factors acts not only on Fn production, but also on Fn unfolding and stiffness, we pre-conditioned 3T3-L1 as described above and conducted FRET analysis. To only analyze Fn fibrils deposited to the newly deposited Fn matrix and exclude artifacts mediated by the glass surface this analysis was performed only on the portions of the matrix that were >2.25 µm away from the glass (Figure 2.5). Matrices assembled by tumor-pre-conditioned cells (Figure 2.6A) exhibited a decreased mean FRET intensity relative to matrices deposited by control cells as visualized by the color shift from yellow-green (control) to blue (tumor) in Figure 2.6B, the left-shift of the histograms accumulating FRET intensities of the entire z-stack of that field of view (Figure 2.6C), and the corresponding box and whisker plots of multiple fields of view (Figure 2.6D). Correlation of these changes in FRET intensity with Fn strain (based on the calibration in Figure 2.1D indicates that tumor-associated 3T3-L1 cells generate highly-strained fibers (220% average strain), while control cells deposit more relaxed fibers (120% average strain) correlating with a 83% change in Fn fiber strain. When relating Fn fiber strain to the stiffness of individual Fn fibers as recently published (Klotzsch et al 2009), these data also suggest that Fn fibers generated by tumor-associated cells are more than three times stiffer than fibers deposited by control cells (tumor-associated Fn: 0.5-0.6 MPa; control: 0.1-0.2 MPa). These differences suggest that 3T3-L1 cells exposed to tumor-derived soluble factors are capable of increasing the population of partially unfolded, stiffer Fn fibers. Additionally, the spread of Fn conformations was significantly narrower in the tumor case as suggested by the FRET values (tumor: ~0.5 to 0.7; control: ~0.5 to 0.8) and width of the corresponding histograms (Figure 2.6C) of one representative experiment and calculated changes for 6 independent experiments (Figure 2.7). This suggests that tumor-derived factors prevent stromal cells from generating their usual heterogeneous Fn matrix (consisting of a broad range of Fn conformations from almost compact to unfolded) and instead stimulate them to generate highly stretched, and hence stiffer, partially unfolded fibers. Figure 2.6D summarizes FRET data for multiple fields of view per condition and illustrates the global effect of tumor-derived soluble cues on matrix conformation and stiffness by indicating a significant decrease in FRET intensity for Fn matrices

produced by tumor pre-conditioned cells compared to control cells. Therefore, in addition to up-regulating matrix thickness, tumor-secreted soluble factors enrich the population of highly stretched, stiffer Fn fibers in 3T3-L1-deposited matrices.

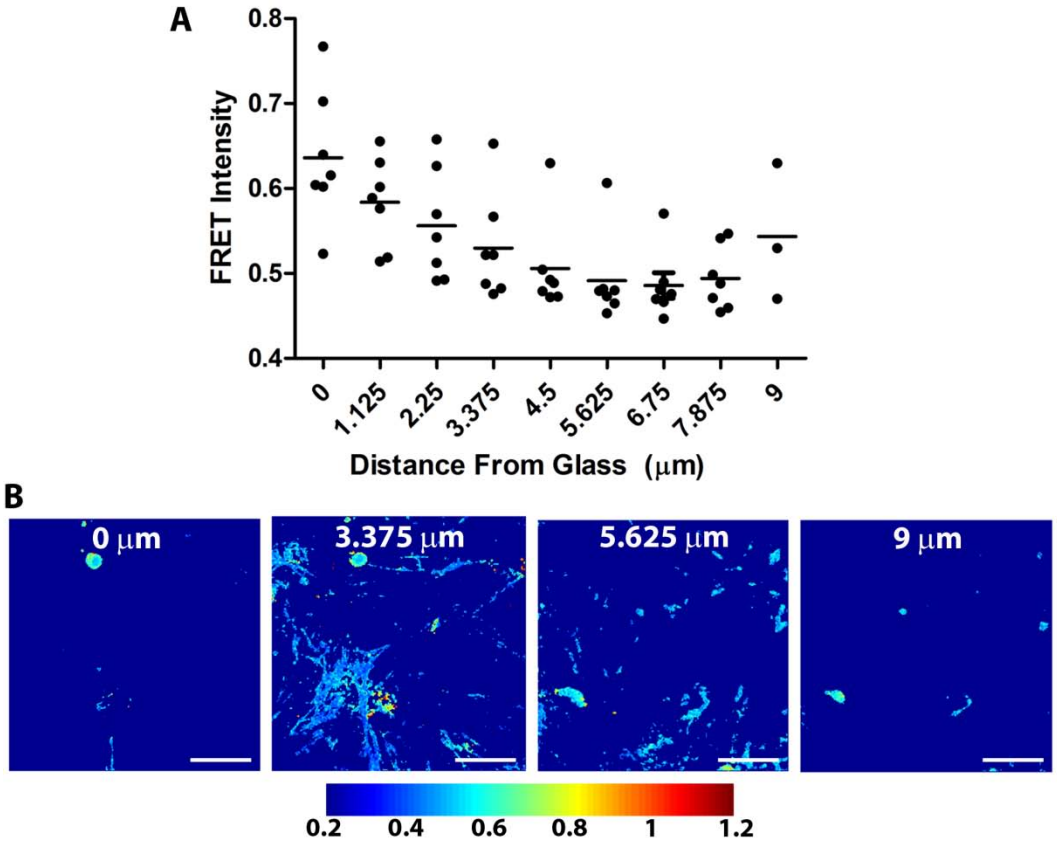

Figure 2.5 Variation of FRET intensity through the matrix

(A) The FRET intensity through the matrix, i.e., along the z-axis from the glass/matrix interface (z = 0 μm) to the matrix/medium interface (z = 9 μm) is indicated for one condition (Tumor-Pre), showing a line to represent the average intensity per image as a function of z. Representative FRET images of the matrix along z showing higher FRET fibrils (appearing like small aggregates anchored to the glass) at z = 0 and rather constant lower FRET fibrils above a certain distance from the glass (z > 2.25 um). (B) These constant FRET values are the ones that were averaged and reported in this study, intentionally discarding fibers at the glass interface to eliminate effects mediate by Fn-substrate interactions (scale bar = 50 μm).

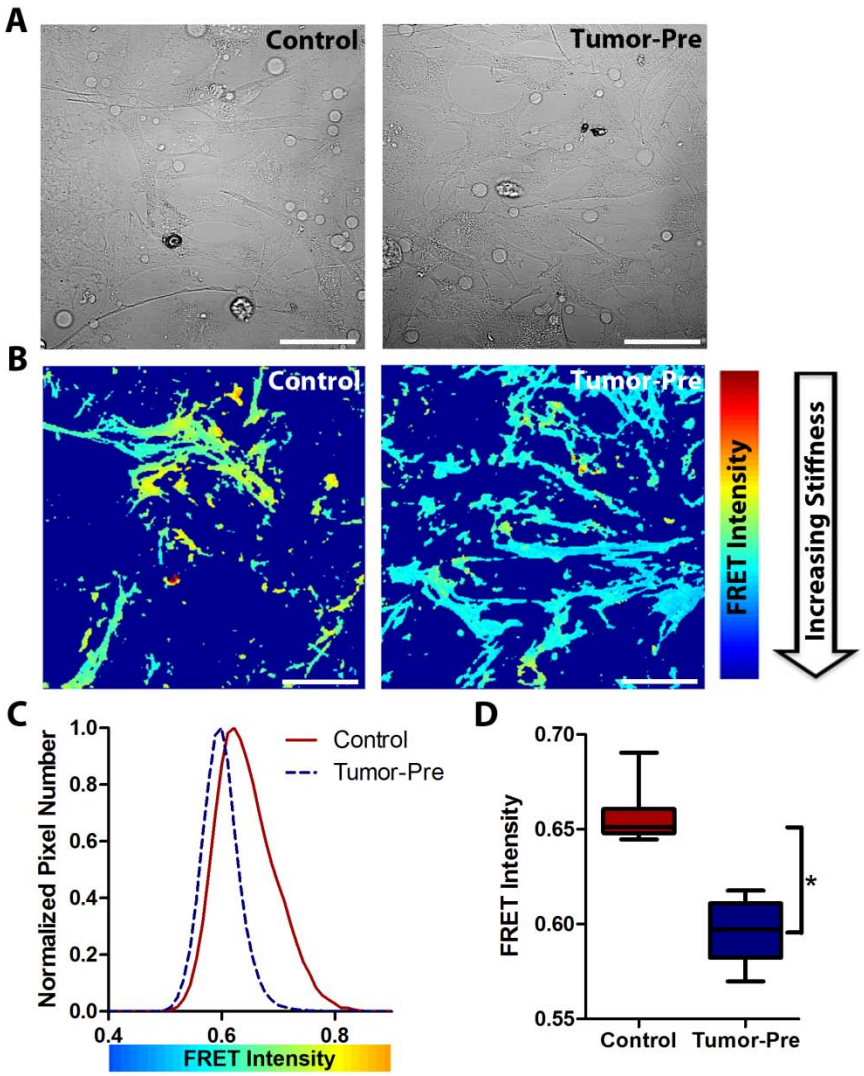

Figure 2.6 Fn matrix unfolding and stiffening in response to tumor-conditioned media

3T3-L1 cells pre-conditioned in the presence of tumor-derived soluble factors (Tumor-Pre) promote Fn unfolding and stiffness relative to the same cells pre-conditioned in control media (Control). (A) Bright field images of representative fields of view (scale bar = 50 μm). (B) Confocal Z-stack slices of the same fields of view in which the FRET intensity for each pixel was color-coded and mapped to the images shown in A (scale bar = 50 μm). (C) Histograms of the FRET intensity derived from analysis of the complete z-stack of that field of view. (D) Box and whiskers plots of the FRET intensity determined by analysis of 6-8 representative fields of view per condition indicate the intensity of the FRET for each condition ($n = 7$, * $p < 0.05$).

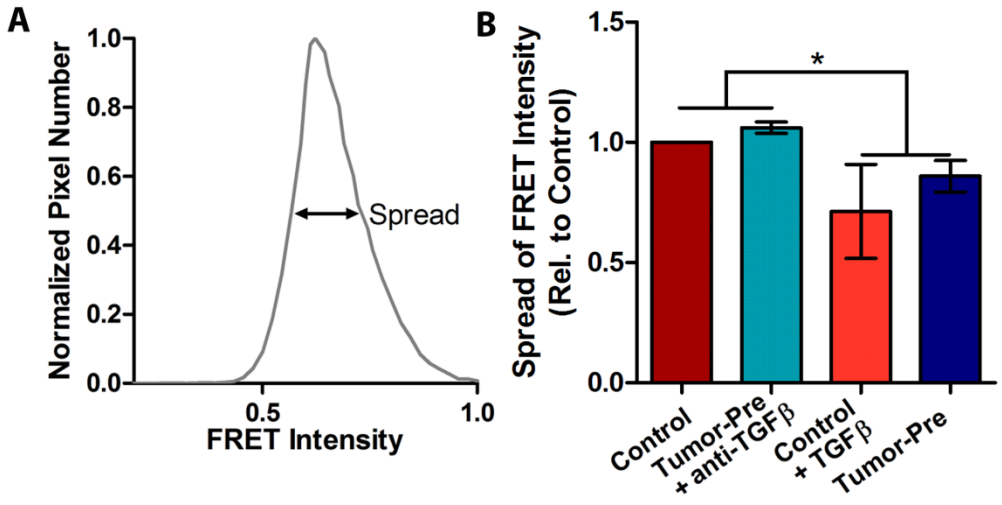

Figure 2.7 Effect of tumor-conditioned media and TGFβ on Fn fiber heterogeneity

(A) Fn fiber heterogeneity was assessed by quantifying the standard deviation (i.e., spread) of the FRET intensity for each condition. (B) Pre-conditioning of 3T3-L1 cells with tumor-conditioned media (Tumor-Pre) or TGFβ (Control + TGFβ) significantly decreases the spread of the FRET intensity (i.e., increases fiber homogeneity) relative to control conditions (Control) and tumor-preconditioning in which TGFβ signaling has been inhibited via the addition of a neutralizing antibody (Tumor-Pre + anti-TGFβ) ($n = 2$ or 6, $*p < 0.05$).

Tumor-derived TGF-β plays a key role in regulating Fn matrix unfolding and stiffness

To determine if tumor-derived TGFβ contributes to the matrix modifications described above, we first measured the levels of TGFβ in both control and TCM and detected increased concentrations of TGFβ (up to 1.75 ng/mL) in TCM (Figure 2.8A). We next pre-conditioned 3T3-L1cells in the presence or absence of TGFβ, mimicking levels in the TCM, followed by a 24 hour incubation period with Fn (8% dual-labeled Fn-DA) for FRET measurements (Figure 2.8B). Qualitative and quantitative FRET analysis revealed that the presence of TGFβ affected matrix characteristics in a manner similar to TCM. More specifically, the mean FRET intensity decreased for matrices assembled by TGFβ-pre-conditioned cells (0.50) as compared to control conditions (0.54), indicating the formation of more stretched and stiffer Fn

fibers in the presence of TGFβ (Figure 2.8 C-E). The width of the corresponding histograms additionally revealed that the distribution of Fn conformations was narrower in the TGFβ case relative to controls, and, in fact, recapitulated conditions generated by tumor-preconditioned cells (Figure 2.7B, 2.8D). These changes suggest that TGFβ plays a role in the assembly of a Fn population that mostly consists of unfolded and stiffer fibers. Finally, TGFβ enhanced the quantity of assembled fibers, which resulted in a 23% increase in matrix thickness relative to control conditions (Figure 2.8F) and a corresponding increase in protein content as detected by Western Blot analysis (Figure 2.8G).

We next evaluated whether inhibition of TGFβ can normalize Fn matrix assembly by tumor-associated 3T3-L1 cells. To this end, 3T3-L1 cells were pre-conditioned in TCM that was either supplemented with TGFβ neutralizing antibody or left untreated (Figure 2.9A). Subsequent FRET analysis of the resulting matrices revealed that inhibiting TGFβ in the TCM has two significant effects on matrix characteristics: (i) stabilization of Fn fibers from cell-mediated stretching and unfolding (Figure 2.9 B-D), and (ii) down-regulation of fiber formation (as detected by the decrease in matrix thickness in Figure 2.9E and corresponding Western Blot analysis (Figure 2.9F). The spread of FRET intensity also increased with TGFβ antibody treatment and mimicked decreased fiber homogeneity in a manner similar to control conditions (Figure 2.6). Collectively, these results suggest that tumor-secreted TGFβ plays a key role in deregulation of Fn matrix assembly in tumor microenvironments and that blocking its signaling normalizes the assembly of Fn matrices and reduces their corresponding stiffness.

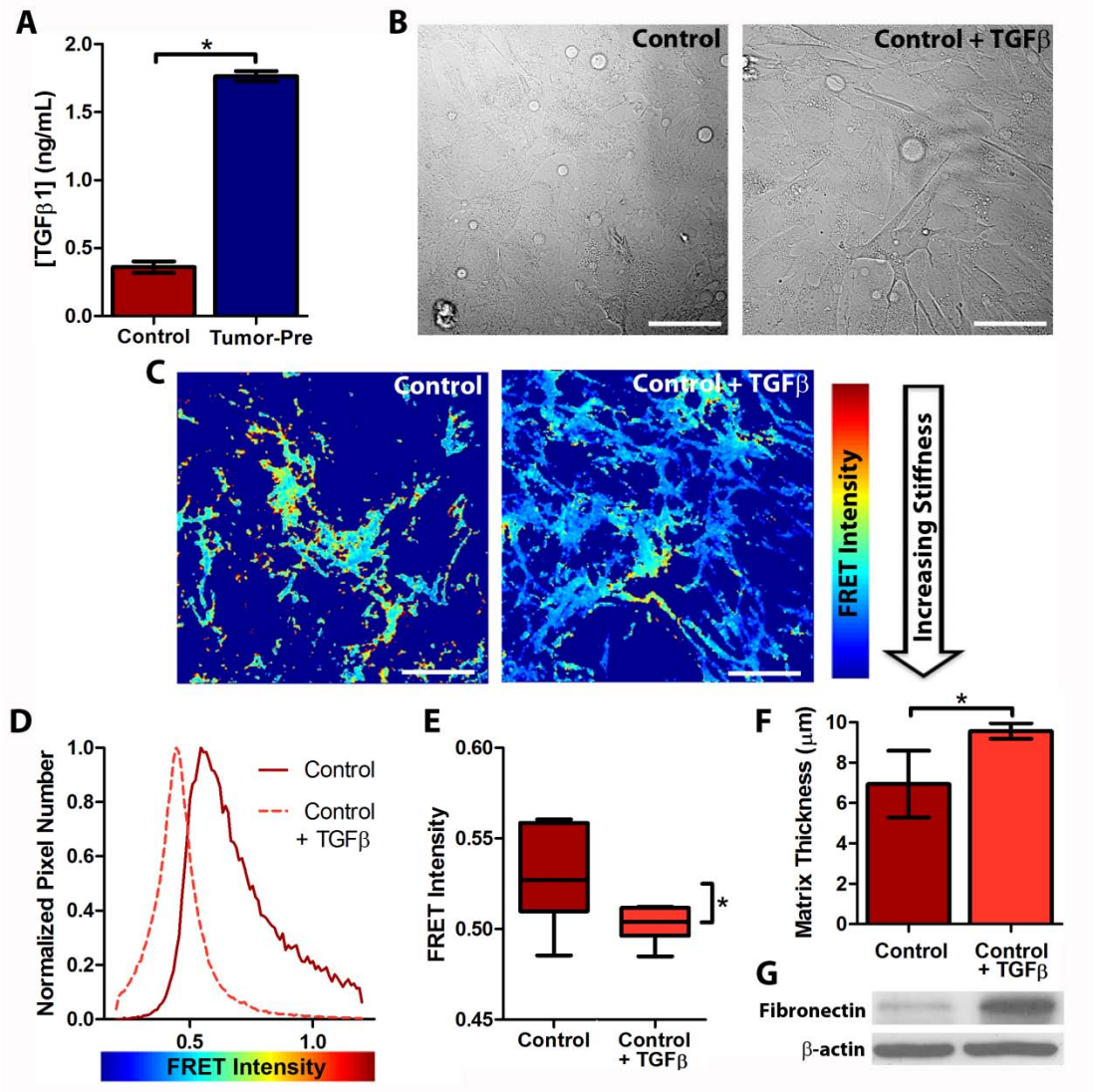

Figure 2.8 Fn matrix characteristics in response to TGFβ

Pre-conditioning of 3T3-L1s with TGFβ as a mimic of tumor cell secretion (Control+TGFβ) promotes Fn matrix unfolding, stiffness, and thickness relative to pre-conditioning with control media (Control). (A) ELISA indicates increased concentrations of TGFβ in tumor-conditioned media (TCM) relative to control media (Control) (n = 3). (B) Representative bright field images of 3T3-L1 cells preconditioned with or without TGFβ at concentrations similar to those in the tumor-conditioned media (scale bar = 50 μm). (C) Confocal z-stack slices of the same fields of view in which the FRET intensity for each pixel was color-coded and mapped to the images shown in B (scale bar = 50 μm). (D) Histograms of the FRET intensity derived from analysis of the complete z-stack of that of view as well as (E) a box and whiskers plot of the

FRET intensity determined by analysis of 6-8 representative fields of view per condition indicate the distribution of the FRET for each condition (n=6, *p < 0.05). (F) Fn matrix thickness as determined by confocal analysis of z-stack images for four independent experiments (n = 4, *p < 0.05). (G) Fn levels as measured by Western Blot analysis.

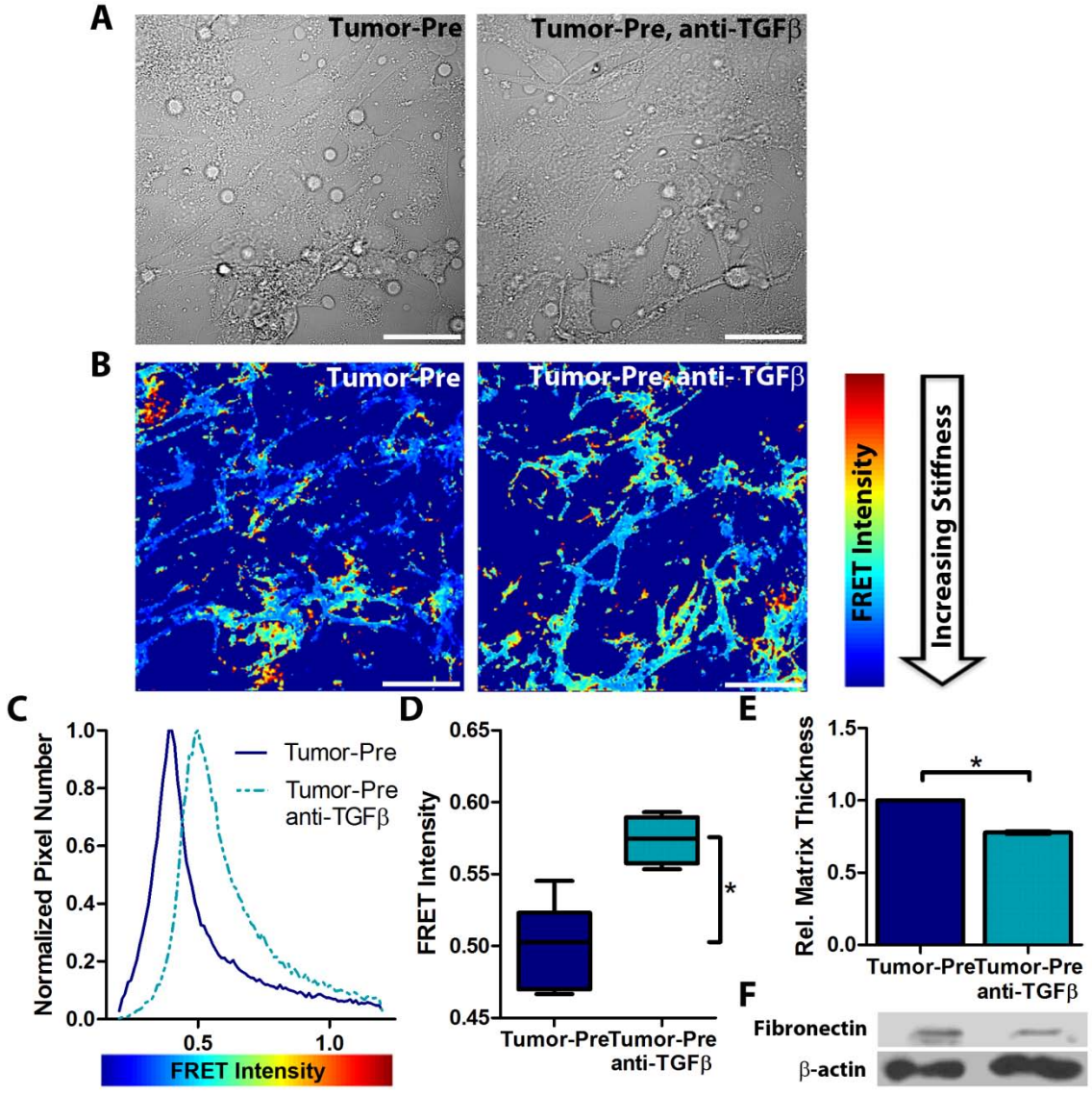

Figure 2.9 Fn matrix characteristics in response to tumor-conditioned media with inhibition of TGFβ

Inhibition of TGFβ by supplementing tumor-conditioned media with neutralizing antibodies (Tumor-Pre, anti-TGFβ) inhibits Fn matrix unfolding, stiffness, and thickness mediated by 3T3-L1s relative to tumor-

conditioned media (Tumor-Pre). (A) Representative bright field images of 3T3-L1 cells pre-conditioned in tumor-conditioned media with or without TGFβ neutralizing antibody (scale bar = 50 μm). (B) Confocal z-stack slices of the same fields of view in which the FRET intensity for each pixel was color-coded and mapped to the images shown in A (scale bar = 50 μm). (C) Histograms of the FRET intensity derived from analysis of the complete z-stack of that field of view (D) as well as a box and whiskers plot of the FRET intensity determined by analysis of 6-8 representative fields of view per condition (n=7 or 4, * $p < 0.05$) indicate the distribution of the FRET for each condition. (E) Fn levels in the different cultures as determined by confocal analysis of matrix thickness (n = 2, *$p < 0.05$) and (F) Western Blot analysis.

Note, absolute FRET intensities for these experiments (Figures 2.8 & 2.9) varied from those shown in Figure 2.6. This variation can be explained by the fact that the FRET efficiency of the Fn-DA aliquot, which was utilized for the entire study naturally (slowly) decreased with time. The loss of FRET efficiency is not linear with time because of intrinsic differences between donor and acceptor fluorophores, and because of the higher number of donors vs. acceptors on each Fn-DA molecule. Nevertheless, the FRET dependency on strain maintains the same trend (FRET decreases with applied strain, due to extension or unfolding in regions of Fn within approximately 10 nm of $FnIII_7$ and $FnIII_{15}$ where acceptors fluorophores are located) only with a different, usually smaller, slope. Averaging of the relative changes of FRET intensity across multiple experiments verified the relevance of our results and yielded statistically significant differences (Figure 2.7).

2.6 Discussion

It has been known for almost 30 years that solid tumors contain increased levels of Fn (90), yet the underlying mechanisms and resulting effects on cancer still remain unclear. Our studies now provide experimental evidence that paracrine signaling between breast cancer and adipose progenitor cells

regulates Fn deposition and remodeling. Furthermore, our findings support that the resulting modifications of the Fn matrix contribute to the enhanced rigidity of mammary tumors, which is associated with tumorigenesis and metastasis (51, 73, 115). More specifically, our results reveal that tumor-derived soluble factors promote Fn expression and unfolding by adipose progenitor cells and that TGFβ serves as a soluble cue underlying these changes. Lastly, our *in vivo* data provide pathological relevance by indicating a denser and more fibrillar Fn matrix in tumors that were formed in the presence of ASCs although we cannot directly confirm this is due to the presence of the ASCs.

Previous studies indicate that stromal cells up-regulate Fn in tumor microenvironments and that these changes promote tumor malignancy (77, 97). By performing a combination of biochemical and physical science measurements our data not only support this observation, but furthermore suggest that the conformation and stiffness of the tumor-associated Fn matrix is altered within our *in vitro* matrices. Using a previously established FRET technique (109) we reveal that tumor-conditioned stromal cells increase Fn unfolding, thereby exposing cryptic binding sites and enhancing the population of stiffer Fn fibers in the ECM (91). In our studies, the estimated stiffness of individual Fn fibers was significantly higher than the macroscopic stiffness of tumors *in vivo*. This difference can be attributed to the mesoscopic regime of deformations in individual fibers, whereas in tumors the deformation is distributed over a network of disordered and connected fibers that respond collectively to strain (initially by ordering/aligning along the strain axis). In addition to these direct effects, Fn unfolding may also indirectly influence matrix mechanics as it leads to the subsequent deposition of a more unfolded (hence stiffer) matrix (116). These changes are likely due to enhanced traction forces that cells exert on stiffer substrates and that increase unfolding of the newly assembled Fn (48, 117). Finally, it is conceivable that altered Fn characteristics modulate tumor rigidity by changing the specific properties of other ECM components. For example, Fn fibers act as templates and are necessary for the deposition of collagen (75). In addition, the specific binding of collagen type I's α1 chain to the gelatin-binding domain of Fn (located on modules FnI_6, $FnII_{1\text{-}2}$ and $FnI_{7\text{-}9}$) is necessary for the initial co-deposition of collagen (118). Because the interaction between Fn and collagen is likely conformation-dependent, the unfolded/highly-strained

Fn fibers generated by ASCs may dramatically affect collagen fibrillogenesis, either by disrupting the exposed binding site for collagen type I or by exposing cryptic sites with enzymatic activity such as FnCol-ase, which is a metalloprotease in the collagen binding domain of Fn, capable of digesting collagen (119). Consequently, Fn unfolding may regulate the biological and physical characteristics of tumor-associated collagen I that ultimately contribute to tumorigenesis (73, 120).

The recruitment of mesenchymal stem cells to the tumor stroma and their contribution to breast tumorigenesis has been actively investigated in the past. While most studies have focused on bone marrow-derived mesenchymal stem cells (56), relatively little is known about the role of adipose tissue-derived mesenchymal stem cells (i.e., ASCs) in the tumor microenvironment. Our data suggest that ASCs regulate the physicochemical properties of the mammary tumor microenvironment by altering the composition and stiffness of the tumor stroma. In addition to modulating tumor cell signaling, these changes may be of particular relevance to tumor angiogenesis, a hallmark of cancer (121). Specifically, ASCs are able to differentiate into endothelial cells (122) and to incorporate into tumor vessels (123). As both cell differentiation and blood vessel growth are directly regulated by mechanical signals (49, 50), it is possible that paracrine signaling between ASCs and mammary tumor cells provides a mechanism by which tumors recruit blood vessels for further growth and metastasis. We have performed our *in vitro* studies with 3T3-L1 preadipocytes as a representative of ASCs. It has to be noted that the differentiation potential of these cells is limited to the adipose lineage, while ASCs are multipotential (52). Nevertheless, our *in vivo* studies with ASCs support the relevance of our findings. Additionally, we have conducted studies comparing the proliferation and differentiation potential of 3T3-L1 and ASCs in tumor-conditioned media and observed similar responses (Figure 4.1). Collectively, our data implicate ASCs as an important stromal cell type that contributes to tumorigenesis.

TGFβ is a global modulator of tumorigenesis (e.g., by modulating metastasis and interactions with immune cells (33, 124)) that is secreted by mammary tumor cells (19). It also regulates ECM deposition (92). However, its specific role in regulating the stiffness of the mammary tumor stroma remains less well understood. Previous studies have attributed TGFβ a role in ECM stiffening, though

most of this work has been conducted in the context of myofibroblast-mediated stiffening of collagen (125). In the context of wound healing, TGFβ contributes to fibrosis and the related changes in fibroblast behavior depend on Fn matrix production (126). Our data now suggest that TGFβ acts as a paracrine signal that stimulates ASCs to produce a denser and stiffer Fn matrix in tumors. TGFβ-mediated matrix remodeling contributes to tumor metastasis (127), and metastasis, in turn, is enhanced on stiffer matrices (73). Therefore, it is possible that TGFβ enhances metastasis through altering Fn assembly by ASCs.

Collectively, our results contribute to an improved understanding of Fn matrix assembly in the breast tumor microenvironment and future experiments will help to further clarify the role of adipose progenitor cells in this process. For example, our studies have been performed on 2-D glass surfaces, and as both substrate rigidity and culture dimensionality can modulate changes in cell behavior a more relevant culture system should be implemented in the future. More specifically, the glass substrates utilized in our studies do not reflect the tumor-inherent matrix stiffness that may affect cell-mediated changes of Fn matrix conformation and mechanics. Future experiments using culture substrates of varying stiffness (e.g., polyacrylamide gels (116)) may illuminate the mechanical properties of the newly assembled Fn matrix as a function of the initial substrate stiffness. Furthermore, matrix assembly and remodeling depends upon the formation of focal adhesion complexes whose functional properties differ in 2-D and 3-D cell culture (128, 129). By expanding upon our work, FRET-studies in a physiologically relevant 3-D matrix (e.g., collagen gels) could lead to additional insights into Fn matrix assembly by tumor-associated adipose progenitor cells.

2.7 Conclusion

A combination of biochemical and physical science tools was utilized to evaluate the role of ASCs in Fn matrix assembly and stiffness enhancement. Our results suggest that paracrine signaling between tumor cells and ASCs contribute to matrix stiffening in tumors and that TGFβ is a critical regulator of this process. While this study was specifically designed to characterize the Fn matrix

deposited by tumor-conditioned ASCs, our experimental approach may be broadly applicable to studying other tumor-stroma interactions. For example, fibroblasts are fundamental to the organization of the tumor ECM (13) and the combination of conditioned media studies with FRET analysis may help to evaluate Fn matrix assembly by these cells in tumors. Additionally, analysis of stiffness-related mechanotransduction (e.g., via activation or inhibition of the Rho-ROCK pathway (130)) in conjunction with FRET analysis of the resulting Fn characteristics will allow us to better understand the interdependence of these two parameters. Insights gained by these studies improve our knowledge of how cell-microenvironment interactions promote mammary tumorigenesis and may ultimately help to improve the clinical prognosis of cancer patients.

2.8 Acknowledgements

The authors would like to thank Bo Ri Seo for help with *in vivo* experiments, Shengling Hu and Kunjal Patel for aid in Matlab FRET analysis, and Dr. David Infanger for aid in manuscript preparation.

CHAPTER 3

STIFFNESS OF PHOTOCROSSLINKED RGD-ALGINATE GELS REGULATES ADIPOSE PROGENITOR CELL BEHAVIOR

Published in *Biotechnology & Bioengineering* (131)

3.1 Contributors

Co-authors to this work made the following contributions: Caroline M. Berglund and William J. Polacheck, undergraduates in the Kirby lab at the time the work was completed, aided in the preparation and analysis of the photocrosslinked alginate gels. Jason S. Lee, an undergraduate and then M. Eng. Student in the Fischbach lab working under my supervision, aided in the culture, seeding, and analysis of cells within the photocrosslinked systems. Jason P. Gleghorn, a post-doctoral fellow in the Kirby lab, aided in the design of studies to analyzed the photocrosslinked alginate gels. The work was completed as a collaboration between the labs of Brian J. Kirby and Claudia Fischbach who both contributed greatly to the preparation of the manuscript presenting this work.

3.2 Abstract

Adipose progenitor cells (APCs) are widely investigated for soft tissue reconstruction following tumor resection; however, the long-term success of current approaches is still limited. In order to develop clinically relevant therapies, a better understanding of the role of cell-microenvironment interactions in adipose tissue regeneration is essential. In particular, the effect of extracellular matrix (ECM) mechanics on the regenerative capability of APCs remains to be clarified. We have used artificial ECMs based on photocrosslinkable RGD-alginate to investigate the adipogenic and pro-angiogenic potential of 3T3-L1 preadipocytes as a function of matrix stiffness. These hydrogels allowed us to decouple matrix stiffness from changes in adhesion peptide density or extracellular Ca^{2+} concentration and provided a physiologically relevant 3-D culture context. Our findings suggest that increased matrix rigidity promotes

APC self-renewal and angiogenic capacity, whereas it inhibits adipose differentiation. Collectively, this study advances our understanding of the role of ECM mechanics in adipose tissue formation and vascularization and will aid in the design of efficacious biomaterial scaffolds for adipose tissue engineering applications.

3.3 Introduction

Adipose progenitor cells (APCs) are widely used for breast reconstruction following tumor resection (132). In these applications, APCs are frequently transplanted on biomaterial scaffolds and then used to stimulate soft tissue formation by both readily differentiating into adipocytes and through paracrine signaling with surrounding host cells (103). For example, APCs secrete pro-angiogenic factors (e.g., vascular endothelial growth factor [VEGF]) that promote the recruitment of endothelial cells and angiogenesis (133, 134). New blood vessel formation, in turn, ensures the functionality of the newly developing adipose tissue by providing routes for endocrine and metabolic signaling (135, 136). While increasing experimental evidence indicates that cell-microenvironment interactions play a critical role in guiding adipogenesis (137, 138), the effect of dynamic changes of the extracellular matrix (ECM) mechanics on APC behavior remains largely unknown. This information is critical to the design of biomaterial scaffolds for adipose tissue engineering applications.

Changes in ECM rigidity broadly regulate cell behavior and may also impact the regenerative capabilities of APCs. ECM rigidity is largely controlled by the composition, crosslinking, and contraction of its protein components (35), and these parameters may vary locally at the site of APC implantation. Specifically, the mechanical properties of the ECM change during adipogenesis as the initially fibrillar ECM transforms into a laminar matrix structure (139). Additionally, APCs may be exposed to pathologically enhanced ECM stiffness when they are located next to scars resulting from surgery (140) or tumors that may recur after resection (47). While matrix stiffness regulates the proliferation (141, 142), differentiation (49), malignancy (51), and angiogenesis (50) of various cell types, its specific effect on

APC differentiation and pro-angiogenic activities is less well understood.

Matrices with adjustable mechanical but fixed chemical properties are necessary to study APC behavior in response to matrix stiffness. Frequently, Matrigel™ and collagen gels of variable concentrations are used to evaluate the relationship between ECM mechanics and cell behavior (143, 144). However, this approach entails changes in adhesion ligand density, which regulates cellular functions independent of matrix stiffness (145). Artificial ECMs may overcome these limitations by permitting decoupling of the physical and chemical matrix characteristics. Specifically, the rigidity of RGD-modified alginate hydrogels can be readily adjusted by ionic crosslinking with varying concentrations of Ca^{2+} (146). This approach, however, may not be suitable for studies of adipogenesis as it typically yields gels that are much stiffer than adipose tissue and because local concentrations of Ca^{2+} regulate APC functions (e.g., proliferation and differentiation (147, 148)). Photocrosslinked, alginate-based hydrogels (149-152) may provide suitable alternatives to examine the effect of matrix stiffness on adipogenesis.

The goal of this study was to establish a biomaterial-based 3-D culture system in order to evaluate the effect of matrix stiffness on the self-renewal, differentiation, and pro-angiogenic capacity of APCs under biologically relevant conditions. To this end, we have cultured 3T3-L1 preadipocytes, a well established cell model for the study of adipogenesis (153), within photocrosslinked, RGD-modified alginate hydrogels that recreate tissue dimensionality and ECM mechanics representative of normal and pathological adipose tissue. Our results identify mechanical stiffness as an important regulator of APC function that must be considered in the design of efficacious and safe biomaterials for adipose tissue engineering.

3.4 Materials and Methods

Cell culture

3T3-L1 cells (ATCC) were routinely cultured in MEM (α-modification, Sigma) containing 10%

fetal bovine serum (FBS, Tissue Culture Biologicals) and 1% antibiotic (penicillin/streptomycin, Gibco). To induce adipogenesis, cells were maintained for 2 days in MEM (α-modification), 5% FBS, 1% antibiotic containing 1 μM insulin (Sigma), 100 nM corticosterone, 200 μM isobutylmethylxanthine, and 60 μM indomethacin (all from EMD) as previously described (137). Subsequently, differentiation media (MEM [α-modification], 5% FBS, 1% antibiotic, 1μM insulin) was added, and cells were cultured under these conditions for 6 days, with media changes every other day.

Cell viability in response to photocrosslinking conditions

Cell viability in response to photocrosslinking conditions was tested in 2-D culture by exposing 3T3-L1 cells to increasing concentrations of VA-086 (Wako), Irgacure-2959 (Ciba), and varying durations of ultraviolet (UV) light (365 nm longwave, 2 $\mu W/cm^2$) in the absence of polymer. Specifically, cells were seeded into 12-well plates at equal densities and allowed to adhere overnight. Cultures were then treated with photoinitiators and/or UV light (using a Spectroline UV crosslinker) to simulate the conditions during hydrogel crosslinking. For these experiments, VA-086 and Irgacure-2959 were dissolved in water and 70% ethanol, respectively. Due to the different photoinitiator activities, 10-fold greater concentrations of VA-086 (0.1 - 0.4 %, w/v) were used as compared to Irgacure-2959 (0.01 - 0.04 %, w/v). Subsequently, dead cells were removed by rinsing the culture dishes with PBS, while adherent viable cells were trypsinized and quantified using a Beckman Coulter counter.

Fabrication and characterization of photocrosslinked alginate hydrogels

Photocrosslinkable alginate was synthesized by reacting Protanal® LF10/60 (FMC Biopolymer) with methacrylic anhydride (Alfa Aesar), replacing secondary alcohols on the polymer with methacrylate groups (Figure 3.1) (152, 154, 155). To this end, methacrylic anhydride (Alfa Aesar) was added to a 2.5% w/v solution of alginate in deionized water while the pH was maintained with 5M NaOH. After 72 hours of reaction time, the alginate was washed with ethanol and filtered twice prior to lyophilization. In a

second reaction, the obtained material was modified with GGGGRGDSP (Peptides International) adhesion peptides using standard carbodiimide chemistry as previously described (156). To remove unreacted, low-molecular weight components, the alginate was purified by dialysis, and then the methacrylated RGD-alginate was sterile filtered and lyophilized. To prepare hydrogel disks for further analysis, a 3% (w/v) solution of methacrylated RGD-alginate in PBS was cast between two glass plates (separated by 1 mm spacers) and crosslinked in an UV crosslinker (Spectroline) for 5 minutes. The same modified polymer was used for all hydrogel systems; stiffness was altered by adjusting VA-086 concentrations to 0.1 (compliant gels), 0.2 (moderate gels), and 0.4 (stiff gels) % (w/v). Disks were punched out of the crosslinked slab of hydrogel using sterile biopsy punches (d=6 mm).

Aggregate moduli of photocrosslinked alginate were measured under radial confinement and uniaxial compression using a mechanical tester (ELF 3100, Bose). Alginate hydrogels were incrementally loaded at steps of 5% compression with the reported aggregate modulus measured from the slope fit to the stress–strain curve at 15% strain. To ensure that gel modulus was maintained through experiments, the aggregate moduli of different batches were measured. Additionally, for experiments where direct comparisons were made between conditions, the same batch of material was used. To ensure maintenance of gel mechanical character for the duration of the culture experiments, the aggregate modulus of compliant alginate gels was measured in the same manner as described above over a period of 2 weeks. Gel swelling was assessed by measuring the wet and dry weights of alginate gels, pre- and post-lyophilization, respectively, over a 6 week period. To encapsulate 3T3-L1 into 3-D hydrogels, cells were suspended in the alginate solution prior to gelation at a concentration of 1.5×10^6 cells/mL. The resulting matrices were subsequently cultured under dynamic conditions on a Bellco orbital shaker. The day of cell encapsulation was considered day 0.

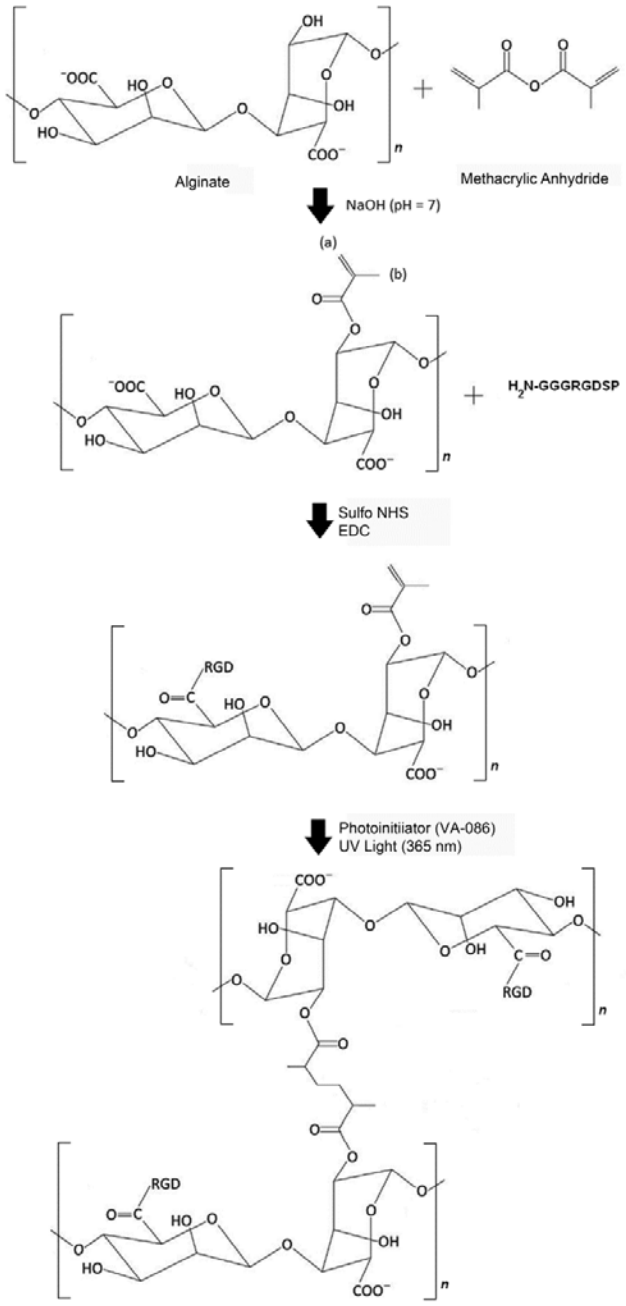

Figure 3.1 Development of photocrosslinked RGD-alginate hydrogels

Methacrylated alginate was synthesized by reaction of LF10/60 alginate with methacrylic anhydride and was subsequently modified with RGD-adhesion peptides using carbodiimide chemistry. Exposure of the resulting material to UV light in the presence of a photoinitiator yielded photocrosslinked RGD-alginate hydrogels.

Analysis of cell adhesion and proliferation

Cell adhesion was measured under 2-D conditions. 3T3-L1 preadipocytes were seeded onto non-modified and RGD-modified alginate disks of equal aggregate modulus (~12 kPa). After 16 hours of culture, cells were fixed and stained with Alexa Fluor 568 phalloidin (Invitrogen, 1:100) and DAPI (Invitrogen, 1:5000). The cells were visualized using a fluorescent microscope (Zeiss Observer Z.1), and three representative images per gel were taken with an AxioCam MRN camera. Cell spreading was quantified via image analysis (ImageJ, NIH) by measuring the average surface area per cell for three gels per condition.

Cell proliferation was tested under 3-D conditions. Cells were released from their matrices by dissolution of the gels in a solution of alginate lyase (3.3 units/g alginate, Sigma) in PBS on days 0, 3, and 7. Cell numbers in the resulting cell suspension were determined with a Beckman coulter counter. Additionally, cell-encapsulating alginate disks were subjected to live/dead staining using calcein (Invitrogen, 1ug/mL for 15 mins) and propidium iodide (Sigma, 10ug/mL for 5 mins), respectively. Eight representative images of three gels per condition were taken at randomly selected locations on each gel for viability quantification via image analysis.

Analysis of adipose differentation

Cells were harvested from their 3-D matrices by alginate lyase treatment as described above 8 days after induction of differentiation. The resulting cell pellet was lysed on ice in a buffer containing 50mM Tris, 1mM EDTA, and 1mM β mercaptoethanol (all from J.T. Baker). Subsequently, glycerol-3-phosphate dehydrogenase (GPDH) activity was measured using a spectrophotometer as previously reported (137). Briefly, supernatants obtained from the lysates were mixed with dihydroxyacetone phosphate and the oxidized form of nicotinamide adenine dinucleotide (NADH). GPDH activity was assessed by quantifying the decrease in NADH absorbance at 340 nm over a 7-minute period. Enzyme activity was normalized to total protein content as measured by the Bio-Rad Protein assay per

manufacturer's protocol. To visualize lipid accumulation, cell-incorporating gels were fixed overnight in formalin, stained with Oil Red O (Sigma, 0.3% w/v solution in 60% isopropyl alcohol) for 2 hours, and then interrogated with bright field microscopy.

Analysis of VEGF secretion

On day 3, cell-incorporating hydrogel disks were transferred to new culture dishes containing MEM (α-modification) with 1% FBS and 1% antibiotic. Media were collected after 24 hours and analyzed for VEGF (Quantikine ELISA, R&D). To additionally determine the amount of matrix-sequestered VEGF, alginate constructs were dissolved with alginate lyase as described above and the VEGF content of the resulting solution was measured. Prior studies verified that alginate lyase treatment does not compromise VEGF analysis as incubation of recombinant VEGF with alginate lyase and subsequent ELISA yielded similar VEGF concentrations as samples not exposed to alginate lyase (Figure 3.2). Indicated values represent the total amount of VEGF quantified in the conditioned media as well as the gel lysate. VEGF data were normalized to cell number as determined at the time of media harvest to account for cell proliferation differences between conditions.

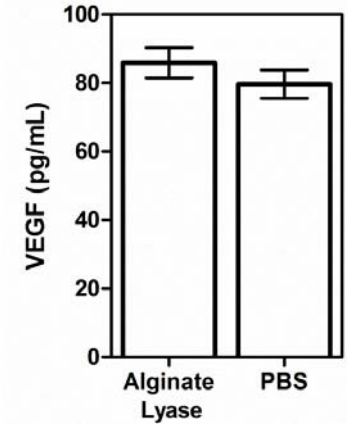

Figure 3.2 Alginate lyase treatment does not alter VEGF ELISA readings

Control experiment of recombinant VEGF levels measured in samples diluted with alginate lyase and PBS show that treatment with alginate lyase does not compromise ELISA readings as similar values are found in both solutions.

Analysis of endothelial cell behavior

Human umbilical vein endothelial cells (HUVECs, Lonza) were routinely cultured in endothelial growth medium (EGM-2, Lonza). 3T3-L1-conditioned media was collected as described above for VEGF analysis, concentrated two-fold using Amicon centrifugal filter units (Millipore, MWCO = 3kDa), and subsequently reconstituted with EGM-2 from which growth factors were omitted. HUVEC proliferation was assessed by cell counting after 5 days of culture in reconstituted conditioned media. To assess cord formation, HUVECs were seeded onto Matrigel™ (BD) in conditioned media. After 24 hours, the cells were stained with calcein (Invitrogen, 1 μg/mL) and imaged on a Zeiss Observer Z.1 microscope using an AxioCam MRN camera. Three randomly selected areas were imaged and analyzed per well with three wells per condition. The connectivity and length of the tubular structures were assessed using a MATLAB®-based program (AngioQuant) (157).

Statistical analysis

All data are reported as means ± standard deviations and were analyzed by one-way analysis of variance (ANOVA) followed by the Newman-Keuls method to make *post hoc* pair wise comparisons using Prism 5 (GraphPad Software) with $\alpha = 0.05$ (*, $p<0.05$; **, $p<0.01$ between noted conditions).

3.5 Results

Establishment of photocrosslinking conditions

To enable cytocompatible photocrosslinking, we initially tested the effect of two widely used photoinitiators, Irgacure-2959 and VA-086 (151, 155), on 3T3-L1 viability. For these experiments, relevant concentrations of these two substances were added to the media of standard 2-D cell cultures (i.e., in the absence of the polymer). Our results indicated that VA-086 in 10-fold higher mass concentration is less toxic to 3T3-L1 cells than Irgacure-2959 (Figure 3.3 A,B), both with and without

UV exposure. Specifically, 0.04 % Irgacure-2959 in conjunction with 15 min UV (i.e., conditions necessary to produce the stiff gels [see below]) dramatically decreased cell viability to 2% (Figure 3.3A). In contrast, exposure to 0.4 % VA-086 and 5 min UV (i.e., conditions needed to produce similarly stiff gels [see below]) resulted in 82% viability. To assess whether these differences were due to the varying UV exposure times we additionally irradiated cultures with VA-086 for 15 min. In these experiments, cell viability was slightly reduced as compared to treatment for 5 min, but still remained at 77% for the highest VA-086 concentration (Figure 3.3B). The reduced viability in the 0% Irgacure-2959 condition relative to the 0% VA-086 condition after 15 min of UV may be caused by the different solvents (ethanol for Irgacure-2959, water for VA-086). Nevertheless, the different solvents do not account for the observed changes in cell viability in the presence of photoinitiators because VA-086 is also less cytotoxic than Irgacure-2959 when dissolved in ethanol (149). Collectively, treatment with VA-086 (0.4%; 5 min UV) yields 41-fold enhanced 3T3-L1 cell numbers as compared to Irgacure-2959 (0.04%; 15 min UV) and was, therefore, used for all experiments involving photocrosslinking of cell-incorporating alginate matrices.

Development of artificial ECMs with relevant matrix stiffnesses

Next, we tested our ability to generate 3-D hydrogel matrices of biologically relevant stiffness by photocrosslinking methacrylated alginate with VA-086. The crosslinking density of the gels was adjusted by altering the concentration of the photoinitiator VA-086. Mechanical testing confirmed that the elastic moduli of the resulting matrices were 3.3 kPa, 7.9 kPa, and 12.4 kPa and, therefore, representative of physiological (~2kPa), intermediate, and pathological (~12kPa) stiffness ranges detected, for example, during tumorigenesis (47) (Figure 3.4A). These moduli were maintained throughout the time of 3-D culture, as no significant changes were detected over 2 weeks (Figure 3.4B). Additionally, measurement of gel wet and dry weight indicated no significant swelling during the duration of the experiment that would otherwise alter the mechanical characteristics of the gels (Figure 3.4C).

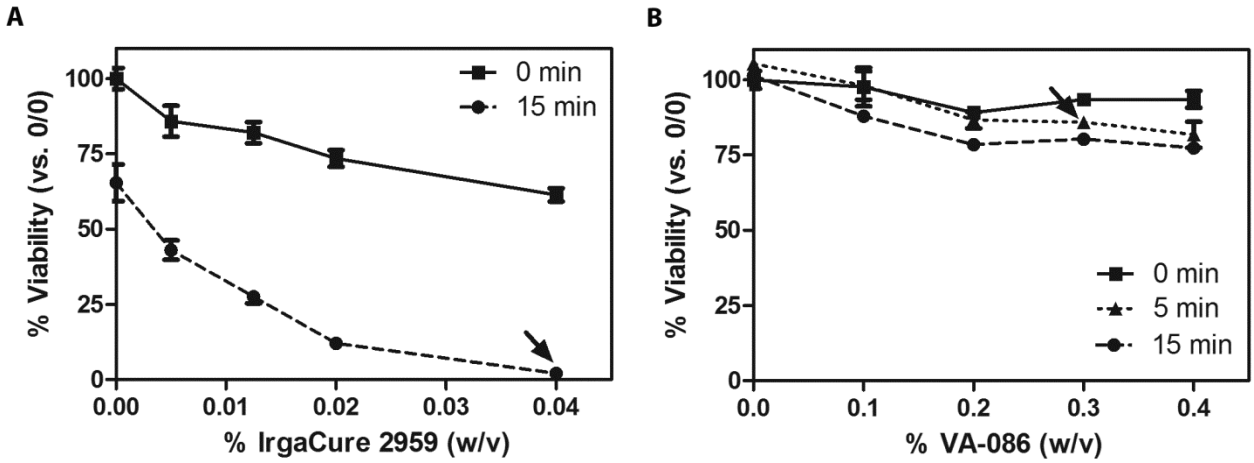

Figure 3.3 Cell viability in response to photocrosslinking conditions.

Control experiments in 2-D cell culture indicate that 3T3-L1 viability is lower following photocrosslinking with Irgacure-2959 (A) compared with VA-086 (B). The percentage of viable cells is expressed relative to control conditions in which cells were neither treated with photoinitiator nor exposed to UV light (0/0); however, an equal volume of the solvent (water or 70% ethanol for VA-086 or Irgacure-2959, respectively) was added to the control condition. Arrows indicate photocrosslinking conditions that would be necessary to produce gels with a modulus of 12 kPa (stiff condition).

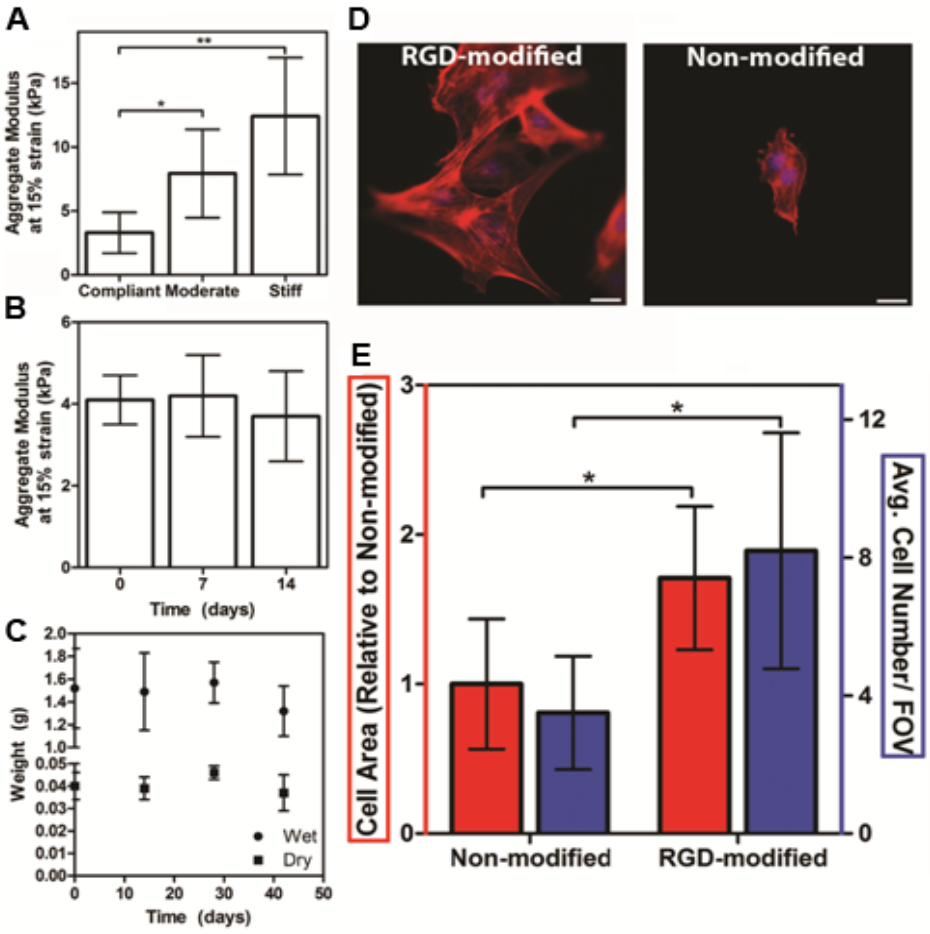

Figure 3.4 Characterization of the developed materials

Mechanical testing verified that gels that mimicked moduli of normal (compliant), intermediate (moderate), and pathological (stiff) adipose tissue could be engineered by controlling photoinitiator concentration (A, n = 5 or 6) and that the modulus did not change significantly during the culture time period (B, n = 4). No significant swelling in the gels was seen after initial equilibration as the wet and dry weights of the alginate gels were maintained for periods longer than the duration of the experiments (C, n=3). Covalent modification of methacrylated alginate with RGD adhesion peptides promoted 3T3-L1 adhesion and spreading on 2-D hydrogel disks. Fluorescent staining was performed with DAPI and phalloidin to visualize actin (red) and nuclei (blue), respectively. (D, scale bars = 20 μm). Average cell area and number of adhered cells per field of view (FOV) were quantified by analyzing the images (E, n = 3). (*, $p < 0.05$; **, $p < 0.01$)

Subsequently, we modified the photocrosslinkable alginate by covalent coupling of adhesive RGD peptides according to a previously established protocol (Figure 3.1) (156). This reaction resulted in the introduction of two cellular binding sites per alginate chain (158) and enabled integrin engagement necessary for cells to sense changes in matrix stiffness (159). Successful RGD modification was confirmed with a simple 2-D adhesion assay in which cells were seeded on top of hydrogel disks with aggregate modulus of 12 kPa. 3T3-L1 cells readily adhered and spread on RGD-modified alginate, whereas cell adhesion was dramatically reduced on non-modified alginate (Figure 3.4D). Specifically, both cell numbers and cell surface areas were significantly increased on RGD-modified disks relative to non-modified cultures (Figure 3.4E).

3T3-L1 proliferation and viability within hydrogels with different modulus

We determined 3T3-L1 number and viability within the 3-D hydrogel matrices to assess the effect of mechanical stiffness on adipose progenitor cell self-renewal. The number of 3T3-L1 cells within 7.9 kPa (moderate) and 12.4 kPa (stiff) hydrogels increased over time, while no significant change was detected in 3.3 kPa (compliant) matrices (Figure 3.5A). At day 0, cellularity was similar for all conditions, suggesting that the detected differences were due to changes in cell proliferation rather than encapsulation efficiency. Live/dead staining after 7 days in culture, furthermore, indicated that culture within compliant gels promoted cell death as compared to culture within moderate and stiff gels. The resulting changes in cell viability likely contributed to the detected variations in cell number by mediating a decrease in the population of proliferative cells (Figure 3.5 B,C).

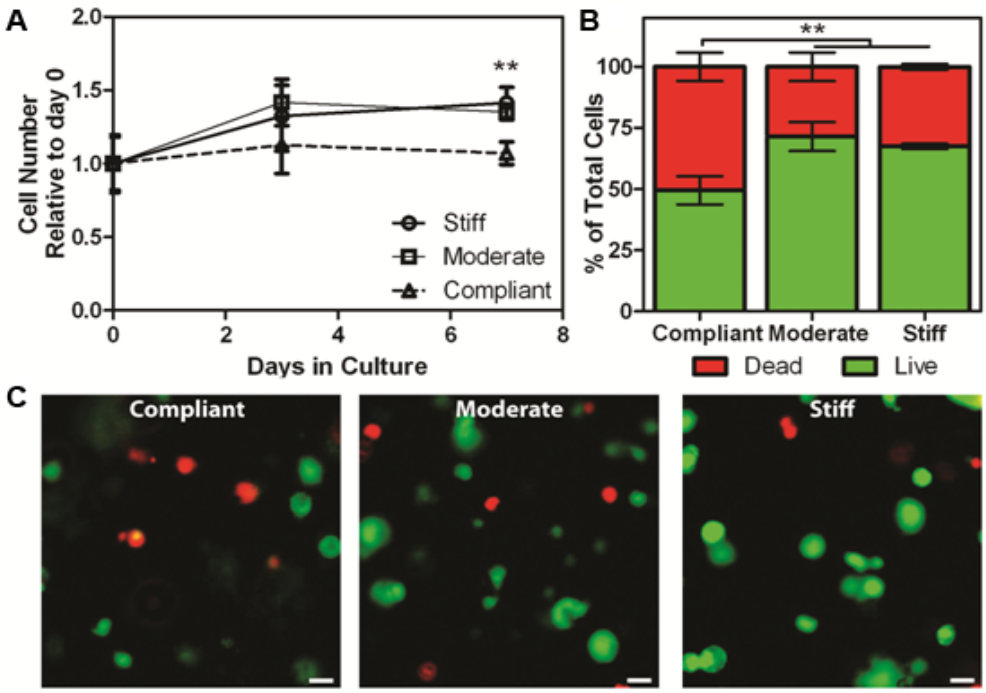

Figure 3.5 Proliferation and viability within 3-D hydrogel cultures

Significantly more 3T3-L1 cells were observed following culture within the stiff and moderately stiff gels compared with the compliant gels (A, n = 4). At day 7, cell viability in the stiff and moderate gels was higher relative to the compliant gels as assessed by image analysis (B, n = 4) of live and dead cells following staining with calcein (green) and propidium iodide (red), respectively. (C, scale bars = 20 μm). (**, $p < 0.01$)

3T3-L1 differentiation within hydrogels of varying stiffness

To evaluate the effect of matrix stiffness on adipogenesis, typical markers of lipid biosynthesis were analyzed 8 days following induction of differentiation. GPDH activity, a key enzyme involved in lipid accumulation, decreased with increasing ECM stiffness (Figure 3.6). Specifically, 3T3-L1 cells that differentiated within stiff gels exhibited 1.4-fold and 2.4-fold reduced GPDH activity relative to the same cells maintained within moderate and compliant gels, respectively (Figure 3.6A). Visualization of lipid biosynthesis via Oil Red O staining further confirmed that cells in compliant matrices produced enlarged fat droplets as compared to cells cultured within the stiffer matrices (Figure 3.6B). Because 3T3-L1

differentiation was induced immediately after seeding, no proliferation phase occurred and these results cannot be attributed to changes in cell numbers due to altered proliferation. Consequently, our data suggest that adipose differentiation of 3T3-L1 cells is inhibited in stiff matrices and that a combination of chemical and mechanical cues contributed to this as no adipogenesis was observed in the absence of hormonal induction.

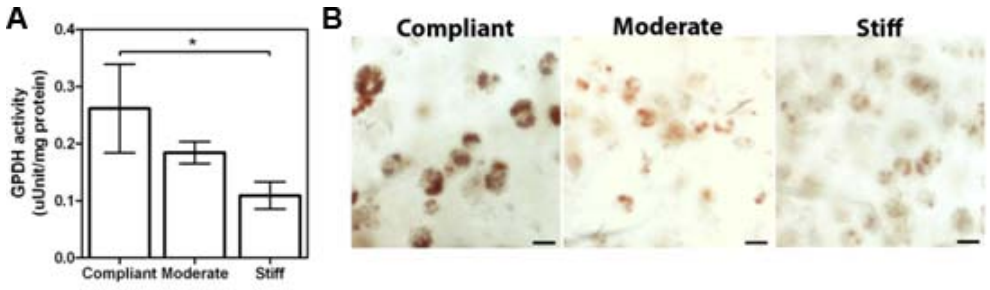

Figure 3.6 Adipose differentiation within 3-D hydrogel cultures

As determined by analysis of GPDH activity, adipogenesis of 3T3-L1 cells was higher within compliant gels relative to stiffer gels (A, n = 4) and microscopic evaluation of lipid droplet size following Oil Red O staining one week after inducing differentiation. (B, scale bars = 20 μm). (*, $p < 0.05$)

Pro-angiogenic capacity of 3T3-L1 in response to varying stiffness

We analyzed VEGF secretion of 3T3-L1 preadipocytes in the different hydrogels to assess the effect of 3-D matrix stiffness on the pro-angiogenic potential of these cells. 3T3-L1s cultured within stiff gels secreted significantly more VEGF as compared to the same cells contained within compliant gels (Figure 3.7A). No significant difference in VEGF secretion was detected between the compliant and moderate culture systems. The observed effects can be attributed to changes in secretion rather than variable sequestration within the different matrices, because similar amounts of VEGF were retained in compliant (45 ± 13 % of total VEGF) and stiff gels (47 ± 5 % of total VEGF). In these experiments, VEGF secretion was normalized to cell number at the time of harvest, thus the differences indicate altered secretion and

not differences in cell number. To evaluate the physiologic relevance of these changes, we analyzed HUVEC behavior in response to media collected from the different substrates. Media conditioned by 3T3-L1 cells in stiff matrices promoted HUVEC proliferation (Figure 3.7B) and tube formation on Matrigel™ (Figure 3.7 C,D) as compared to media collected from cells within compliant substrates. Additionally, conditioned media from stiff cultures promoted transwell migration of endothelial cells (305 ± 24 HUVECs/FOV) relative to media from compliant cultures (286 ± 34 HUVECs/FOV).

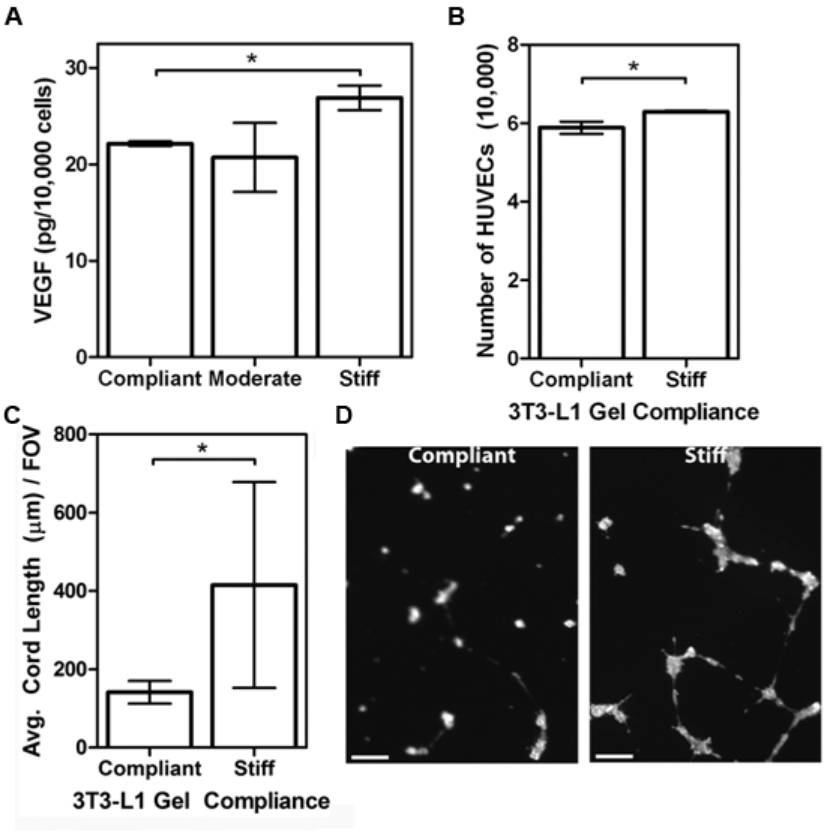

Figure 3.7 Pro-angiogenic potential of 3T3-L1 in 3-D hydrogel cultures

3T3-L1 cells cultured within stiff hydrogel matrices secreted larger concentrations of VEGF normalized to cell number compared with those maintained within more compliant gels (A, n = 4). Conditioned media collected from cells maintained in stiffer matrices enhanced HUVEC proliferation (B, n = 4) and capillary tube formation on Matrigel (C[n = 3], D[scale bar = 50 μm]) relative to media obtained from compliant cultures. (*, $p < 0.05$)

3.6 Discussion

We have characterized a biologically relevant 3-D culture system for 3T3-L1 cells and used it to evaluate the effect of matrix stiffness on the self-renewal, differentiation, and pro-angiogenic capacity of APCs. This model system is based on photocrosslinked RGD-modified alginate and through its use, we decoupled matrix stiffness from changes in adhesion peptide density or extracellular Ca^{2+} concentration, which may independently affect adipose progenitor cell behavior (145, 147, 148). Our data indicate that enhanced matrix rigidity significantly decreases adipose differentiation of APCs, whereas it increases the number and angiogenic capacity of these cells. Collectively, our results define matrix stiffness as an important design parameter for the development of biomaterial scaffolds for adipose tissue engineering.

We used the developed RGD-alginate gels to study APC behavior in response to varying stiffnesses under 3-D culture conditions. Previous studies have indicated that matrix elasticity regulates the proliferation and differentiation capacity of stem cells on 2-D substrates (49, 141, 142), and that compliant matrices may be a prerequisite for adipose differentiation in 2-D culture (160). However, integrin mechanoreceptors may signal differently in 2-D and 3-D culture (128), and we, therefore, aimed at investigating APC behavior under 3-D conditions. Our results suggest that, according to previous 2-D studies, adipose differentiation is greatest in matrices with a modulus that is similar to adipose tissue, whereas less compliant substrates inhibit this process and increase the proliferative and angiogenic potential of APCs. These differences may be related to adhesion-dependent changes in cell contractility. In particular, cells encapsulated in stiff matrices exhibit increased integrin engagement, cell proliferation, and angiogenic factor expression as compared to those in compliant matrices (35, 161), and changes in cytoskeletal tension and intracellular signaling may contribute to this (162, 163). In contrast, adipose differentiation is favored in softer environments with which cells interact less strongly and consequentially undergo morphological changes that favor adipogenesis (163). Future studies using pharmocological inhibition of the associated signaling pathways will help to probe these connections.

Vascularization of adipose tissue is mediated by a concerted and complex interplay between multiple pro- and anti-angiogenic factors. For example, VEGF dynamically interacts with basic fibroblast

growth factor (bFGF) and interleukin-8 (IL-8) (164) to activate endothelial cell proliferation and migration that leads to the formation of new blood vessels, while anti-angiogenic factors such as thrombospondin inhibit these processes (165). To the best of our knowledge, our studies for the first time suggest that mechanical stiffness results in the up-regulation of VEGF in APCs. Nevertheless, the detected differences in VEGF secretion may only partially account for the significant increase in tube formation observed on Matrigel™. It is likely that a stiffness-mediated increase of other pro-angiogenic molecules, or downregulation of anti-angiogenic factors, contributes to the detected angiogenic effects in our experiments; this deserves future study.

The reported results have important implications for the design of biomaterial scaffolds for adipose tissue engineering. Successful adipose tissue engineering approaches rely on both adipose differentiation and the rapid recruitment of a vascular network to meet the metabolic requirements of the newly formed fat pad (132). It may be possible to satisfy these biological design parameters by the development of hydrogel composites that consist of spatially defined compliant and stiff compartments that drive adipose tissue regeneration by promoting adipogenesis and pro-angiogenic factor secretion, respectively. Such polymeric systems would be particularly useful when combined with endothelial cells (166). Specifically, our results indicate that co-implanted endothelial cells may be able to accelerate vascularization by increased proliferation and tube formation in response to the elevated concentration of pro-angiogenic factors (e.g., VEGF) from APCs. In contrast, implantation of APCs within matrices exhibiting stiffnesses >10kPa may not result in efficacious and safe therapies, as the encapsulated cells may undergo very limited differentiation into adipocytes, while potentially promoting pathological angiogenesis. In particular, enhanced concentrations of pro-angiogenic factors can activate the angiogenic switch in dormant tumors (167), which is critical to tumor induction, progression, and metastasis. This process may be further enhanced because increased matrix rigidity promotes blood vessel formation by directly altering endothelial cell behavior (50). This possible perturbation of blood vessel homeostasis represents a particularly important problem, as adipose tissue engineering is predominantly pursued for reconstruction therapies for breast cancer patients who carry the risk of tumor recurrence (132).

While the focus of this study was to investigate the role of mechanical stiffness on APC proliferation, adipose differentiation, and pro-angiogenic capability in a 3-D culture context, a number of related questions could also be studied with the developed hydrogels. For example, does mechanical stiffness also influence the behavior of fully differentiated adipocytes? What happens if APCs are not exposed to differential mechanical environments until after they are hormonally induced to undergo differentiation? Would they still respond differently to soft and stiff matrices? Finally, APCs are multipotential and have been shown to differentiate into other lineages including chondrocytes, osteoblasts, and endothelial cells (52). To what extent are mechanical cues involved in guiding these cells along a specific lineage? The materials described in this study provide an important platform that can be used to address all of these questions. As the developed photocrosslinkable materials can be processed into 2-D and 3-D substrates, they may also be useful to assess differences as a function of tissue dimensionality.

3.7 Conclusions

We explored RGD-functionalized, photocrosslinkable alginate gels to evaluate the effect of ECM mechanics on APC behavior under physiologically relevant 3-D culture conditions. Using these model systems, we revealed that increased ECM stiffness inhibits adipose differentiation, while increasing the proliferative and angiogenic potential of these cells. Based on these observations, it may be possible to enhance adipose regeneration by implanting APCs in composite hydrogels that consist of both compliant and stiff compartments. Our results suggest that this approach might simultaneously promote adipogenesis and angiogenesis, two processes critical to the long-term success of engineered adipose tissue. In total, our results provide an improved understanding of the role of ECM stiffness in adipose tissue regeneration, and inform adipose tissue engineering approaches.

3.8 Acknowledgements

The authors would like to thank Dr. Lawrence Bonassar for use of equipment and for helpful discussions and Weilin Yang for help with swelling data collection.

CHAPTER 4

IMPLANTED ADIPOSE PROGENITOR CELLS AS PHYSICOCHEMICAL REGULATORS OF BREAST CANCER

Accepted for publication in *Proceedings of the National Academy of Sciences (168)*

4.1 Contributors

Co-authors to this work made the following contributions: Bo Ri Seo, a Ph.D. candidate in the Fischbach lab, is an equally contributing co-first author to this work. She primarily did the *in vivo* work in addition to some of the analysis of myofibroblastic differentiation. Joseph P. Califano, a Ph.D. student in the Reinhart-King lab, collected and analyzed the traction force microscopy (TFM) data. Roberto Andresen Eguiluz, a Ph.D. student in the Gourdon lab, aided in the collection and analysis of the dynamic mechanical thermal analyzer (DMTA) data. Jason S. Lee, an undergraduate and later M. Eng. student in the Fischbach lab collected the data on the secretion of progenitor cells on variably stiff polymer gels. Christine J. Yoon imaged the cells stained for phosphorylated focal adhesion kinase. James X. Wang, an undergraduate student in the Fischbach lab, cultured adipose-derived stem cells in collage gels which were analyzed for matrix stiffening by David T. Tims, an M. Eng. student in the Fischbach lab. Le Cheng, a post-doctoral researcher in the Nikitin lab, aided in the orthotopic implantation of tumor cells into mice. Sunish Mohanan, a board certified pathologist, identified markers of malignancy within the H&E stained tumor sections. Mark R. Buckley, a Ph.D. student in the Cohen lab, and Itai Cohen developed a previously published method to measure gel stiffness utilized to measure the stiffness of collagen gels in this work. Alexander Yu Nikitin aided in the design of the *in vivo* experiments. Rebecca M. Williams aided in the imaging and analysis of the collagen fibers within the tumors. Delphine Gourdon aided in the measurement of tumor stiffness using DMTA as well as in the preparation of the manuscript. Cynthia A. Reinhart-King provided her expertise in the implementation of TFM to measure forces generated by

progenitor cells on variably stiff gels and aided in the preparation of the manuscript. The thrust of this work was completed in the lab of Claudia Fischbach who contributed greatly to the design of experiments and the preparation of the manuscript presenting this work.

4.2 Abstract

Multipotent adipose-derived stem cells (ASCs) are increasingly used for regenerative purposes, such as soft tissue reconstruction following mastectomy. However, the ability of tumors to commandeer ASC functions to advance tumor progression is not well understood. Through the integration of physical sciences and oncology approaches we investigated the capability of tumor-derived chemical and mechanical cues to enhance ASC-mediated contributions to tumor stroma formation. Our results indicate that soluble factors from breast cancer cells inhibit adipogenic differentiation while increasing proliferation, pro-angiogenic factor secretion, and myofibroblastic differentiation of ASCs. This altered ASC phenotype led to varied extracellular matrix (ECM) deposition and contraction, thereby enhancing tissue stiffness, a characteristic feature of breast tumors. Increased stiffness, in turn, facilitated changes in ASC behavior similar to those observed with tumor-derived chemical cues. Orthotopic mouse studies further confirmed the pathological relevance of ASCs in tumor progression and stiffness *in vivo*. In summary, altered ASC behavior can promote tumorigenesis, and thus their implementation for regenerative therapy should be carefully considered in patients previously treated for cancer.

4.3 Introduction

Adipose-derived stem or progenitor cells (ASCs) are widely used in tissue engineering due to their multipotency, ability to enhance vascularization, and relative ease of isolation from the stromal vascular fraction of adipose tissue (52, 169). In particular, ASCs are increasingly considered for reconstructive procedures following surgery for breast cancer, which compose the majority of the 93,000

breast reconstructions performed in the U.S. per year (170). ASCs offer several advantages over commonly utilized silicone and saline implants including their ability to regenerate functional adipose tissue, which reconstitutes a large fraction of the breast (60, 171). However, malignantly transformed cells may be present in breast cancer survivors without manifest disease, and it remains unclear whether implanted ASCs may increase the risk of tumor development and relapse (172) by establishing a microenvironment conducive to nascent or recurrent tumorigenesis.

Mammary tumors are stiffer than normal mammary gland tissue (47, 173), due in part to tumor cell-secreted morphogens that vary extracellular matrix (ECM) assembly. Altered ECM deposition and contraction not only enhances tumor rigidity (41), but further modulates tumor progression by perturbing epithelial morphogenesis (51) and vascular development (50). Myofibroblasts regulate these outcomes by controlling the mechanical properties of the tumor-associated ECM and by functioning as a major source of host-derived pro-angiogenic factors (e.g., vascular endothelial growth factor [VEGF]) (41, 174). Generally, local fibroblasts are considered the primary origin of myofibroblasts and regulator of this desmoplastic reaction, but bone marrow- and tissue-derived mesenchymal stem cells may also contribute to this cell population. Specifically, ~20% of tumor-associated α-smooth muscle actin (α-SMA)-positive myofibroblasts originate from bone marrow, whereas non-bone marrow tissues including adipose tissue contribute to the remainder (175, 176). However, the integrated effects of tumor-associated physicochemical cues on ASC-dependent tumorigenesis are not well understood.

Here, we applied a physical sciences-based approach to correlate tumor-mediated changes in ASC phenotype with tissue stiffness, vascularization, and growth. Our findings support that ASCs can develop into myofibroblasts in response to physicochemical factors provided by cancerous cells. This phenotypic change not only enhanced angiogenesis, but also ECM rigidity, which further increased the tumor-promoting capacity of ASCs in a positive feedback loop. These findings support the role of ASCs as key regulators of mammary tumor progression and recurrence, which warrant review of current tissue engineering therapies following mastectomy and may be explored towards more efficacious therapies for breast cancer patients.

4.4 Materials and Methods

Cell Culture

3T3-L1, MDA-MB231, MCF-7 (all from ATCC), and MCN1 and MCN2 mammary tumor cells isolated from the mammary epithelium of MMTV-Cre, $p53^{L/L}$ and MMTV-Cre, $p53^{L/L}$ $Rb^{L/L}$, respectively (177), were routinely cultured in MEM (α-modification [αMEM], Sigma) containing 10% FBS (Tissue Culture Biologicals) and 1% antibiotic (penicillin/streptomycin, Gibco). MCF-10A (ATCC), MCF10AT1, and MCF10ACA1a (both from Barbara Ann Karmanos Cancer Institute (178)) were maintained in DMEM/F12 supplemented with horse serum, epidermal growth factor (EGF), hydrocortisone, cholera toxin, insulin, and penicillin/streptomycin (all from Invitrogen) as previously described (179). ASCs and human umbilical vein endothelial cells (HUVECs) (both from Lonza) were cultured in their corresponding growth media (ADSC-GM and EGM-2, respectively; Lonza). Lonza isolates ASCs from lipoaspirates based on expression of stem cell-associated surface markers (180), cryopreserves cells at passage 1, and does not pool cells from multiple sources. Here, ASCs from two separate, female donors were utilized at passages less than 7.

Analysis of ASC proliferation, adipogenesis, pro-angiogenic capability, and migration

Conditioned media was collected from the different tumor and epithelial cell lines in αMEM (1% FBS, 1% antibiotic) over 24-hours, normalized to cell number, concentrated 10-fold in an Amicon centrifugal filter unit (Millipore, MWCO = 3kDa), and subsequently reconstituted with media containing 1% FBS (Tissue Culture Biologicals) and 1% antibiotic (Gibco) specific to the treatment cell type (Table 4.1). Control medium was incubated for 24-hours without exposure to cells and then processed similarly. Conditioned media was globally tested for cytokines using Human Cytokine Antibody Arrays (Affymetrix) and specifically for IL-8 using ELISA DuoSets (R&D). Following 3 days of treatment in control media or TCM, cell counting was performed using a Z2 Beckman Coulter counter. To assess

proliferation, 10 μM BrdU (Sigma) was added to cells 20 hours prior to fixation in 4% paraformaldehyde. Then samples were incubated in ice-cold 1N HCl, followed by 2N HCl at 37°C, and then 0.1 M borate buffer prior to adding biotinylated mouse anti-BrdU. Subsequently, BrdU and nuclei were stained with streptavidin-conjugated Alexa Fluor 555 (both from Invitrogen) and DAPI (4',6-diamidino-2-phenylindole), respectively. The percentage of BrdU-positive nuclei was determined from 5 images per samples with 4 samples per condition.

Table 4.1 TCM Reconstitution Medium

Cell Type	Reconstitution Medium	Additives
3T3-L1 (ATCC), MCN1, MCN2 (177)	MEM (α-modification) (Sigma)	1% FBS (Tissue Culture Biologicals) 1% antibiotic (Gibco)
HUVEC (Lonza)	EBM-2 (Lonza)	Heparin (Lonza) Gentamicin/amphotericin-B (Lonza) 1% FBS (Lonza)
ASC (Lonza)	DMEM/F:12 (Invitrogen)	1% FBS (Tissue Culture Biologicals) 1% antibiotic (Gibco)

Adipogenesis of 3T3-L1s and ASCs was induced as previously described (137) and by using ADSC-GM SingleQuots® (Lonza), respectively. Differentiation into adipocytes was assessed by Oil Red O staining, immunofluorescence analysis of peroxisome proliferator-activated receptor gamma (PPARγ), as described in the staining procedures section, and by measuring glycerol-3-phosphate dehydrogenase (GPDH) activity. For the latter, supernatants collected after lysing cells on ice in a buffer containing 50mM Tris, 1mM EDTA, and 1mM β mercaptoethanol (all from J.T. Baker) were mixed with dihydroxyacetone phosphate and oxidized nicotinamide adenine dinucleotide (NADH). The decrease in NADH absorbance at 340 nm was quantified on a spectrophotometer over a 7 min period. Enzyme activity was normalized to total protein content as measured by protein assay (Bio-Rad). To visually assess differentiation into lipid-rich adipocytes, cells were fixed in formalin prior to staining with Oil Red O (Sigma) for 2 hours. Samples were imaged with a bright field microscope.

For analysis of pro-angiogenic activities, 3T3-L1s or ASCs were preconditioned in control or TCM for 3 days, then fresh media containing 1% FBS and 1% antibiotic specific to the treatment cell type

(Table 4.1) was added, collected after 24 hours, and processed as described above. VEGF secretion of preconditioned ASCs or 3T3-L1s was analyzed via human or mouse Quantikine ELISA (R&D Systems), respectively, and normalized to cell number determined by Z2 Beckman Coulter counter. To assess the effect of altered VEGF secretion on HUVEC migration, ASCs and 3T3-L1 cells were preconditioned for 3 days. Collagen-coated transwell inserts seeded with HUVECs were placed atop tumor-preconditioned 3T3-L1 or ASCs cells in fresh αMEM (1% FBS, 1% antibiotic). After 24 hours, inserts were formalin-fixed following a swabbing of the top of the membrane to remove non-migrated HUVECs. Cells on the lower side of the membrane were stained with DAPI and nuclei were counted. The number of migrated HUVECs was then normalized to the number of progenitor cells within each well.

To determine the effect of tumor-derived soluble factors on adipose progenitor recruitment, 3T3-L1 cells were seeded on top of collagen I (PureCol, Inamed)-coated Nunc 10 mm Tissue Culture inserts (8.0 μm pore) with either TCM or control medium beneath the membrane. After 18 hours, 3T3-L1s were formalin fixed following a swabbing of the top of the membrane to remove non-migrated cells. Cells on the lower side of the membrane were stained with DAPI and the average number of nuclei was counted in 8-10 images per sample.

Analysis of myofibroblast differentiation and matrix stiffening

Differentiation into myofibroblasts was assessed by immunofluorescence analysis of α-SMA, procollagen I, and collagen I as described below. Transforming growth factor β (TGF-β) signaling was modulated by supplementing control or TCM with 2 ng/mL recombinant human TGF-β1 or 0.5 μg/mL anti-human LAP (neutralizing TGF-β1 antibody) (both from R&D Systems), respectively. Interleukin-8 (IL-8) signaling was evaluated by supplementing growth media with 3-30 ng/mL recombinant human IL-8 (R&D). For contraction assays, ASCs were suspended in 15 mg/ml collagen (1×10^6 cells/ml) isolated from rat tails (181), cast into circular molds 0.5 mm thick and 4 mm in diameter (182), and cultured in TCM or control medium under free-floating conditions on an orbital shaker for 2 weeks, with media

changes every other day. To inhibit proliferation, initial addition of TCM or control medium was supplemented with 4 µg/mL mitomycin C (Fisher Scientific) as previously described (183). Actin polymerization and pROCK signaling were inhibited by supplementing culture media with 1 µM cytochalasin D or 20 µg/ml Y-27632 (both from Tocris), respectively. Gel contraction was determined by measuring the surface area of each gel using the magnetic lasso tool in Photoshop (Adobe) to trace the apical surface circumference. For the analysis of cell matrix stiffening, these same collagen gels were stained with dichlorotriazinylaminofluorescein (5-DTAF), sandwiched between two glass plates, and imaged with a Zeiss LSM 510 confocal microscope as previously described (184). A shear stress was applied to the gel while a photobleached line in the sample was imaged. As described previously, a MATLAB algorithm was then used to calculate the gel modulus based on the displacement of the photobleached line (184).

Western Blot Analysis

Cells were lysed in RIPA buffer (Thermo Scientific) containing protease inhibitor (Sigma), phosphatase inhibitor cocktail (Sigma), and 1mM phenylmethylsulfonyl fluoride (PMSF) in isopropyl alcohol. Equivalent quantities of protein were loaded as measured by BCA protein assay (Thermo Scientific). Proteins were separated by SDS-PAGE and transferred to a PVDF membrane (Bio-Rad). Primary antibody to α-SMA (Abcam) was incubated with the membrane overnight at 4°C, followed by a 1 hour incubation with HRP-conjugated anti-rabbit secondary antibody (Novus Bio) at room temperature. Chemiluminescence detection was performed to visualize probed protein using ECL kit (GE healthcare) based on manufacturer's protocol.

Analysis of ASC response to matrix mechanical properties

For traction force microscopy (TFM) analysis, polyacrylamide gels 1, 5, and 10 kPa in stiffness were prepared with embedded fluorescent beads, and cellular traction stresses were measured using TFM

as previously described (114, 185-187). Briefly, images of the gels in a stressed and relaxed state were taken pre- and post-removal of the cells with trypsin, respectively. The substrate strains were converted to traction stresses using the LIBTRC analysis library developed by Professor Micah Dembo of Boston University, who also invented the basic theory that underlies TFM. Polyacrylamide gels of the same stiffness were used for immunofluorescence analysis of phosphorylated focal adhesion kinase (pFAK[Y397]) as described in staining procedures section. For studies of the combined effects of stiffness and TCM, cells were seeded on 0.2-30 kPa stiff polyacrylamide gels and cultured in either control media or TCM for 10 days followed by staining and analysis as further outlined in the staining procedures section.

For studies using RGD-modified alginate substrates, alginate (Protanal LF 20/40, FMC) was modified with GGGGRGDSP (Peptides International) as previously described (1). 3%, 1.5%, and 0.75% (w/v) solutions of alginate in αMEM were cast between glass plates with 1 mm spacers and crosslinked in a solution of 0.1 M $CaCl_2$, 0.01 M HEPES (J.T. Baker) prior to punching out topographically flat disks 1 cm in diameter. The aggregate moduli of these gels were measured on a mechanical tester (ELF 3100, Bose) under radial confinement and uniaxial compression at 15 % strain. Cells were seeded on top of the gels and cultured in well plates. For analysis of cell numbers and adipogenic differentiation, cells were harvested by dissolving these constructs in 50mM EDTA (J.T. Baker) in PBS and analyzed as described above. To analyze VEGF secretion, cell-seeded gels were transferred to a new culture dish (containing fresh media with 1% FBS, 1% antibiotic). After 24 hours, media and cells were collected and analyzed as described above.

In vivo studies

Media, ASCs and/or MDA-MB231 cells (1×10^6 in 20 µL of DMEM/ Ham's F-12, 10 % FBS, 1 % antibiotic) were injected into the cleared mammary fat pad of at least six 3 week-old female SCID/NCr mice (Charles River Labs, 01S11) (2 tumors per mouse) per condition in accordance with Cornell

University animal care guidelines. Explants were harvested 6 weeks after implantation, imaged, weighed, and divided for subsequent formalin-fixation/paraffin-embedding and lysis in T-PER buffer (Pierce). H&E-stained sections were broadly evaluated for pathological features of malignancy. Cross-sections were characterized further via immunohistochemical staining for CD31, α-SMA, procollagen I, and desmin, while collagen was stained via Masson's Trichrome. Staining procedures and image analysis methods are described in the following sections. VEGF and IL-8 content in lysates was measured via VEGF and IL-8 DuoSets (R&D) and normalized to protein content as determined via BCA protein assay (Thermo Scientific).

Staining procedures

For immunocytochemistry, formalin-fixed cells were rinsed with 0.05% Triton-X in PBS (PBS-X) followed by incubation with 2% BSA in PBS-X (PBS-X/BSA) for blocking. Afterwards, the cells were incubated with the desired primary antibody diluted in PBS-X/BSA overnight at 4°C. Following two washes in PBS-X, samples were incubated with secondary antibodies diluted in PBS-X/BSA for 1 h at room temperature. The following primary antibodies were used: rabbit anti-mouse PPARγ (Cell Signaling), rabbit anti-FAK [pY397] (Invitrogen), mouse anti-α-SMA (Abcam), rabbit anti-procollagen I (SP1.D8, Developmental Studies Hybridoma Bank, Univ. of Iowa), and rabbit anti-collagen I (Millipore). DAPI was used as a nuclear counterstain, Alexa Fluor 488 or 568 served as the secondary antibody, and Alexa Fluor 568-conjugated phalloidin enabled detection of the F-actin cytoskeleton (all from Invitrogen). Imaging was performed on a Zeiss Observer Z.1 microscope and AxioCam MRm camera unless otherwise noted. Cells cultured within collagen gels and stained with α-SMA primary and AlexaFluor 488-conjugated secondary antibody, phalloidin, and DAPI were imaged on a Zeiss 710 Confocal Microscope.

Paraffin sections of *in vivo* samples were subjected to antigen retrieval treatments (proteinase K [Dako] for CD31 staining, antigen retrieval system [Dako] for α-SMA, and 0.1M citrate buffer for

alternate stains) prior to standard immunostaining procedures. Subsequently, samples were rinsed and blocked in 0.05% Tween-20 PBS (TBST) with SuperBlock (Thermo Fisher). An additional blocking treatment was required for α-SMA and procollagen I staining using M.O.M kit (Vector laboratories) and Vectastatin ABC kit (Vector laboratories), respectively. In addition to those previously listed, rat anti-CD31 (Pharmingen), mouse anti-α-SMA (Invitrogen), and rabbit anti-desmin (Abcam) were used. For CD31 staining, the TSA biotin system (PerkinElmer) was used for signal amplification. For DAB-based immunohistochemistry, peroxidase activity was blocked using 3% hydrogen peroxide and an HRP-conjugated secondary antibody (Novus) and 3,3´-diaminobenzidine (DAB) substrate kit (Thermo Fisher) was used for color development. Samples were counter-stained with Gill's hematoxylin (EMD chemicals). IgG isotopes and primary antibody-lacking sections served as negative controls.

For picrosirius red staining, 4 μm thick sections of paraffin–embedded tissue were stained with 0.1% Sirius red F3B (Sigma) in saturated picric acid for two hours at room temperature followed by washes in 1% acetic acid and distilled water. Stained sections were imaged with a Nikon Eclipse TE2000-S microscope equipped with a rotating filter for polarized light under 10x magnification. Microscope setting (light intensity, exposure time, condenser opening, gain, and gamma parameter) was identically applied to all samples.

Image Analysis

For image analysis, raw data images of *in vitro* samples and histological cross-sections were utilized. Background staining was excluded from images of various samples prior to isolating positive pixels of interest using Adobe Photoshop. Isolated positive pixels were then quantified in ImageJ (NIH). Positive pixel density was averaged for 8-10 representative images per sample for 4 samples per *in vitro* condition and for 15-20 representative images per explant. Staining intensity was normalized to cell number as determined by semi-automated counting of DAPI-stained nuclei utilizing ImageJ. Alpha-SMA positive cells in *in vitro* samples were manually quantified. Cell alignment was determined by using

ImageJ to measure the angle of lines drawn through the long axis of up to 20 randomly selected cells per image. The average cell angle was then calculated for each image, and the individual cell deviation from the average was computed and plotted. For all conditions, a total of 8-10 images were examined per sample with 4 samples per condition.

Collagen fiber maturity in picrosirus stained sections was analyzed by their birefringence color appearing as red/orange, green, or blue/white according to fiber thickness. The birefringence color pixels (red, green, and blue) of collagen fibers were segmented using RGD stacks in ImageJ and the separated pixels were quantified. Threshold was manually adjusted based on grayscale images, and kept constant throughout all samples. Five to six images were analyzed per tumor for a total of three tumors per condition.

Multiphoton Second Harmonic Generation Imaging and Analysis

Multiphoton microscopy was performed on a previously described, custom-built multiphoton microscope (188). Tumor samples were fixed in placed, immersed in PBS, and imaged with 780 nm illumination using an Olympus 20x/0.95W XLUMPlanFl objective. For each specimen, six Z-series (2 μm steps, from 60 μm to 100 μm deep) were acquired. Emissions were separated into SHG (360-405 nm, pseudocolored blue) and autofluorescence (420-550 nm, pseudocolored yellow) channels. Only the SHG channel was used for image quantification of collagen matrix properties. In order to analyze the mean structural characteristics of the collagen matrix, a 2D spatial autocorrelation was computed from the SHG channel image. An isocontour was fit to 1/e of the maximum value of each image autocorrelation. The mean radius of this isocontour (the mean correlation distance in the image) indicates the size scale of the collagen framework in any image. For the collagen fibril linearity (FL) assessment, individual fibrils were traced throughout each Z-stack. Specifically, both the full-length and the shortest distance between fibril ends were measured using Fiji (a packaged version of ImageJ). The ratio of the linear distance over the full fibril length was calculated to be the collagen FL. 30-50 fibrils per z-stack were measured, and the

collagen FL of each condition was obtained by averaging the FL of 4 z-stacks in each tumor. A total of 3 tumors per condition were analyzed.

Dynamic Mechanical Thermal Analysis of tumor sections

Fixed tumors were cut with a vibratome into sections ranging from 0.7 to 2.7 ± 0.1 mm in thickness as determined optically. These sections were punched into cylindrical thick sections of 2.6 ± 0.1 mm in diameter, fixed between the Dynamic Mechanical Thermal Analyzer (DMTA) parallel plates, and fully immersed in PBS in a standard submersion-compression clamp configuration at room temperature (25^{o}C). A controlled force was applied by the upper plate while the lower plate held the sample in a fixed position. Two series of compressive tests were then run on each tumor sample following an initial application of 9% pre-strain to ensure full sample engagement and homogeneous compression before measurement. In the first series, the maximum force applied was set at 0.01 N to exclusively probe the low-strain (9-14%) elastic regime to avoid plastic deformation, while it was set at 0.4 N in a second series to investigate the full elastic regime and the onset of material to plastic deformation (up to 30% strain). The rate of force application was kept constant at 0.025 N/min in all tests. The force F (force sensitivity of 0.001 N) and thickness L (distance resolution of 0.05 μm) were measured simultaneously and converted into engineering stress-strain plots as follows: strain, $\varepsilon=(L_o-L)/L_o$ (where L_o is the initial zero-strain sample thickness and L the thickness during compression) and stress, $\sigma=F/A_o$ (where F is the force during compression, and A_o the initial zero-strain sample cross-sectional area). The mean Young's modulus, E, was obtained for each sample from the slope of the stress-strain curve, $\sigma = E\ \varepsilon$ in the low-strain (9-14%) elastic regime.

Analysis of the Effect of Altered Progenitor Cell ECM

3T3-L1-derived matrices were prepared as previously described (189). More specifically, 3T3-L1s were seeded in 12-well plates and cultured for 8 days in either TCM or control media supplemented with

50 µg/mL ascorbic acid (Sigma) with media changes every other day. On day 8, the matrix was incubated at 37°C for 15 minutes in extraction buffer (20 mM NH_4OH and 1% Triton-X in PBS). After washing in deionized (DI) H_20 and PBS followed by blocking with 1% BSA, Vybrant DiO (Invitrogen)-labeled MDA-MB231 cells were seeded atop the matrix. pROCK signaling was inhibited by supplementing culture media with 20 µg/mL Y-27632 (Tocris). The number of MDA-MB231 cells was assessed by counting 10 images per sample for 6 samples per condition.

Statistical analysis

Statistical analysis was performed using GraphPad Prism 5©. Student's t-tests were used to compare two data sets while ANOVA was applied to determine the statistical significance of the differences between data sets of 3 or more using the Tukey method to make post-hoc pairwise comparisons. A p-value less than 0.05 was considered statistically significant. Data are represented as average ± standard deviations with the exception of the traction force measurements which are shown with standard errors.

4.5 Results and Discussion

TCM regulates the adipogenic and pro-angiogenic capability of ASCs

To evaluate the effects of tumor cell-secreted soluble factors on ASC behavior, human ASCs were cultured in conditioned media (TCM) from commonly used highly (MDA-MB231) or less (MCF-7) aggressive human breast cancer cell lines. Additionally, mouse 3T3-L1 preadipocytes – a well-characterized cell model for studies of adipogenesis (89) – were used to verify the broad implications from primary ASC studies. Analysis of cell numbers and BrdU incorporation suggested that tumor-secreted factors promoted ASC and 3T3-L1 proliferation (Figures 4.1A and 4.2A). In contrast, these factors inhibited adipose differentiation of both cell types, as indicated by attenuated activity of the

lipogenic enzyme GPDH (Figure 4.1B), reduced activation of the key adipogenic transcription factor PPARγ (Figure 4.2C), and inhibition of lipid droplet accumulation (Fig. 4.2B). An experiment in which ASCs and 3T3-L1s were first exposed to TCM and then evaluated for VEGF secretion further suggested that exposure to tumor-derived soluble factors enhances pro-angiogenic factor release by these cells (Figure 4.1D). This increased pro-angiogenic potential is relevant to tumor angiogenesis as tumor-preconditioned ASCs and 3T3-L1s significantly enhanced VEGF-dependent migration of human umbilical vein endothelial cells (HUVECs) as compared to control cells (Figure 4.1E). Notably, the magnitude of these changes directly correlated with tumor aggressiveness since MDA-MB231-TCM induced greater phenotypic changes than media collected from MCF-7 cultures (Figures 4.1 and 4.2). Comparison of effects mediated by isogenically matched normal MCF10A, premalignant MCF10AT, and fully malignant MCF10ACA1a cells confirmed these results. Specifically, premalignant cells had no significant effect on ASC adipogenic differentiation and VEGF secretion, but promoted ASC proliferation, whereas MCF10ACA1a cells mediated outcomes similar to MDA-MB231 (Figure 4.2C-E). The described observations were broadly relevant as TCM collected from two murine mammary tumor cell lines (177) also enhanced the proliferative and pro-angiogenic phenotype of adipose progenitor cells, and inhibited adipose differentiation (Figure 4.3A-C).

To assess whether tumor cells actively recruit ASCs, we performed a transwell migration assay with TCM, which revealed that tumor cells attract adipose progenitor cells towards their respective location by enhancing their directed migration (Figure 4.3D). Collectively, these data suggest that tumor cell-secreted soluble factors enhance the pro-angiogenic cell population in the tumor stroma by guiding ASC behavior. As TCM similarly modulated ASC and 3T3-L1 behavior, and because data generated with primary cells are typically more robust and generalizable the studies described in the following experiments were primarily performed with ASCs.

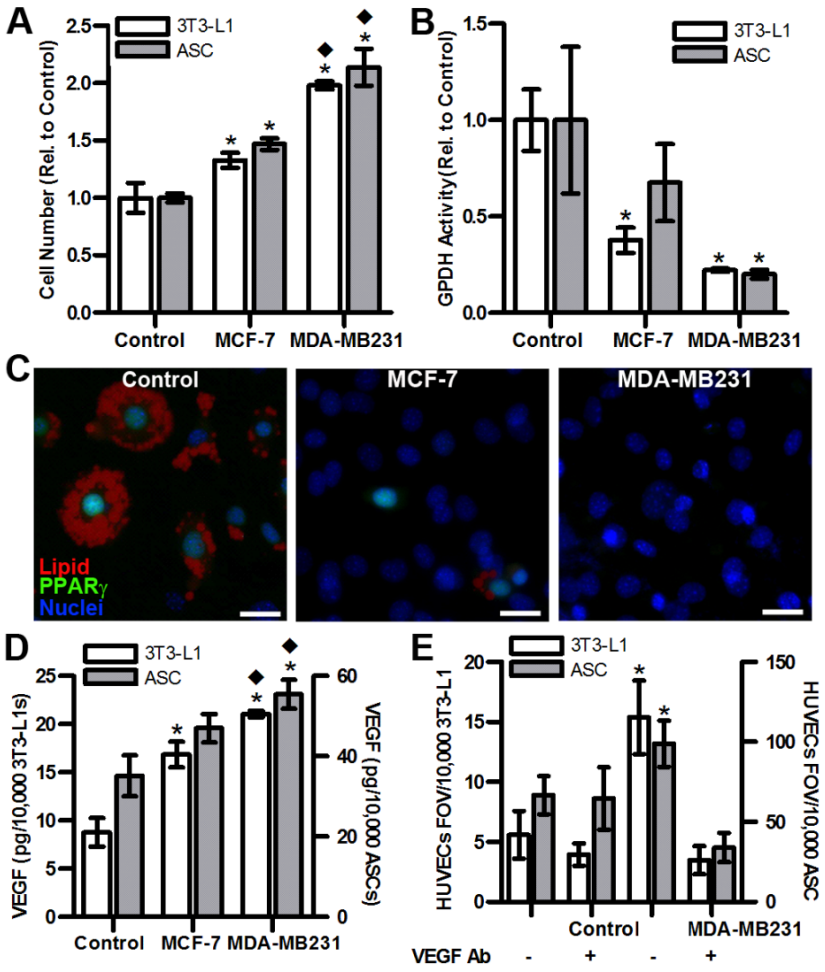

Figure 4.1 Tumor-secreted soluble factors regulate ASC function

(A) TCM from MCF-7 and MDA-MB231 increases 3T3-L1 and ASC cell numbers relative to control (n = 4). (B) TCM treatment significantly decreases the adipogenic capability of 3T3-L1 and ASCs relative to control as determined by spectrophotometric analysis of GPDH activity (n = 4). (C) Immunofluorescence analysis of the transcription factor PPARγ in 3T3-L1s confirmed that TCM inhibits adipogenic differentiation (Scale bar = 20 μm). (D) ELISA suggested that ASCs and 3T3-L1s increase VEGF secretion when pre-conditioned with TCM from either MCF-7 or MDA-MB231 (n = 4). * $p < 0.05$ from control; ♦ $p < 0.05$ from MCF-7 condition. (E) 3T3-L1s and ASCs that were previously pre-conditioned with TCM from MDA-MB231 enhanced HUVEC migration in a transwell assay as compared to 3T3-L1s and ASCs pre-conditioned with control media; addition of a VEGF neutralizing antibody decreased migration to control levels (n = 4). * $p < 0.05$ from all other conditions of the same cell type.

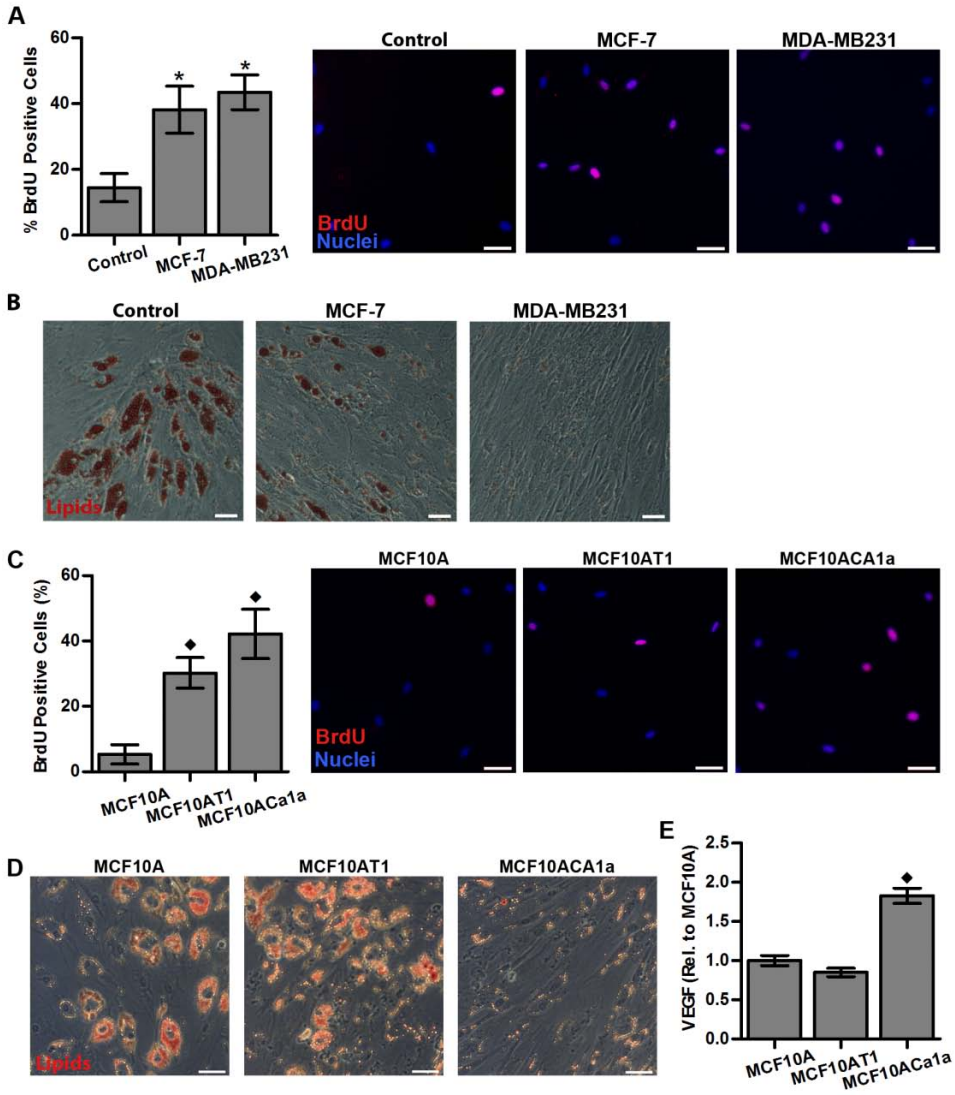

Figure 4.2 Tumor-secreted soluble factors alter ASC functions

(A) TCM from MCF-7 and MDA-MB231 enhanced ASC proliferation as assessed by quantification of BrdU positive cells (Scale bar = 50 μm). (B) Differentiation of ASCs in control medium resulted in large lipid droplet formation, whereas ASCs cultured in TCM from MCF-7 or MDA-MB231 exhibited decreased lipogenesis, evidenced by diminished Oil Red O-staining (Scale bar = 50 μm). (C) Quantification of BrdU positive ASCs after culture in conditioned media of isogenically matched MCF10A (normal), MCF10AT1 (premalignant), and MCF10ACA1a (malignant) cells confirms that increased ASC proliferation represents a function of tumor malignancy (Scale bar = 50 μm). (D) Adipogenic differentiation of ASCs in conditioned medium from normal and premalignant cells resulted

in lipid droplet formation, whereas ASCs cultured in TCM from MCF10ACA1a cells exhibited decreased lipogenesis, evidenced by diminished Oil Red O-staining (Scale bar = 100 μm). (E) MCF10ACA1a TCM also significantly increased VEGF secretion by ASCs as measured by ELISA (n = 4). * $p < 0.05$ from control condition; ♦ $p < 0.05$ from MCF10A condition.

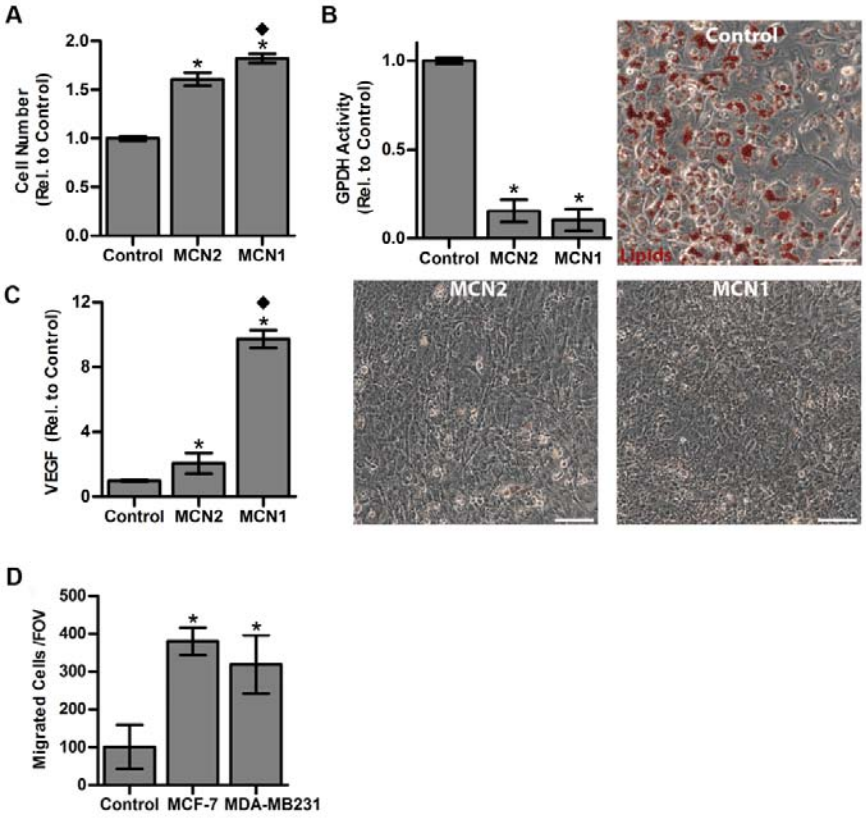

Figure 4.3 Effect of tumor-derived soluble signals on 3T3-L1 cells

(A) Cell counting indicated enhanced 3T3-L1 cell numbers with TCM supplementation from two mouse breast cancer cell lines (MCN1, MCN2) as compared to control medium (n = 4). (B) Adipogenic differentiation significantly decreased with murine TCM treatment relative to control conditions as assessed by spectrophotometric analysis of GPDH activity and Oil Red O staining (n = 4) (Scale bar = 20 μm). (C) Murine TCM also significantly increased VEGF secretion by 3T3-L1s as measured by ELISA (n = 4). (D) Using a transwell assay, 3T3-L1 migration was enhanced towards TCM from MDA-MB231 and MCF-7 as compared to control medium (n = 3). * $p<0.05$ from control; ♦ $p<0.05$ from MCN2 condition.

TCM enhances ASC differentiation into ECM-stiffening myofibroblasts

Myofibroblasts represent an abundant and pro-angiogenic cellular component of the tumor stroma whose differentiation is enhanced in the presence of reduced signaling by the adipogenic transcription factor PPARγ (190, 191). Accordingly, ASCs exposed to TCM exhibited increased expression of α-SMA relative to control conditions (Figure 4.4A), whereby MDA-MB231 exerted a more pronounced effect than MCF-7 (Figure 4.4B). Next, we evaluated whether tumor cell-derived TGF-β (192), which is pivotal to myofibroblast differentiation and secreted at higher levels by more malignant tumor cells (193) may be involved in inducing phenotypic changes of ASCs. Control media was supplemented with TGF-β at levels found in MDA-MB231-TCM, and this treatment induced ASC differentiation into myofibroblasts as suggested by immunofluorescence and Western Blot analysis (Figures 4.4 A,C). Furthermore, addition of a TGF-β epitope-blocking antibody to TCM abrogated myofibroblast differentiation. While these data verify that tumor-secreted TGF-β functions as an upstream mediator of ASC differentiation into myofibroblasts (Figure 4.4A) other molecules may also play a role. Comparison of control media as well as TCM from MCF-7 and MDA-MB231 via a cytokine antibody array revealed that interleukin-8 (IL-8), VEGF, tumor necrosis factor receptor 1 (TNFR1), and matrix metalloproteinase 3 (MMP3) were enhanced in the TCM (Figure 4.4D). As IL-8 has been related to myofibroblast differentiation in prostate cancer (194) and was enhanced in MDA-MB231 vs. MCF-7 TCM (Figure 4.4E), we assessed its effect on ASC myofibroblast differentiation. Results from these studies elucidated that IL-8 regulates ASC differentiation into myofibroblasts in a dose-dependent manner (Figure 4.4F). These findings are of particular interest as myofibroblasts themselves can up-regulate IL-8 (195), which may further promote ASC differentiation into myofibroblasts.

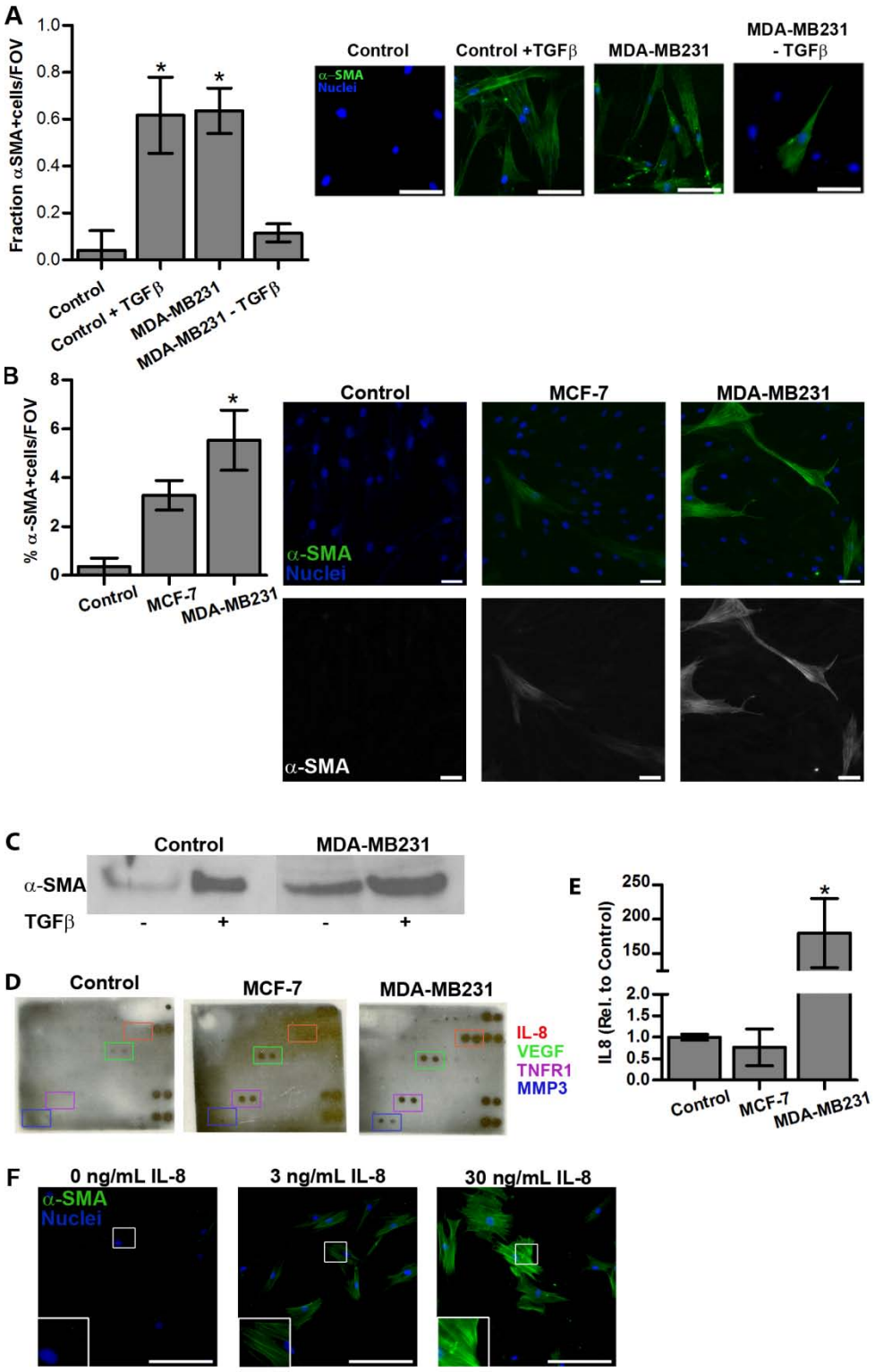

Figure 4.4 Effect of tumor-derived soluble factors on ASC myofibroblast differentiation.

(A) Treatment of ASCs with TCM from MDA-MB231 significantly increased the number of α-SMA (green) positive cells as quantified by immunofluorescence image analysis. Addition of TGF-β to control

media (control + TGF-β) mimicked this effect, while blockade of TGF-β in TCM using a neutralizing antibody (MDA-MB231 - TGF-β) inhibited it (n = 4) (Scale bar = 100 μm) * $p < 0.05$ from control and MDA-MB231-TGF-β conditions. (B) Immunofluorescence analysis indicates that ASCs up-regulate α-SMA more significantly with TCM from MDA-MB231 as compared to TCM from MCF-7 or control cells (n = 4) (Scale bar = 50 μm). (C) Western blot analysis of equally loaded samples shows elevated levels of α-SMA in ASCs treated with MDA-MB231 TCM, which were further enhanced by addition of TGF-β. (D) Cytokine array analysis indicates increased levels of noted cytokines within TCM as compared to control media. (E) ELISA of IL-8 detects greatest levels within MDA-MB231 TCM (n = 3). (F) Exposure of ASCs to relevant concentrations of IL-8 increased α-SMA and stress fiber formation (insets) in a dose-dependent manner (Scale bar = 200 μm). * $p < 0.05$ from control (B) or from all other conditions (E).

Myofibroblasts mediate tissue stiffening by altering ECM composition and enhancing contraction. In particular, increased collagen I deposition has been associated with increased tumor stiffness and malignancy (73). Our results support that ASC exposure to tumor-derived paracrine signals may contribute to this because ASCs produced significantly more procollagen I (6.0 ± 1.1-fold) and collagen I (4.2 ± 1.1-fold) when treated with TCM rather than control media (Figure 4.5). Furthermore, ASCs seeded into microfabricated, free-floating 3-D collagen disks differentiated into myofibroblasts, developed stress fibers, and contracted significantly more when cultured in the presence of TCM as compared to control media (Figures 4.6 B,C). These variations in gel contraction were mediated by differences in TCM-mediated changes in myosin-mediated cell contractility rather than proliferation. Specifically, pharmacological inhibitors cytochalasin D (i.e., an agent preventing actin polymerization) or Y-27632 (i.e., an inhibitor of pROCK and thus RhoA signaling) added at levels not affecting cell viability restored the diameter of previously contracted gels (Figure 4.6C), whereas disks cultured in TCM in the presence of mitomycin C contracted markedly more than similarly treated control disks (Figure 4.6A). To

more fully elucidate whether the integrated effects of varied ECM deposition and contraction indeed contribute to enhanced tissue rigidity, the mechanical properties of ASC-seeded disks were analyzed following culture in control or TCM. The shear modulus of these constructs was determined by applying a shear force to one side of a sandwiched gel while measuring the displacement of a photobleached line within the gel (184). Our results indicate that TCM-treated collagen cultures were 1.5-fold stiffer than the control constructs (Figure 4.6D), confirming the effect of tumor-derived soluble factors on ASC-mediated changes in tissue stiffness. These changes may be explained by varied matrix contraction and irreversible changes in ECM deposition mediated, for example, by increased collagen crosslinking due to enhanced lysyloxidase (LOX) expression by myofibroblasts (196) and/or deposition of additional fibrillar ECM components such as fibronectin (93).

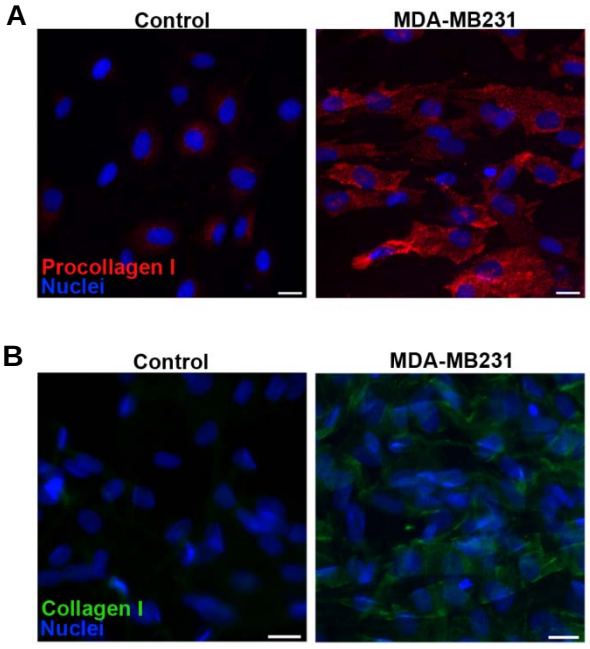

Figure 4.5 Effect of tumor-secreted soluble factors on ASC collagen deposition.

ASCs cultured in MDA-MB231 TCM exhibited increased collagen type I matrix assembly relative to ASCs maintained in control medium as indicated by positive staining for (A) type I procollagen and (B) collagen (Scale bar = 20 μm).

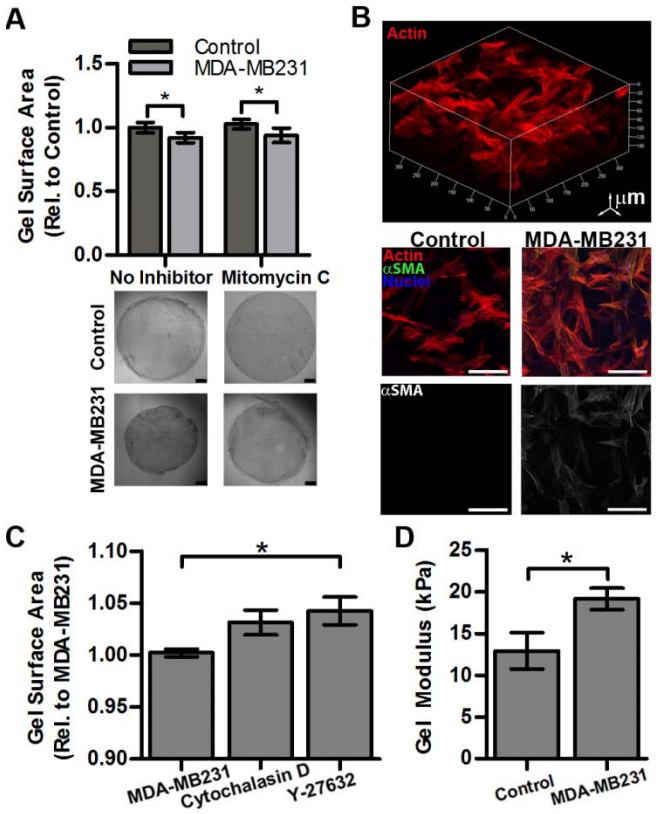

Figure 4.6 Altered matrix mechanics with ASC differentiation into myofibroblasts

(A) Collagen gels seeded with ASCs contracted significantly more when cultured in TCM as compared to control medium (n = 6), which occurred even in the presence of the proliferation inhibitor mitomycin C (Scale bar = 500 μm). (B) Confocal imaging revealed that ASCs within these gels developed stress fibers necessary to generate contractile tension, but only differentiated into α-SMA positive cells in the presence of TCM (Scale bar = 100 μm). (C) Pharmacological inhibition of cytoskeletal tension using cytochalasin D and Y-27632 contributed to the release of the contracted gels as determined via an increase in surface area (n = 3). (D) ASC-seeded collagen gels cultured in the presence of TCM were significantly stiffer relative to gels maintained in control media as determined by confocal-based stiffness measurements (n = 5) * $p < 0.05$.

ASCs respond to ECM mechanical properties in a tumor-dependent manner

Both normal and tumorigenic cells respond to increased matrix stiffness by adjusting integrin-dependent adhesion, traction forces, and subsequent downstream signaling (51, 197) with effects on cell proliferation and differentiation (49). To test the ability of ASCs to react to tumor-derived and/or self-imposed changes in matrix stiffness we evaluated their adhesion characteristics and corresponding activation of mechano-regulated signaling pathways using hydrogels of pathologically-relevant stiffness (47). Specifically, use of collagen-coated polyacrylamide gels allowed control over mechanical properties of the culture substrates without affecting adhesion ligand density, which can independently affect cell behavior (198). ASCs spread significantly more on substrates mimicking breast tumor rigidity (~10kPa (47)) relative to substrates approximating premalignant (~5kPa) and adipose tissue (~1kPa (47)) stiffness (Figure 4.7A). TFM confirmed that these morphological changes were accompanied by greater traction forces of ASCs on stiffer relative to more compliant matrices (Figure 4.7A). These observations directly correlated with the recruitment of pFAK to focal adhesions (Figure 4.7B), a result of activated Rho-ROCK signaling due to force-induced changes in adhesion dynamics (199). Accordingly, ASC number was greater on stiffer matrices, and administration of cytochalasin D and Y-27632 inhibited this effect (Figure 4.7C) confirming that Rho-ROCK mediated changes in cytoskeletal tension enable ASCs to respond to ECM stiffness.

To broadly assess stiffness-dependent cellular responses to a more relevant, biocompatible material that can be used for adipose tissue engineering and breast reconstruction applications (200, 201), we cultured adipose progenitors on RGD-modified alginate disks similarly mimicking normal, premalignant, and cancerous breast tissue stiffness. Interestingly, increased stiffness recapitulated the effects of TCM and enhanced cell numbers and VEGF-secretion of these cells, while inhibiting their adipogenic differentiation (Figure 4.8). These results are consistent with previous studies, which indicate elevated adipocyte conversion on more compliant matrices (49, 131) and with less spread, rounder cell morphology (163).

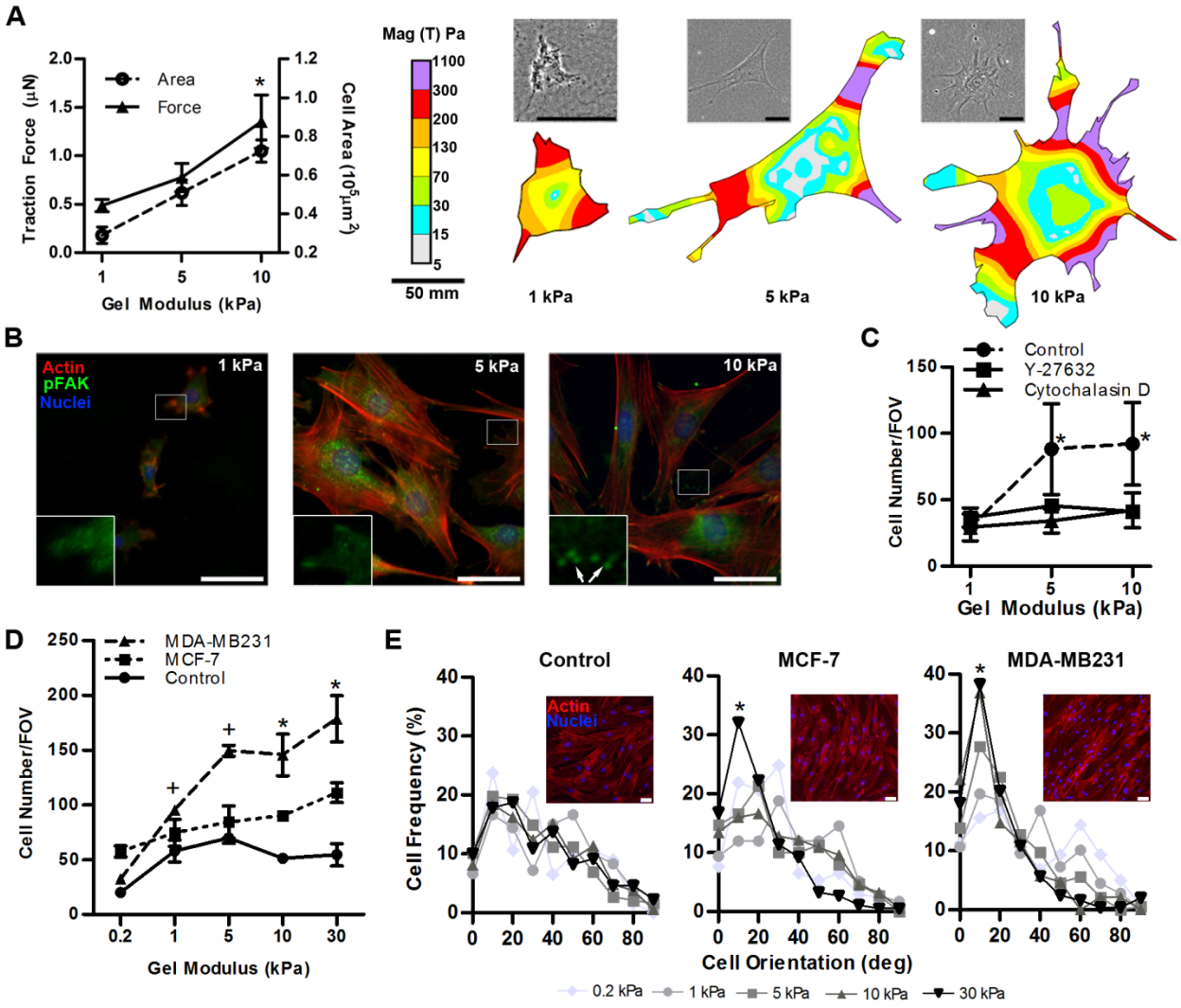

Figure 4.7 ASC response to matrix mechanical properties

(A) Traction Force Microscopy indicated that ASCs cultured on hydrogels of increased stiffness spread significantly more and exert greater traction forces relative to cells cultured on soft matrices; representative ASC phase images with corresponding traction maps are shown (n = 13-32, error bars represent standard errors) (Scale bar = 50 μm) * $p < 0.05$ from 1 kPa condition. (B) Immunofluorescence indicates increased recruitment of pFAK[Y397] to ASC focal adhesions on stiffer matrices (white arrows) (Scale bar = 20 μm). (C) Cell counting suggested that increased matrix stiffness enhances ASC numbers and that pharmacological inhibition of cytoskeletal tension with Y-27632 or cytochalasin D inhibits this effect (n = 4). (D) ASC numbers on stiff matrices were further enhanced with culture in TCM whereby TCM from MDA-MB231 exerted a more pronounced effect than TCM from MCF-7 (n = 3) * $p < 0.05$

between all conditions; $^{+}$ $p < 0.05$ between MDA-MB231 and control conditions. (E) Image analysis of the deviation from the average angle of phalloidin-stained cells revealed that ASC alignment represented an integrated effect of both substrate stiffness and tumor malignancy; while ASCs on 30 kPa gels had enhanced alignment in MCF-7 TCM, this occurred on gels of even lower stiffness in MDA-MB231 TCM. (Scale bar = 50 μm) * $p < 0.05$.

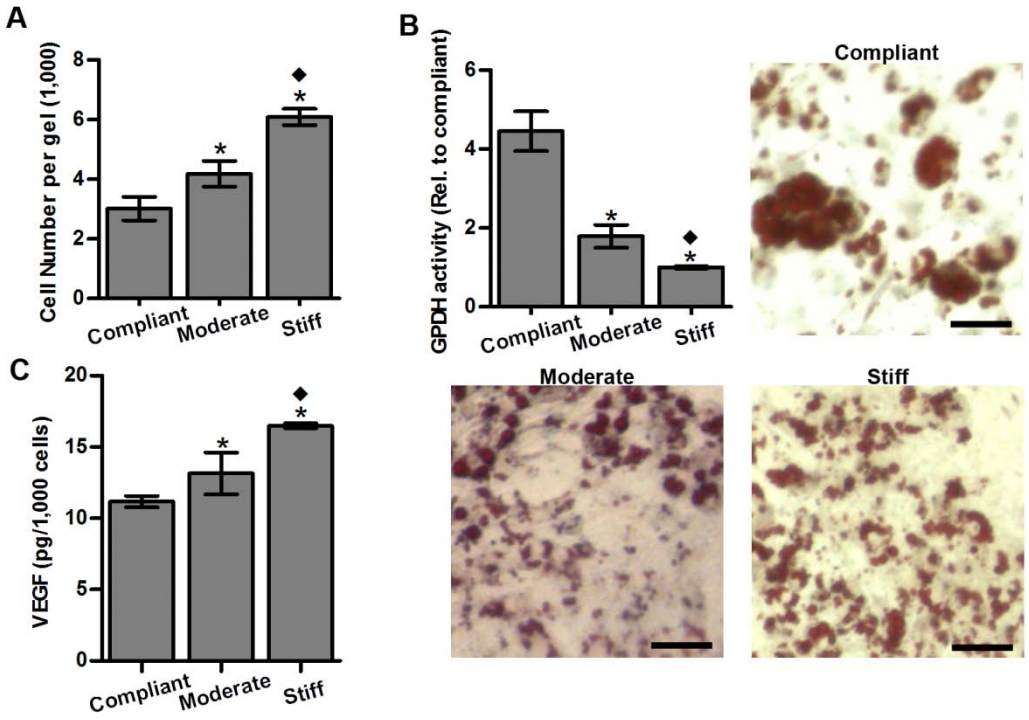

Figure 4.8 Effect of matrix stiffness on adipose progenitors

Culture of 3T3-L1s on RGD-modified alginate hydrogels mimicking stiffness of normal (compliant, ~1.8 kPa), moderately diseased (~5.2 kPa) and malignant breast tissue (stiff, ~12 kPa) demonstrate that matrix mechanical properties mediate similar effects on adipose progenitors as tumor-derived soluble factors. (A) Enhanced matrix stiffness increased cell numbers (n = 8), (B) decreased adipogenesis as determined by GPDH analysis and Oil Red O-staining, (n = 3), and (C) enhanced VEGF secretion as measured by ELISA (n = 4). * $p < 0.05$ from compliant condition. ♦ $p < 0.05$ from moderate condition (Scale bar = 50 μm).

To investigate whether tumor-secreted soluble factors enhance ASC response to ECM rigidity, ASCs were cultured on polyacrylamide substrates of a broad range of stiffnesses (0.2-30 kPa)), in the presence or absence of TCM from MCF-7 or MDA-MB231. Cell growth was commensurate with increasing stiffness whereby the level of tumor malignancy affected ASC stiffness response. More specifically, TCM from the more malignant MDA-MB231 cells increased cell growth on gels of lower stiffness relative to TCM of the less malignant MCF-7 (Figure 4.7D). Furthermore, the combined effects of ECM stiffness and tumor-derived soluble factors promoted cellular alignment on stiffer, but not soft, matrices, and this effect was more pronounced with TCM from MDA-MB231 than MCF-7 (Figure 4.7E). Collectively, these results suggest that tumor-secreted factors dramatically enhance adipose-derived stem cell responses to stiffness leading to (i) an increased contractile cell population, and (ii) directed force generation (202), which may ultimately exacerbate tumor rigidity and hence malignancy.

ASCs modulate tumor progression in vivo

To determine the relevance of our *in vitro* findings to tumor growth *in vivo*, ASCs and MDA-MB231 cells were injected individually or in combination into the cleared mammary fat pad of immunocompromised mice. Co-injection of MDA-MB231 with ASCs yielded larger tumors than delivery of tumor cells alone in accordance with previous results (123, 203) (Figure 4.9A). In contrast, injected ASCs largely formed adipose tissue, as seen in histological sections (Figures 4.9C and 4.13A, B), that was similar in size to explants from sham-injected media suggesting that the difference in tumor size was caused by varied tumor malignancy rather than the additional volume assumed by the co-injected ASCs (Figure 4.9A). Furthermore, tumors resulting from the mixture of ASCs and MDA-MB231 cells appeared more locally invasive upon explantation relative to MDA-MB231-borne tumors, which were easily demarcated for dissection. Pathological evaluation of H&E-stained cross-sections confirmed this assessment and revealed an enhanced degree of local invasion and desmoplasia for the co-implanted tumors versus the control tumors (Figures 4.10A, B). Additionally, cytological features of malignancy

(multinucleated cells and rosettes) were augmented in the co-implanted group as compared to the MDA-MB231 group (Figure 4.10C).

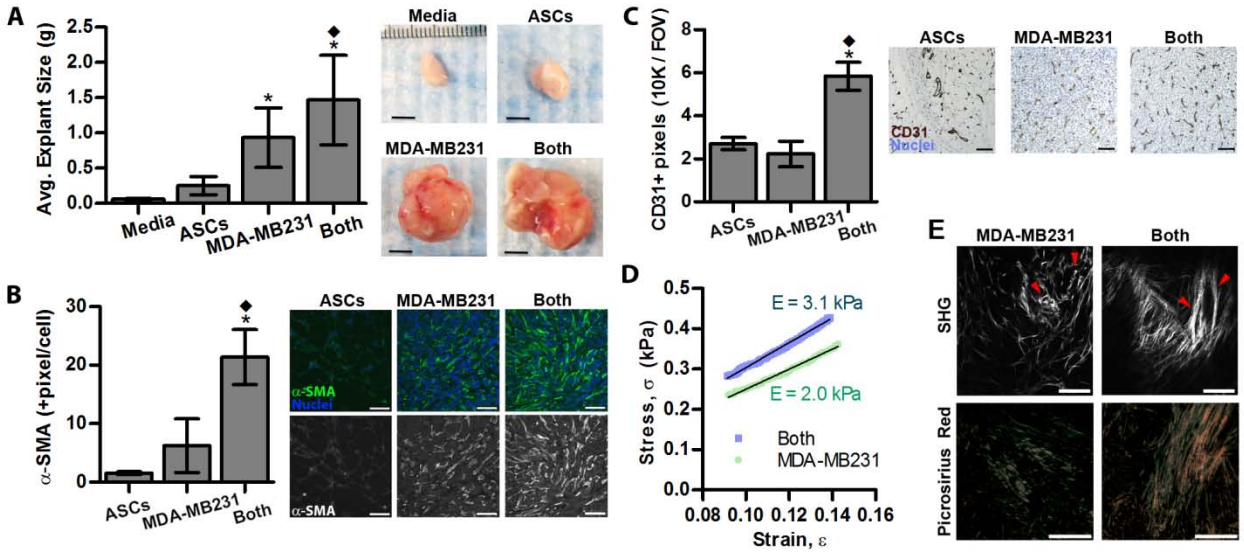

Figure 4.9 ASCs modulate tumor progression *in vivo*.

(A) Tumors resulting from the co-injection of ASCs and MDA-MB231 cells (Both) (n = 14) were significantly larger than tumors formed by MDA-MB231 cells alone (n = 16). Soft tissue explants generated from injected ASCs (n = 12) or Media (n = 2) are shown for a comparison (Scale bar = 5 mm). (B) Immunofluorescence analysis indicates that α-SMA levels were greatest in the explants resulting from co-implantation of ASCs and MDA-MB231 cells as compared to those from MDA-MB231 and ASCs alone (Scale bar = 50 μm). (C) Similarly, the density of CD31+ blood vessels was enhanced in explants from the co-implanted group (Scale bar = 20 μm). For α-SMA and CD31+ image analysis, ASC (n = 6), Both (n = 6), and MDA-MB231 (n = 12) explants were analyzed. (D) Mechanical analysis of tumor sections via DMTA. The mean stress-strain profile was measured in PBS at room temperature through the low-strain (9-14%) elastic regime. The engineering stress σ versus strain ε curve represents the average of 2 compressions per tumor section performed on 4 tumor sections from MDA-MB231 alone, and 9 tumor sections from the co-implantation group (see Materials and Methods). The mean Young's modulus, *E*, was extracted from the slope of the stress-strain curve, $\sigma = E\,\varepsilon$. (E) Compared to

tumors from MDA-MB231, co-injected tumors contain more mature and linearized collagen fibers as revealed by picrosirius red staining of cross-sections and second harmonic generation (SHG) imaging (Scale bar = 100 μm), which is further quantified in Fig. S9. For (A-C) *p < 0.05 from ASCs condition; ♦p < 0.05 from MDA-MB231 condition.

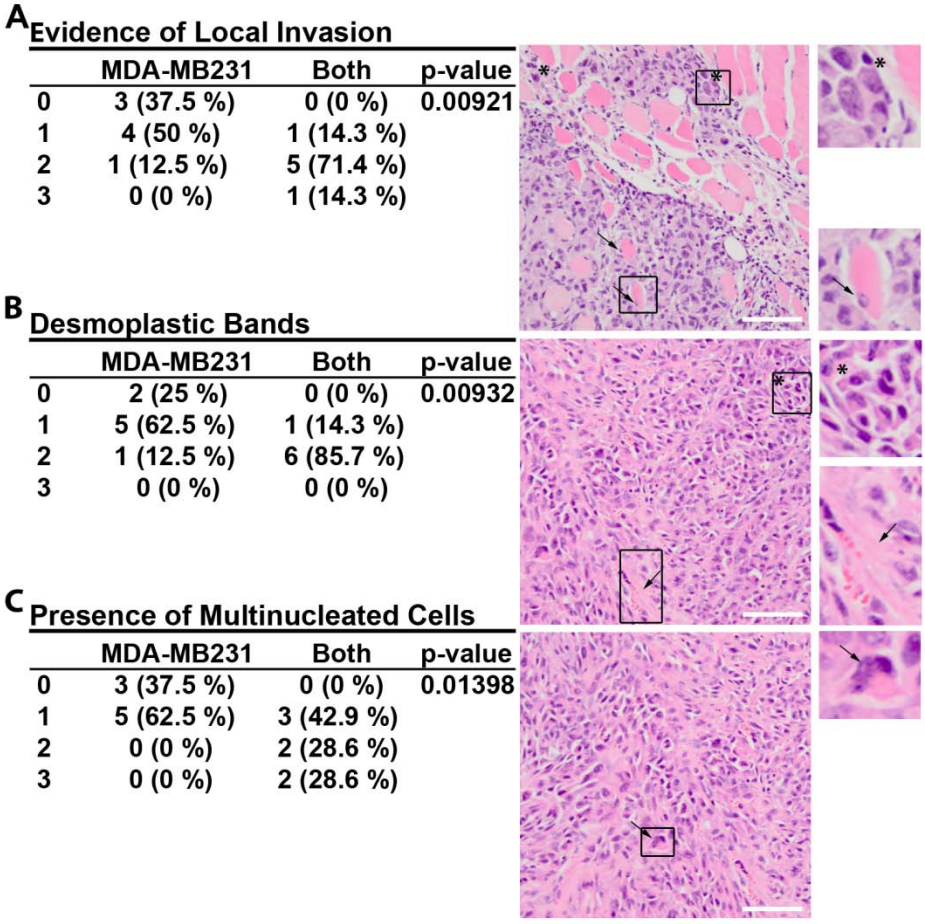

Figure 4.10 ASCs modulate tumor progression *in vivo*

Representative H&E sections of tumors resulting from co-injection of ASCs and MDA-MB231 cells (Both) (n = 7) or MDA-MB231 cells alone (n = 8) scored for pathological features of malignancy are shown (Scale bar = 40 μm). P-values were calculated from the total population of scores for each section type. (A) Co-implanted tumors exhibited enhanced local invasion relative to MDA-MB231 tumors as evidenced by indistinct tumor boarders. Tumor cells infiltrated and separated skeletal myofibers (*) and

often surrounded atrophic skeletal myofibers (→). (B) Enhanced desmoplasia in the co-implanted group was evident as variably sized, pale to brightly eosinophilic, loose bands of connective tissue (→) scattered within the tumor. Additionally, rossettes (*) which indicate an anaplastic phenotype in tumors, were evident in the co-implanted tumors. (C) Multinucleated tumor cells (→), indicating the breakdown of cell division machinery, are also more evident in the co-implanted tumors as compared to MDA-MB231 tumors alone.

To correlate variations in tumor growth with differences in myofibroblast differentiation, immunohistochemical analysis was performed, which confirmed that the density of α-SMA myofibroblastic cells (Figure 4.9B) was increased in tumors originating from co-injection of both cell types rather than tumor cells alone. Circulating ASCs can be recruited to and associate with blood vessels in the form of α-SMA pericytes (204). In our co-implantation studies, however, immunohistochemical analysis of desmin, a pericyte marker (205), verified that the majority of α-SMA positive cells were myofibroblasts rather than pericytes as desmin staining showed no significant difference ($p=0.33$) between co-implanted and control tumors. Nevertheless, blood vessel density was greater in the co-implantation group (Figure 4.9C), and ELISA of tumor lysates suggested that ASC/myofibroblast secretion of pro-angiogenic VEGF and IL-8 (174, 195) may have contributed to these differences (Figure 4.11).

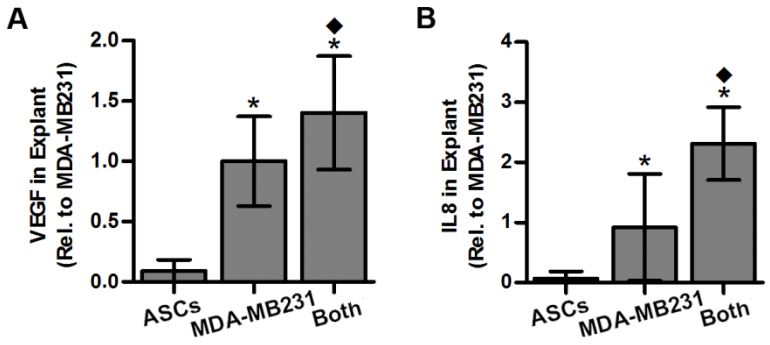

Figure 4.11 ASCs increase pro-angiogenic factor levels in tumors

(A) VEGF and (B) IL-8 content was enhanced within tumors containing ASCs as compared to those from only MDA-MB231 cells as revealed by ELISA of lysates. * $p < 0.05$ from ASC condition; ♦ $p < 0.05$ from MDA-MB231 condition. ASC (n = 6), ASC/MDA mixture (n = 6), and MDA (n = 12) implants were analyzed.

To evaluate if varied myofibroblast content correlated with increased stiffness, we determined the mechanical properties of the different tumors via DMTA compression tests on tumor sections, in the elastic regime of deformation. The mean Young's modulus (*E*) was more than 50% higher in tumors generated by co-implantation of ASCs than in those generated in the absence of ASCs (3.1 ± 1.2 kPa vs. 2.0 ± 0.8 kPa, $P < 0.04$) (Figures 4.9D and 4.12). Data from the full elastic and plastic regime of deformation (Figure 4.12B) additionally indicated that tumors from the co-implanted group exhibit both higher stiffness and a smaller range of elastic (reversible) deformation than tumors grown without ASCs. Consistent with these results, tumors resulting from co-injection contained more procollagen I and collagen (Figures 4.13A, B), were characterized by enhanced collagen fibril maturity and linearity (Figures 4.13C, D), and likely also comprised increased fibronectin (93). Such changes are indicative of enhanced desmoplasia and aggressiveness (73) and may further contribute to ASC-mediated changes in tumor growth; decellularized matrices of TCM-preconditioned adipose progenitors increased tumor cell growth relative to matrices from control cells in a manner dependent on generation of cytoskeletal tension

(Figure 4.13E). Nevertheless, additional conditions including paracrine signaling between ASC-derived cells and tumor cells may also contribute to the observed changes in tumor growth in our studies (123).

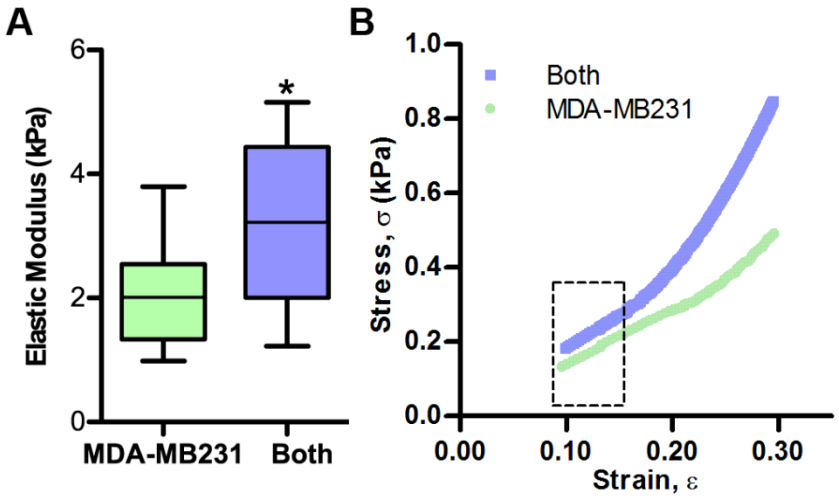

Figure 4.12 ASCs increase tumor stiffness

Tumors formed *in vivo* by MDA-MB231 alone (MDA-MB231) or MDA-MB231 in the presence of ASCs (Both) were analyzed for stiffness via DMTA of cross-sections in PBS at room temperature (n = 8-18). (A) The lines within the boxes indicate the mean Young's modulus for each condition, while the colored boxes span the 25th to 75th percentile. The whiskers correspond to the maximum and minimum measured Young's modulus values. The mean Young's modulus of the tumor sections from the co-implanted group (Both = 3.1 ± 1.2 kPa) is approximately 50% higher than that of the sections from the tumors grown without ASCs (MDA = 2.0 ± 0.8 kPa). (B) DMTA mean stress-strain profiles of tumor sections over the full regime of elastic and plastic deformation (n = 4-9). The boxed-in area corresponds to the low-strain (9-14%) regime from which the Young's moduli (shown in A) were extracted. Tumors from the co-implanted group (Both) exhibit not only higher moduli but also a smaller range of elastic deformations, i.e., earlier onset to plastic deformation than tumors grown without ASCs (17% versus 23%), and more pronounced stiffening prior to rupture, as indicated by the steeper stress-strain slope at high strains in the co-implanted group. * $p < 0.05$ from MDA-MB231.

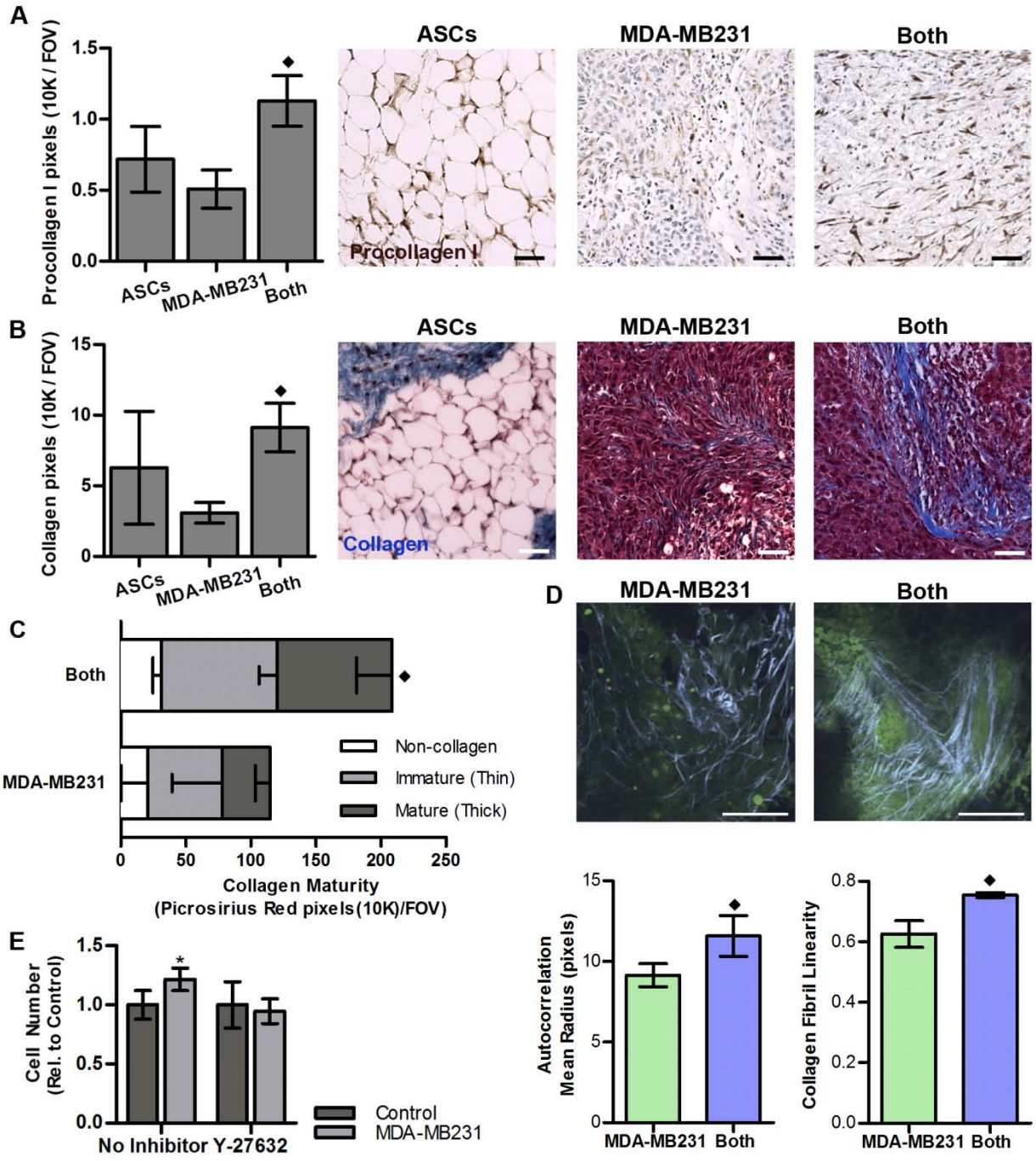

Figure 4.13 ASCs enhance tumor growth by modulating collagen deposition and structure

(A) Immunohistochemical analysis of tissues subjected to co-injection of ASCs and MDA-MB231 cells (Both) or either cell type alone indicated increased collagen synthesis with co-injection, as indicated by greater levels of the precursor type I procollagen (brown). (B) Masson's Trichrome staining confirmed greater collagen deposition (blue) in tumors formed by both ASCs and MDA-MB231 cells as compared

to tumors formed by MDA-MB231 only. For procollagen I and collagen image analysis, ASC (n = 6), ASC/MDA mixture (n = 6), and MDA (n = 12) implants were analyzed (Scale bar = 20 μm). (C) Images captured from picrosirius red-stained cross-sections via polarized light microscopy (as shown in Figure 4.9E) were analyzed for non-collagen (white), immature/thin collagen (green), and mature/thick collagen content. Co-implanted tumors (Both) contained more mature collagen fibrils than control tumors. (D) A 2D spatial autocorrelation analysis based on SHG images showed that the average collagen framework size (autocorrelation mean radius) in the ASC-containing tumor explants (Both) was significantly greater than their counterparts (MDA-MB231) (Scale bar = 100 μm). Additionally, analysis of fibril linearity (a ratio of the shortest distance to the full-length between fibril ends) indicated that collagen fibrils in tumors from the co-implantation group (Both) were straighter than those from control tumors. For picrosirius red and SHG image analysis, MDA-MB231/ASC (n = 3) and MDA-MB231 (n = 3) explants were analyzed. (E) MDA-MB231 grew more on decellularized matrices from MDA-MB231-conditioned 3T3-L1 than matrices from 3T3-L1 preconditioned with control media. These differences were related to varied cytoskeletal tension as treatment with the pROCK inhibitor Y-27632 inhibited this effect (n = 6). ♦ $p < 0.05$ from MDA-MB231 condition; * $p < 0.05$ from control.

4.6 Conclusions:

Breast cancer cell signaling may undermine normal ASC function to form a physicochemical microenvironment that promotes tumorigenesis. Epidemiologically, controversy still exists as to whether fat grafting procedures contribute to recurrence of breast cancer (206). Our findings suggest this possibility and long-term follow up studies will be needed in which not only the use of ‘simple’ fat, but implants concentrated with ASCs are evaluated. Additionally, the results presented herein provide a possible explanation for why obesity - associated with an increased pool of ASCs - represents a risk factor for breast cancer (207, 208), and highlight novel design parameters for ASC-based breast reconstruction. Specifically, ASCs are frequently applied using relatively rigid biomaterial scaffolds or hydrogels (209,

210), but vehicles mimicking the mechanical properties of adipose tissue and potentially co-delivery of morphogens are needed to ensure adipose tissue functionality. In particular, PPARγ agonists may represent attractive candidate molecules due to their ability to promote adipogenesis, while inhibiting myofibroblast differentiation (191). Determination of whether tumor-related changes of ASC functions are due to selective mechanisms or cell fate instruction will also be needed to help increase the safety of such applications. Although the goal of the present study was to better define the physicochemical contributions of ASCs to breast cancer, a variety of other cancers may also depend on such phenomena. Because ASCs can be activated and released into the circulation to participate in tumor progression at spatially distinct sites they may, for example, impair the prognosis of prostate (211) and colorectal cancer patients (212). Collectively, therapeutic application of ASCs independent of site should be carefully considered in patients previously treated for cancer, and the use of cell delivery vehicles accurately mimicking non-tumorigenic microenvironmental conditions should be a prerequisite.

4.7 Acknowledgements

Dr. David Infanger for aid in manuscript preparation, Kerstin Höger, Ana Martin-Ryals, and Christina Cossell for experimental aid, and Andrea Flesken-Nikitin for help with animal experiments.

CHAPTER 5

CONCLUSIONS

This body of work presents findings on the role of ASCs in breast tumorigenesis. These findings are broadly applicable to both the fields of regenerative tissue-engineering as well as cancer biology. The response of ASCs to signals derived from tumors in the form of soluble secreted molecules and extracellular matrix (ECM) stiffness was measured to assess whether changes in ASC behavior as a result of these signals could contribute to produce a pro-tumorigeneic microenvironment. As ASCs are found within the local host tissue surrounding breast tumors, gaining an understanding of the changes in their behavior when signaled by tumors may provide insight into potential therapeutic targets. Furthermore, the regenerative potential of ASCs is immense; however, without a complete understanding of the potential of these cells, implanted ASCs may have detrimental off-target outcomes. Three main questions were addressed through this work to analyze the changes in the behavior of tumor associated (TA-) ASCs as outlined in the sub-hypotheses in section 1.8.

5.1 ASCs promote tumor stiffening by altering the composition of the ECM

Initially, the ability of TA-ASCs to alter the fibronectin (Fn) ECM structure and composition as a result of tumor-derived chemical cues was assessed. To this end, both biochemical assays and fluorescence resonance energy transfer (FRET) techniques were implemented to measure Fn density and conformation (Chapter 2). Additional work looking at the altered collagen composition and structure within the tumor-ECM in the presence of ASCs was presented in Chapter 4. This work together indicates that as hypothesized, ASCs do promote tumor stiffening by altering the composition and structure of the ECM.

For the initial study, changes were seen in the Fn ECM produced by ASCs in response to tumor-derived chemical cues. More specifically, the amount of Fn within an *in vivo* model of human ASCs and

an *in vitro* model of mouse 3T3-L1preadipocytes was increased in the presence of breast tumor. After seeing an enhancement to the Fn density within tumors due to TA-ASCs, further investigations into the protein conformation were conducted. These studies showed conformational changes to this Fn matrix. FRET analysis indicated that the Fn within TA-3T3-L1-derived matrices, as compared to normal 3T3-L1-derived matrices, was in a more unfolded conformation. This work shows that phenotypic changes in ASCs that occur as a result of tumor-derived chemical cues lead to increased unfolding of Fn, which results in overall Fn fiber stiffening. While we can directly correlate Fn conformation to fiber stiffness, in this work we do not directly show that this results in a total matrix stiffening. TGF-β, which is secreted at high levels by many breast cancer cells, was largely responsible for this phenotypic change in the 3T3-L1 behavior and resultant Fn matrix changes. In addition to Fn matrix changes, TA-ASCs were also shown to produce a more collagen rich tumor ECM, full of elongated fibrils. Stiffness measurements, as shown in Figure 4.12, further confirm that the presence of ASCs does lead to stiffer tumors, which is likely due to the aforementioned ECM protein changes. With an indication that TA-ASCs contribute to tumor stiffening, further analysis of the impact that tissue stiffness has on the function of ASCs was necessary.

5.2 Enhanced tissue stiffness, as seen in tumors, alters ASC function

Next, the ability of the enhanced tissue stiffness as seen at the tumor-host interface to signal these host tissue cells was assessed using a novel photo-crosslinked alginate system (Chapter 3). Additional experiments using Ca^{2+} cross-linked alginate gels as well as polyacrylamide gels in Chapter 4 also show that, over the range of normal to malignant breast tissue stiffness, the behaviors of ASCs is altered. This work confirms the second sub-hypothesis that the enhanced tissue stiffness, as seen in tumors, does alter ASC function.

To enable measurement of the impact of ECM stiffening on the behavior of ASCs, independent of other changes within the ECM that occur when tissue density is increased, namely augmented cell adhesion site density, a novel photo-crosslinked alginate gel system was developed. This is in contrast to

Ca^{2+}-crosslinking methods generally implemented (as used in Chapter 4) where varying polymer concentrations are used to modify stiffness, and thus lead to differences in adhesion site density though conditions. By seeding 3T3-L1 cells within these alginate gels of stiffness ranging from that of normal to malignant breast tissue, changes in ASC behavior as a function of ECM stiffness were studied. The combination of studies presented in Chapters 4 and 5 show that over this range of tissue stiffness, ASC behavior is altered. Specifically, increased stiffness enhances proliferation and pro-angiogenic secretion of ASCs while diminishing differentiation into the mature cell type of adipose tissue, adipocytes. Furthermore, these changes are dependent on the utilization of the Rho/ROCK signaling pathway.

These findings have significance for a variety of ASC applications ranging from the design of scaffolds for regenerative approaches to the impact of TA-ASCs within stiff ECMs as seen at sites of inflammation and disease. When utilizing ASCs for tissue-engineering applications, one must consider the stiffness of the implanted material and/or the tissue surrounding the implantation site to ensure that the ASCs remain efficacious. Additionally, with the potential for these cells to contribute to tissue changes as a result of stiffness, their role at the sites of inflammation and diseases like cancer where enhanced stiffness is a hallmark of the disorder, should be more clearly delineated. In order to more fully capture the role of ASCs in breast tumorigenesis, a comprehensive assessment of the ability of these cells to alter the tumor stroma was then further examined.

5.3 The physicochemical cues of breast tumors promote ASC pro-tumorigenic behaviors

In a final comprehensive assessment, the ability of ASCs to assume a myofibroblastic phenotype within the tumor microenvironment and thus contribute to the desmoplastic response in tumors was measured (Chapter 4). This change in ASC phenotype was due to the combination of chemical and mechanical cues from breast tumors and as stated in the third and final sub-hypothesis these tumor-derived cues do enhance the pro-tumorigenic behavior of ASCs. In total, these studies indicate that physicochemical cues within the breast tumor microenvironment produce a pro-tumorigenic phenotypic

change in ASCs.

To rigorously assess the role of ASCs in altering the tumor stroma, ASCs were cultured in conditions to mimic both the chemical and mechanical cues that TA-ASCs would encounter. Notably, the soluble factors produced by tumor cells initially lead to changes in ASC behavior similar to those seen in response to enhanced tissue stiffness. With further investigation, we showed the ability of TA-ASCs to assume a myofibroblast phenotype, in a TGF-β-dependent manner, and further stiffen the ECM through deposition and matrix contraction. This was consistent with the findings of increased Fn fiber stiffness in the matrices of TA-3T3-L1 cells (Chapter 2). Furthermore, the ability of these cells to then respond to these chemical cues was heighted in the presence of the increased stiffness of malignant breast tissue. To ensure the relevance of these *in vitro* findings, an orthotopic murine model was used which further verified that TA-ASCs contribute to tumor growth and stiffening. These cumulative results indicate that ASCs are induced to take on an altered phenotype in response to tumor-derived chemical and mechanical cues and this phenotypic change further propagates the production of a pro-tumorigenic microenvironment through a positive feedback loop mechanism (Figure 5.1).

As a result of this work the scientific community has gained a greater appreciation for the role that chemical and mechanical cues play in altering the function of ASCs. In the context of tissue-engineering, these findings indicate that ASC differentiation and pro-angiogenic behaviors can be controlled in part through the mechanical character of a material. As the vascularization of implants and the production of the cells types of interest are the keys to regenerating tissues, harnessing this knowledge can aid in our ability to utilize ASCs for the production of replacement tissues. However, this should be done carefully as we have furthermore shown that these cells can contribute to producing a microenvironment conducive to tumor growth. As we now know that these cells contribute to changes in the ECM composition, structure, and stiffness, additional work should be carried out to asses exactly how these changes stimulate tumors. With a more thorough mechanistic understanding of the ASC-tumor communications, the ability to target these interactions would be possible for the purpose of anti-cancer therapeutics.

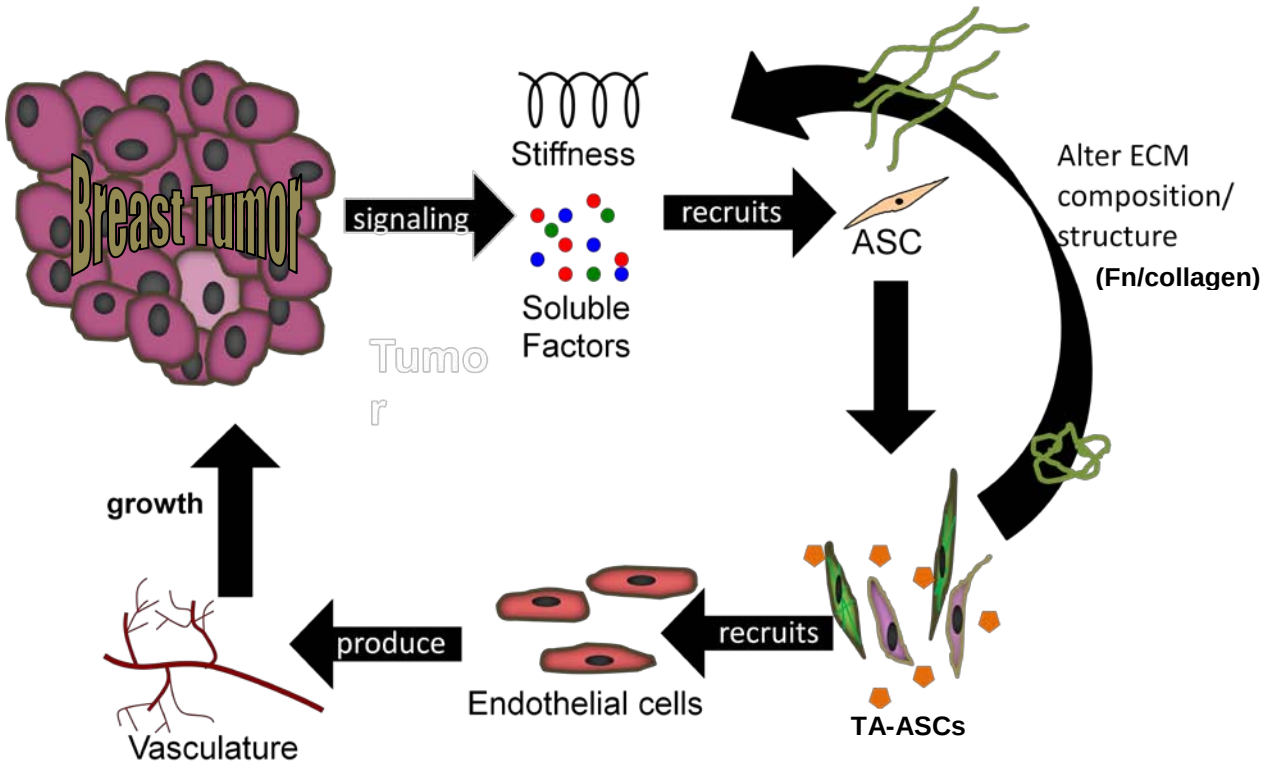

Figure 5.1 Alterations in ASC function within tumor microenvironment

Enhanced tissue stiffness and changes in local signaling molecules are characteristic features of the tumor microenvironment. As cells respond to both chemical and mechanical cues, adipose-derived stem cells (ASCs) assume an altered tumor associated (TA-) phenotype in response to these cues, as would be experienced at the breast tumor-host mammary tissue interface. Namely, these cells take on a more myofibroblastic phenotype producing a denser extracellular matrix (ECM) of fibronectin (Fn) and collagen, within which both proteins are in a more extended form. These TA-ASCs additionally assume a more pro-angiogenic phenotype which contributes to tumor growth by increasing tissue vascularization. In addition to altering ASC function, the ability of the TA-ASCs to enhance tissue stiffness advances the pro-tumorigenic capacity of the tumor stroma as increasing stiffness promotes angiogenesis(50) and tumor cell malignancy(51).

5.4 Future Directions

This dissertation has provided great insight into the changes that occur in ASCs due to altered mechanical and chemical cues as would be encountered within the tumor microenvironment. While making progress in our understanding of the role of stem cells in breast tumorigenesis, the results presented herein broaden our perspective by illuminating additional scientific questions deserving of experimentation. The tumor is an extremely embrangled tissue that requires simplification for the purpose of dissecting out the role of various components; however, once individual constituents have been resolved, the larger, more complicated system must be considered. Future endeavors should entail both of these approaches, by both delving in more depth into the signaling pathways leading to the changes noted as well as by looking further into additional methods of signaling not addressed within this work.

Propagation of signals due to altered ECM

In this dissertation the enhanced ability of the altered ECM to further promote tumor growth was only peripherally investigated. Results shown in Figure 4.13E indicate that these stiffer ECMs do enhance tumor cell growth; however, more extensive studies into other behavioral changes as well as the signaling mechanisms are needed. Initially, the *in vitro* findings indicating an altered Fn conformation within the tumor stroma should be confirmed within *in vivo* samples. Moreover, the ability of this Fn to signal surrounding cells through means independent of the increased stiffness of the fiber should be assessed. These distinct methods may include the exposure of cryptic binding sites resulting in changes in the overall ECM assembly. Indeed, as Fn and collagen work in concert to produce the ECM (75), the combination of the increased Fn and collagen within the TA-ASC ECM likely alters cell-ECM signal propagation throughout the tumor microenvironment. For example, the elongated Fn may decrease the ability of cells to use the $\alpha_5\beta_1$ integrin due to increased spacing between the synergy and RGD adhesion sites which could propagate the pro-angiogenic phenotype by enhancing alternative integrin engagement

(e.g. $\alpha_v\beta_3$). While work has been done to show that stiffness and collagen cross-linking promote tumor malignancy (51, 73), additional work to fully elucidate ECM protein compositional control of tumor microenvironmental signaling in both normal and malignant cells is necessary. Lastly, as cell-ECM interactions have been shown to contribute to fibroblast activation (23), determining whether the changes that TA-ASCs make to the ECM contribute to myofibroblast differentiation would highlight an additional feedback mechanism being utilized within this system.

Therapeutic targets

With an improved understanding of the key signaling pathways involved in tumorigenesis, we are better able to rectify the mechanisms that tumors use to enable their growth leading to the eventual demise of the organism of origin. Here, we have shown that tumor-derived chemical cues, specifically IL-8 and TGF-β, promote the myofibroblastic phenotype and that this further leads to ECM changes which promote tumor stiffening. This would suggest that a combinatorial targeting of these molecules could reduce tumor desmoplasia and inhibit the downstream signals resultant from these ECM alterations. Although some TGF-β therapies are currently being studied (213), including other molecules that may target the same pathway and finding an approach to reduce off-target consequences as TGF-β is an abundantly utilized growth factor are critical. Additionally, incorporation of an anti-angiogenesis therapeutic (29) with these anti-desmoplasia approaches may prove even more beneficial.

Deciphering the role of direct cell-cell communication

As outlined in section 1.4, cell-cell signaling is an important communication means within the tumor microenvironment. The studies presented here have largely focuses on chemical and mechanical signaling; however, as enhanced recruitment of ASCs to the tumor is seen (Figure 4.3D), more analysis of the behavior of these cells when in direct contact with tumor cells is necessary. As cell-cell junctions play a key role in cellular communication and, in particular myofibroblast differentiation (24), further

work evaluating this signaling means between these cell populations would elucidate the role of this communication in this system and whether this too might be a potential therapeutic target.

Altered mechanotransduction in TA-ASCs

A final avenue of investigation that might prove worthy of study is experimental analysis of whether TA-ASCs assume an altered mechanotransducing pathway. As the glycocalyx is known to be altered within tumor (214), gaining an appreciation for how differentiation of ASCs towards a TA-ASC phenotype may change this mechanotransduction pathway as well as others, could prove to elucidate additional pathways which are changed within TA-ASCs that may aid in their ability to promote tumor growth. As an initial means of assessment, one could simply study whether the traction forces of TA-ASCs are altered as compared to normal ASCs, which would be a likely result of an altered glycocalyx, and then delve into the mechanisms through which the cells is able to achieve this result.

CHAPTER 6

CLIMB GK-12 EXPERIENCE: AN INQUIRY-BASED APPROACH TO TEACHING FUNDAMENTALS OF POLYMERS FOR TISSUE ENGINEERING

Submitted to *The Science Teacher* (215) on June 11, 2012

6.1 Contributors

Co-authors to this work made the following contributions: Ann Phinney-Foreman, the science department head at Waverly High School, provided a classroom filled with students eager to conduct inquiry-based experiments. Shivaun Archer, co-leader of the GK-12 CLIMB program, provided assistance in the design of the experiments and preparation of the manuscript. Claudia Fischbach aided in the preparation of the manuscript describing these experiments.

6.2 Introduction

Currently, when patients are in need of new joints, organs, or other tissues the most common sources are either donors or man-made materials. However, the use of donor tissues is limited by availability, which is why more than 7,000 people die each year while waiting on organ transplant lists (based on Organ Procurement and Transplantation Network data as of April 6, 2012). Alternately, material implants are only available for certain applications and their longevity is often not equal to naturally repaired tissues (216, 217). For these reasons scientists have continued to explore our ability to generate replacement tissues through sophisticated cell culture techniques since the inception of the term *tissue engineering*, nearly a quarter-century ago (218). While some tissue-engineered products like the bi-layered Apligraf® skin substitute have made it to market, research into engineering a wide variety of other tissue types is still ongoing. In order to create tissue engineering products for clinical applications biomaterials scaffolds are frequently combined with the cells that make-up a tissue of interest. These

scaffolds can provide cells with an appropriate physicochemical environment to enable them to recreate *in vivo*-like tissue constructs. For example, Apligraf® consists of a biomaterials matrix that allows cells to grow both within and on top to appropriately mimic the different layers of the skin.

A variety of polymers, both natural and synthetic are used as biomaterials for scaffold fabrication. In particular, hydrogels, which are simply hydrophilic polymer chain networks within which a large amount of water is dispersed, are often explored because these systems mimic the extracellular matrix (ECM) surrounding cells within the body. For example, collagen, an abundant ECM component, is routinely utilized in tissue engineering applications due to its relative ease of isolation and ability to instruct physiologically relevant cell behavior. However, collagen isolation underlies batch to batch variations and is relatively expensive, and thus other natural polymers are frequently researched for tissue engineering approaches. Alginate, one such polymer, is derived from algae and used frequently as a food additive, which makes it a safe, affordable material for study in the classroom that forms a gel as ionic bonds are formed between the polymer chains similar.

We have designed an inquiry-based activity, which allows students to explore hydrogel materials properties in the context of tissue engineering. While exploring the mechanisms through which alginate is able to transition from a polymer in solution to a formed gel, students are able to learn about both the chemistry of polymer cross-linking and how hydrogels can be used as innovative biomaterials to improve human health. Initially, students explore methods of polymerizing a solution of alginate into a gel and then study how to adjust the mechanical properties of the resultant hydrogel for different applications. By adjusting the stiffness of the hydrogel, students can learn the importance of modeling tissue stiffness for the purposes of tissue engineering. This activity covers the NY State learning standards (http://www.p12.nysed.gov/ciai/mst/sci/ls.html) - Analysis, Inquiry, & Design; Apply Scientific Concepts to Physical Setting; Relate Math, Science, & Technology as well as highlights concepts in ionic bonding.

6.3 Experimental Details

Concept Introduction

This activity was collaboratively designed by a New York State high school chemistry teacher and a Cornell University biomedical engineering graduate student. The concepts of tissue culture and ECM should be briefly reviewed. A PowerPoint presentation to introduce the necessary material can be found online (http://climb.bme.cornell.edu/biomaterials.php). Although a brief description is provided, further background on the topics of tissue culture and the ECM are described elsewhere (219-221). These materials enable students to become familiar with real world applications that apply concepts covered in the activity. In the review, students should be made aware that tissue culture (or cell culture) is when cells are grown outside the body and separate from the organism from which they originate. Tissue culture is often done by placing cells in plastic dishes and maintaining them in liquid media which provides the nutrients necessary for the cells to survive and grow. When in culture, these cells are generally maintained without the natural ECM in which they would be found in tissues. The ECM, or the portion of a tissue which is not contained within a cell, is scaffolding on which cells are provided support and structure enabling their growth. As researchers begin to better understand how cells interact with the ECM, the need to culture cells using different materials which better mimic the natural ECM within which the cells would be found in the body is more apparent (218). As the ECM is naturally composed of polymers like collagen, other natural polymers are used to create artificial ECMs for tissue culture, hence the use of hydrogels.

Students are also introduced to the concept of polymers as long-chain molecules composed of repeating units referred to as monomers. The polymer of interest in this experiment, alginate is a block co-polymer of mannuronic and guluronic acid. As can be seen in the chemical structure of alginate, the guluronic monomers stick out from the chain more (Figure 6.1A) and are the units which allow the polymer chains to bond and form cross-links by a divalent cation linking 2 chains together (Figure 6.1B). The objective of this activity is for students to design and carry-out investigations that will aide in their

understanding of polymer cross-linking and hydrogel formation. Their design must include an activity to quantify some mechanical characteristic of the crosslinked polymer, and will require organizing and representing their data using Excel software.

Materials and Teacher Preparation

Handouts to accompany this activity can be found online (http://climb.bme.cornell.edu/biomaterials.php). Prior to the initial hands-on activity, sufficient alginate solution should be prepared noting that each student/group should not require more than 10 mL. For a total of 20 groups, 200 mL of alginate solution should be prepared and left stirring overnight to enable complete dissolution. To produce a 4 % (w/v) solution, slowly add 8 g alginate (FMC Biopolymer) to 200 mL de-ionized (DI) H_2O stirring on a stir plate. Once the alginate is dissolved the solution will be very viscous. In order to better visualize the gel, simple food dyes can be added to the alginate solution. Univalent and divalent cation-containing solutions of 0.1 M NaCl, KCl, $CaCl_2$, and $Ba(NO_3)_2$ in DI H_20 are prepared as the potential cross-linking solutions. For the second portion of the activity where the importance of cross-link density on the stiffness of the alginate is determined cross-link density will be adjusted by varying (i) ion concentration with 0.1 mM, 0.001 M, 0.01M 0.1 M, and 1 M of $CaCl_2$ and $Ba(NO_3)_2$ and (ii) polymer concentration with 0.5, 1, 2, 3, and 4 % w/v solutions of alginate all prepared as described above. As the methods implemented to measure stiffness are largely designed by students, additional supplies necessary are outlined by each student. This may include items such as trays, markers, rulers, weights, timers, and circular molds.

Uncovering the process of cross-linking

Students are provided a 4% (w/v) solution of alginate and potential cross-linking solutions containing univalent and divalent cations. They then devise an experimental approach to determine which of the univalent and divalent solutions cause the polymer solution to gel (Figure 6.2a). After

visualizing solid gels forming only in the presence of the divalent cations, students are able to deduce that divalent cations are necessary for alginate to cross-link into a hydrogel network (Figure 6.2b). This is because of the relatively strong ionic interactions between the carboxylic groups from two alginate chains and the Ca^{2+} or Ba^{2+}. A discussion of the activity can further clarify this phenomenon for students as outlined by the questions in Figure 6.3.

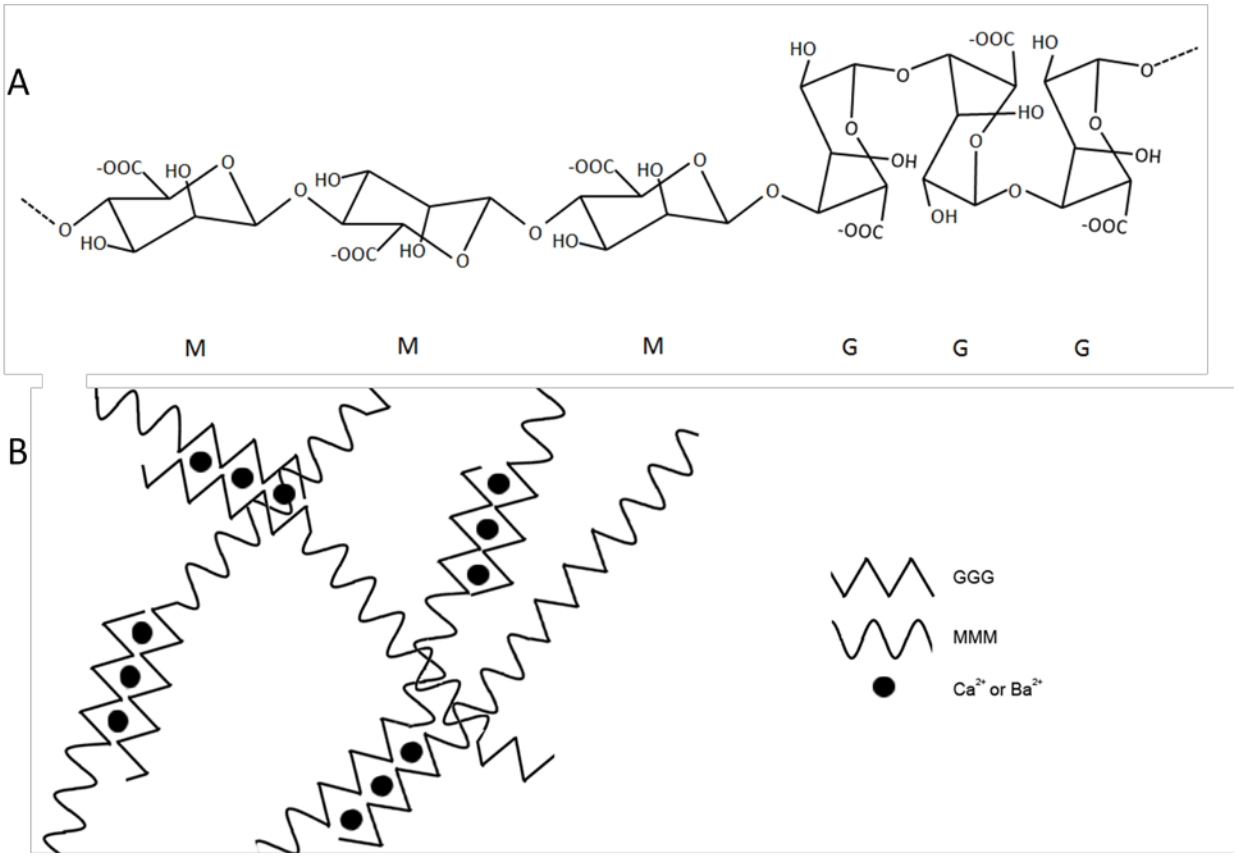

Figure 6.1 Alginate Structure

Alginate is a block co-polymer composed of guluronic (G) and mannuronic (M) acid monomers which are linked in a 1,4 configuration as shown (A) . When divalent cations are added to the guluronic acid monomers, the individual alginate chains are able to create cross-links between the chains, and an intertwined polymer gel is produced (B) which can contain a large amount of water, leading to the term 'hydrogel'.

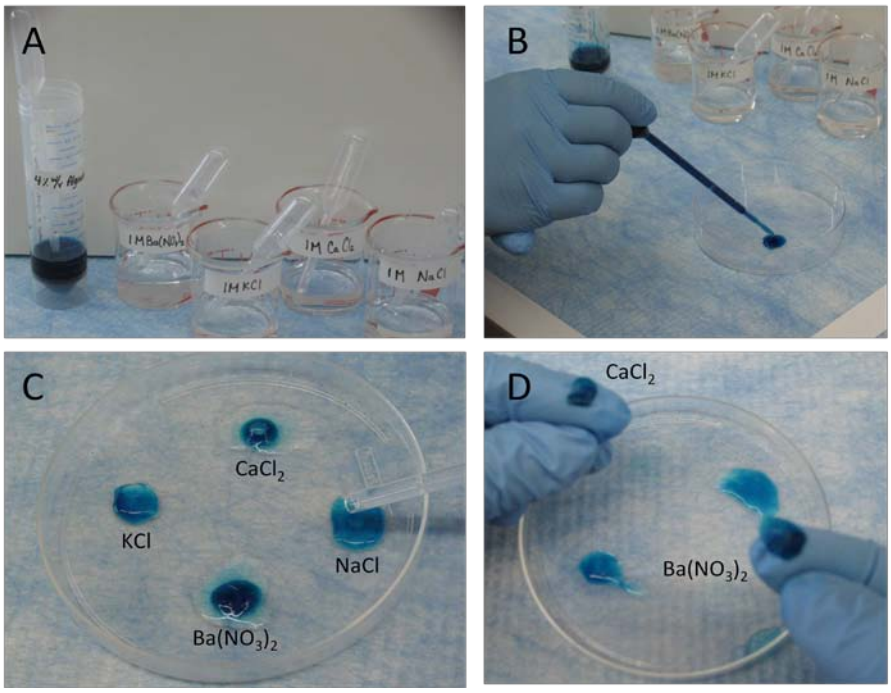

Figure 6.2 Determination of Cross-linking

Each experimental group is provided a 4% (w/v) alginate solution, in this case dyed blue to enable easy visualization, along with all the potential cross-linking solutions (A). By devising a method to simply (B) drop the alginate into a dish and then (C) add each potential cross-linker, students can determine that (D) only when a divalent cation is added to the alginate does the polymer solution gel.

- What changed about the alginate solution when it cross-linked? Why would this occur?
- Which solution(s) caused the alginate to cross-link? Why did this/those solution(s) cause alginate cross-linking? What type of interaction is causing this cross-linking?
- Given that you have now worked with alginate, why do you think that this material might be commonly used in cell culture? There are many reasons, so try to think of a few different reasons that this material might be good for this application.

Figure 6.3 Discussion of Cross-linking

To target the discussion of this activity on what happens when alginate is cross-linked; a few questions for class discussion are provided.

Understanding how cross-link density impacts hydrogel stiffness

Once students discover what is necessary for alginate to become a gelled polymer, the natural progression for the inquisitive student is to investigate how specific gel properties can be achieved by changes in this process. In order for students to delve into this experiment, a spectrum of solutions with varying concentrations of polymer or cross-linker is provided. To encourage inquiry-based investigative skills, students are simply provided a basic description of the supplies and told to develop a method to experimentally determine how the character of the gel is altered with changes in either cross-linker or polymer density. The one caveat to this is that however they choose to measure the gel stiffness it must be quantifiable on a graph. A proposal to students to experimentally determine this relationship is shown in Figure 6.4. Students develop a wide array of techniques to address this including measurement of the distance a polymer moves when placed on an incline following cross-linking or how much the gel deforms when exposed to an equal load (e.g. a small jar, Figure 6.5). After developing their own method, students are then able to better critique their methods to allow for improved measurements. As an example, some students found that when they applied a small amount of solution to a large drop of alginate the exterior of the hydrogel would cross-link while the interior would remain in solution causing it to burst like the Betty Crocker ® snack Fruit Gushers does when a force was applied to it. This then taught the students the alginate solution and crosslinker need to be mixed to properly form a homogeneous gel.

As you previously learned, both Ca^{2+} and Ba^{2+} will crosslink alginate. We would now like to explore how changes in crosslinker or polymer density alter the character of the resulting hydrogel. To do this, first outline the question you would like to ask (your hypothesis), then write-up an experimental plan to test that question, being sure to note what characteristic of the gel you will evaluate and how you will test for this. Try to ensure the method you use to collect data will allow for a graphical representation of your results.

Once you have developed a plan and discussed it with your instructor, complete your experimental plan and analyze your results. You will prepare a write-up of the lab including a graph of your results and discuss the significance of your findings to the use of this biomaterial as an artificial ECM. On the following page more specific details of the lab write-up are provided.
Further exploration: Should time permit, try to determine whether the ionic cross-links formed can be easily broken (i.e. can the alginate hydrogel turn back into an un-gelled solution?).

Figure 6.4 Changes in the Hydrogel

A proposal to students to begin the activity on altering cross-link density will enable them to initiate the second experiment.

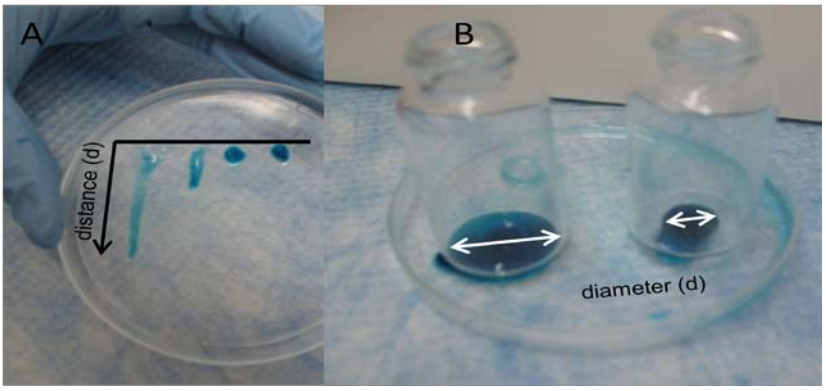

Figure 6.5 Altering Gel Stiffness

By maintaining polymer concentration while varying the concentration of cross-linking ions present, the resultant polymer can vary from dilute solution to rigid gel. Students can implement a variety of methods to measure this. (A) One commonly applied method included measuring the distance the gel traveled when placed on an equal incline, which was produced by simply inclining the plate containing the cross-linked gels. Alternately, students can perform the same test, but measure the time that the gel takes to travel a given distance. (B) Additionally, students chose to apply a given load, in this case a small bottle, to each gel and measured the amount of deformation or spreading that the gels underwent after application of the force.

Producing a Lab Report

An outline of the lab report where students describe their hypothesis and share results learned through this inquiry-based experiment is provided in Figure 6.6. In addition to writing a report, students can use Microsoft® Excel to produce plots of their collected data. This allows them to create a visual means through which they can share their results (Figure 6.7).

Please provide a lab write-up that covers the following questions:
Introduction – In paragraph format be sure to address the following questions:
- What is a polymer?
- How is a hydrogel formed?
- What is alginate?

Hypothesis – What is the question that you explored in your experiment?
Methods – In a step-by-step format describe what you did in the lab to test your hypothesis.
Results – Write a description of what occurred when you tested your hypothesis and provide a clearly labeled plot of your data using Excel.
Discussion – Discuss the following questions:
- Why it is important to understand how cross-linker and polymer concentrations alter hydrogel stiffness? If you were able to fit a trend line to your data, what does this say about this relationship?
- Why is this ability to alter stiffness useful when culturing different types of cells (for example bone vs. fat cells)?
- How might a cell's ability to move on these substrates of varying stiffness differ?
- If you wanted to prepare an artificial ECM for cell culture that was shaped like a particular tissue in the body (for example, the cartilage in the nose) how might you do this using alginate?

Figure 6.6 Lab Write-Up

By following this outline, students can write a lab report to summarize their findings and synthesize their lab data with applications for these materials.

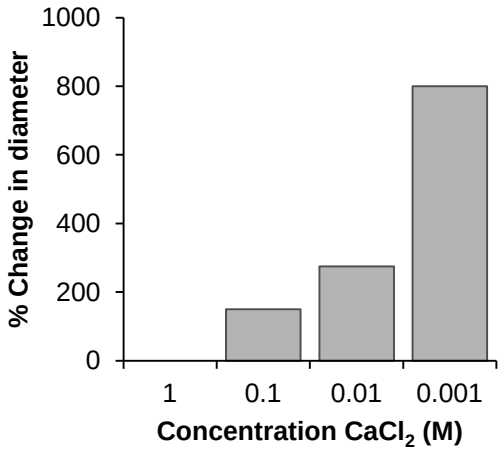

Figure 6.7 Plotting Experimental Results

By first casting gels in molds of a known diameter, the percent change in diameter of the hydrogel when under the same applied force was calculated and plotted.

Following this activity, students can present their results and discuss the role of hydrogel stiffness in tissue engineering as a class. In recent years scientists have found that cells behave very differently when they are cultured within a 3-D scaffold to encourage the production of a more true-to-life tissue. Hydrogels have been shown to be very beneficial for this purpose, and polymers like gelatin and alginate are often used for this approach. The hydrogel provides an aqueous cell environment within which media containing nutrients for cells to grow can easily reach the cells and waste produced by the cells can be removed. Researchers have found that the ability of cells to adhere and move in culture depends on ECM proteins and scaffold material, investigations into the role of the ECM have become much more diverse. In fact, recent work has demonstrated the importance of the matrix stiffness on the behavior of stem cells (49). Through the use of hydrogels, the stiffness of the scaffold on which cells are cultured can easily be adjusted to investigate the effect on cell behavior. Alginate is often used for this purpose, and through this lab students will learn the changes which occur when the material is cross-linked to form a gel and how to adjust this to produce matrices of variable stiffness.

6.4 Hazards

Gloves should be worn to avoid direct contact with barium containing solutions or alginate cross-linked with barium. For this reason, the second activity on understanding the link between cross-link density and stiffness can be performed with $CaCl_2$ solutions only.

6.5 Results and Discussion

This activity was implemented in both a high school AP Chemistry and Organic Chemistry course. Students in both classes showed great enthusiasm for the experiment, some even stated there was 'nothing' they would have changed. Student's knowledge in the area of polymers was greatly increased while gaining an appreciation for how these materials are applied for tissue engineering purposes. By establishing their own procedures, each student or group of students is provided a freedom not often experienced in the classroom. This can help to encourage the students to realize their own abilities and apply their knowledge to explore other topics. By performing a pre- and post- assessment of the students, the knowledge gained through these activities was measured. Students who knew little about polymers initially gained an appreciation for their structure and how they can be used to form hydrogels (Figure 6.8). Discussing a cutting-edge topic like tissue engineering engaged students to think about the broader applications for these materials and provided for great talking-points during the laboratory activity. Interestingly, many students stated that "trying to come up with the experiment" was the least enjoyable portion of the experiment, however students also said that "being able to create our own experiment" was the most interesting part of the activity as well. While freedom can be scary at first, students found it exciting to be able to develop their own experiments – an essential skill to become true scientists.

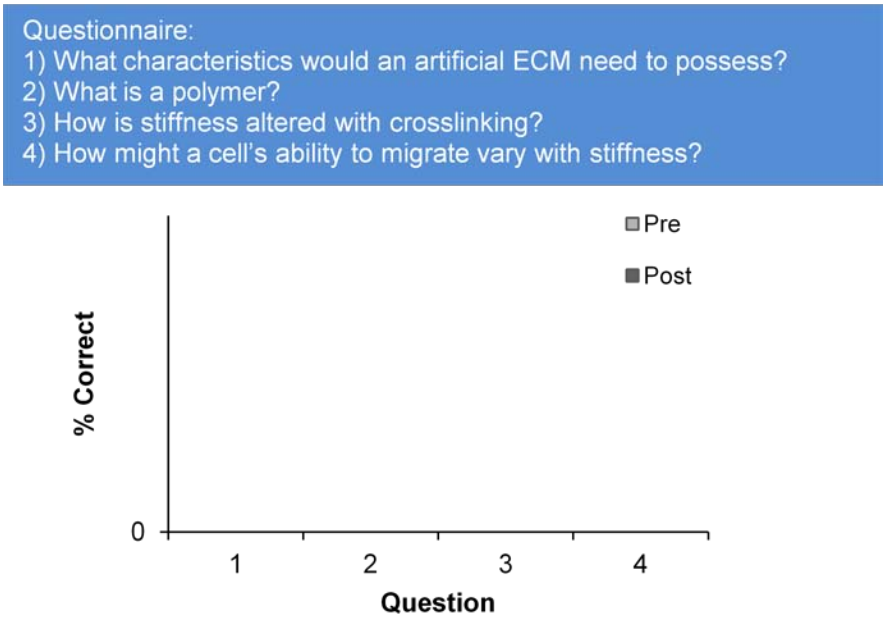

Figure 6.8 Student Impact

Students were provided a questionnaire including the listed questions both prior to and following the experiment. Their ability to answer the questions greatly improved following implementation of this activity, even on questions requiring a great deal of synthesis, like #4.

6.6 Conclusions

A simple inquiry-based experimental approach to introduce students to polymers as synthetic biomaterials that can be used to mimic the ECM is presented. This procedure can be implemented in a wide range of courses including chemistry, biology, or polymer science; however, the material is most suited for students in a course that covers the topic of polymer science. Initially students gain an understanding of how to cross-link alginate and then how to alter the hydrogel stiffness by varying the cross-link density. Students are then able to see an application for this material and gain an appreciation for how this and other polymers can be used to mimic the natural ECM, which spans a broad stiffness range from bone to fat tissue.

6.7 Acknowledgments

Funding for this work was generously provided by the Cornell's Learning Initiative in Medicine and Bioengineering NSF GK-12 grant, DGE 0841291.

REFERENCES

1. Society AC (2011) Breast Cancer Facts & Figures 2011-2012. ed American Cancer Society I (Atlanta).
2. Hanahan D & Weinberg RA (2011) Hallmarks of cancer: the next generation. *Cell* 144:646-674.
3. Siegel R, Naishadham D, & Jemal A (2012) Cancer statistics, 2012. *CA Cancer J Clin* 62:10-29.
4. Sant M, *et al.* (2003) EUROCARE-3: survival of cancer patients diagnosed 1990-94--results and commentary. *Ann Oncol* 14 Suppl 5:v61-118.
5. Hall JM, *et al.* (1990) Linkage of early-onset familial breast cancer to chromosome 17q21. *Science* 250:1684-1689.
6. Wooster R, *et al.* (1994) Localization of a breast cancer susceptibility gene, BRCA2, to chromosome 13q12-13. *Science* 265:2088-2090.
7. Sotiriou C & Pusztai L (2009) Gene-expression signatures in breast cancer. *N Engl J Med* 360:790-800.
8. Slamon DJ, *et al.* (2001) Use of chemotherapy plus a monoclonal antibody against HER2 for metastatic breast cancer that overexpresses HER2. *N Engl J Med* 344:783-792.
9. Mbeunkui F & Johann DJ, Jr. (2009) Cancer and the tumor microenvironment: a review of an essential relationship. *Cancer Chemother Pharmacol* 63:571-582.
10. Boyd NF, *et al.* (2007) Mammographic density and the risk and detection of breast cancer. *N Engl J Med* 356:227-236.
11. Joyce JA (2005) Therapeutic targeting of the tumor microenvironment. *Cancer Cell* 7:513-520.
12. Finak G, *et al.* (2008) Stromal gene expression predicts clinical outcome in breast cancer. *Nat Med* 14:518-527.
13. Kalluri R & Zeisberg M (2006) Fibroblasts in cancer. *Nat Rev Cancer* 6:392-401.
14. Mueller MM & Fusenig NE (2004) Friends or foes - bipolar effects of the tumour stroma in cancer. *Nat Rev Cancer* 4:839-849.
15. Fukumura D, *et al.* (1998) Tumor induction of VEGF promoter activity in stromal cells. *Cell* 94:715-725.
16. Brown LF, *et al.* (1999) Vascular stroma formation in carcinoma in situ, invasive carcinoma, and metastatic carcinoma of the breast. *Clin Cancer Res* 5:1041-1056.
17. Ronnov-Jessen L, Petersen OW, & Bissell MJ (1996) Cellular changes involved in conversion of normal to malignant breast: importance of the stromal reaction. *Physiol Rev* 76:69-125.
18. Aoyagi Y, *et al.* (2004) Overexpression of TGF-beta by infiltrated granulocytes correlates with the expression of collagen mRNA in pancreatic cancer. *Br J Cancer* 91:1316-1326.
19. Massague J (2008) TGFbeta in Cancer. *Cell* 134:215-230.
20. Evans RA, Tian YC, Steadman R, & Phillips AO (2003) TGF-beta1-mediated fibroblast-myofibroblast terminal differentiation-the role of Smad proteins. *Exp Cell Res* 282:90-100.
21. Shao ZM, Nguyen M, & Barsky SH (2000) Human breast carcinoma desmoplasia is PDGF initiated. *Oncogene* 19:4337-4345.

22. Strutz F, *et al.* (2000) Basic fibroblast growth factor expression is increased in human renal fibrogenesis and may mediate autocrine fibroblast proliferation. *Kidney Int* 57:1521-1538.
23. Zeisberg M, Strutz F, & Muller GA (2000) Role of fibroblast activation in inducing interstitial fibrosis. *J Nephrol* 13 Suppl 3:S111-120.
24. Clayton A, *et al.* (1998) Cellular activation through the ligation of intercellular adhesion molecule-1. *J Cell Sci* 111 (Pt 4):443-453.
25. Olumi AF, *et al.* (1999) Carcinoma-associated fibroblasts direct tumor progression of initiated human prostatic epithelium. *Cancer Res* 59:5002-5011.
26. Scott AM, *et al.* (2003) A Phase I dose-escalation study of sibrotuzumab in patients with advanced or metastatic fibroblast activation protein-positive cancer. *Clin Cancer Res* 9:1639-1647.
27. Pugh CW & Ratcliffe PJ (2003) Regulation of angiogenesis by hypoxia: role of the HIF system. *Nat Med* 9:677-684.
28. Folkman J (1971) Tumor angiogenesis: therapeutic implications. *N Engl J Med* 285:1182-1186.
29. Carmeliet P & Jain RK (2011) Molecular mechanisms and clinical applications of angiogenesis. *Nature* 473:298-307.
30. Fischbach C, *et al.* (2009) Cancer cell angiogenic capability is regulated by 3D culture and integrin engagement. *P Natl Acad Sci USA* 106:399-404.
31. Burstein HJ (2011) Avastin for breast cancer, 2005-2011: requiescat in pacem? *J Natl Compr Canc Netw* 9:1321-1323.
32. Samoszuk M, Tan J, & Chorn G (2005) Clonogenic growth of human breast cancer cells co-cultured in direct contact with serum-activated fibroblasts. *Breast Cancer Res* 7:R274-283.
33. Yang L, Pang Y, & Moses HL (2010) TGF-beta and immune cells: an important regulatory axis in the tumor microenvironment and progression. *Trends Immunol* 31:220-227.
34. Larsen M, Artym VV, Green JA, & Yamada KM (2006) The matrix reorganized: extracellular matrix remodeling and integrin signaling. *Curr Opin Cell Biol* 18:463-471.
35. Discher DE, Janmey P, & Wang YL (2005) Tissue cells feel and respond to the stiffness of their substrate. *Science* 310:1139-1143.
36. Verbridge SS, Chandler EM, & Fischbach C (2010) Tissue-engineered three-dimensional tumor models to study tumor angiogenesis. *Tissue Eng Part A* 16:2147-2152.
37. Berx G & Van Roy F (2001) The E-cadherin/catenin complex: an important gatekeeper in breast cancer tumorigenesis and malignant progression. *Breast Cancer Res* 3:289-293.
38. Bremnes RM, Veve R, Hirsch FR, & Franklin WA (2002) The E-cadherin cell-cell adhesion complex and lung cancer invasion, metastasis, and prognosis. *Lung Cancer* 36:115-124.
39. Apostolopoulou M & Ligon L (2012) Cadherin-23 mediates heterotypic cell-cell adhesion between breast cancer epithelial cells and fibroblasts. *PLoS One* 7:e33289.
40. Folkman J (2006) Angiogenesis. *Annu Rev Med* 57:1-18.
41. Butcher DT, Alliston T, & Weaver VM (2009) A tense situation: forcing tumour progression. *Nat Rev Cancer* 9:108-122.
42. Giancotti FG & Ruoslahti E (1999) Integrin signaling. *Science* 285:1028-1032.
43. Juliano R (1994) Signal transduction by integrins and its role in the regulation of tumor

growth. *Cancer Metastasis Rev* 13:25-30.
44. Lukashev ME & Werb Z (1998) ECM signalling: orchestrating cell behaviour and misbehaviour. *Trends Cell Biol* 8:437-441.
45. Bisanz K, *et al.* (2005) Targeting ECM-integrin interaction with liposome-encapsulated small interfering RNAs inhibits the growth of human prostate cancer in a bone xenograft imaging model. *Mol Ther* 12:634-643.
46. Jaalouk DE & Lammerding J (2009) Mechanotransduction gone awry. *Nat Rev Mol Cell Biol* 10:63-73.
47. Samani A, Bishop J, Luginbuhl C, & Plewes DB (2003) Measuring the elastic modulus of ex vivo small tissue samples. *Phys Med Biol* 48:2183-2198.
48. Kong HJ, Polte TR, Alsberg E, & Mooney DJ (2005) FRET measurements of cell-traction forces and nano-scale clustering of adhesion ligands varied by substrate stiffness. *Proc Natl Acad Sci U S A* 102:4300-4305.
49. Engler AJ, Sen S, Sweeney HL, & Discher DE (2006) Matrix elasticity directs stem cell lineage specification. *Cell* 126:677-689.
50. Mammoto A, *et al.* (2009) A mechanosensitive transcriptional mechanism that controls angiogenesis. *Nature* 457:1103-1108.
51. Paszek MJ, *et al.* (2005) Tensional homeostasis and the malignant phenotype. *Cancer Cell* 8:241-254.
52. Gimble JM, Katz AJ, & Bunnell BA (2007) Adipose-derived stem cells for regenerative medicine. *Circ Res* 100:1249-1260.
53. Sakaguchi Y, Sekiya I, Yagishita K, & Muneta T (2005) Comparison of human stem cells derived from various mesenchymal tissues - Superiority of synovium as a cell source. *Arthritis Rheum* 52:2521-2529.
54. Lyden D, *et al.* (2001) Impaired recruitment of bone-marrow-derived endothelial and hematopoietic precursor cells blocks tumor angiogenesis and growth. *Nat Med* 7:1194-1201.
55. Peters BA, *et al.* (2005) Contribution of bone marrow-derived endothelial cells to human tumor vasculature. *Nat Med* 11:261-262.
56. Karnoub AE, *et al.* (2007) Mesenchymal stem cells within tumour stroma promote breast cancer metastasis. *Nature* 449:557-563.
57. McMillin DW, *et al.* (2010) Tumor cell-specific bioluminescence platform to identify stroma-induced changes to anticancer drug activity. *Nat Med* 16:483-489.
58. Panettiere P, Marchetti L, & Accorsi D (2009) The serial free fat transfer in irradiated prosthetic breast reconstructions. *Aesthetic Plast Surg* 33:695-700.
59. Rehman J, *et al.* (2004) Secretion of angiogenic and antiapoptotic factors by human adipose stromal cells. *Circulation* 109:1292-1298.
60. Yoshimura K, *et al.* (2008) Cell-assisted lipotransfer for cosmetic breast augmentation: supportive use of adipose-derived stem/stromal cells. *Aesthetic Plast Surg* 32:48-55; discussion 56-47.
61. Kilroy GE, *et al.* (2007) Cytokine profile of human adipose-derived stem cells: expression of angiogenic, hematopoietic, and pro-inflammatory factors. *J Cell Physiol* 212:702-709.
62. Yu JM, Jun ES, Bae YC, & Jung JS (2008) Mesenchymal stem cells derived from human adipose tissues favor tumor cell growth in vivo. *Stem Cells Dev* 17:463-473.
63. Walter M, Liang S, Ghosh S, Hornsby PJ, & Li R (2009) Interleukin 6 secreted from

adipose stromal cells promotes migration and invasion of breast cancer cells. *Oncogene* 28:2745-2755.
64. Berrier AL & Yamada KM (2007) Cell-matrix adhesion. *J Cell Physiol* 213:565-573.
65. Hynes RO (2009) The Extracellular Matrix: Not Just Pretty Fibrils. *Science* 326:1216-1219.
66. Di Lullo GA, Sweeney SM, Korkko J, Ala-Kokko L, & San Antonio JD (2002) Mapping the ligand-binding sites and disease-associated mutations on the most abundant protein in the human, type I collagen. *J Biol Chem* 277:4223-4231.
67. Gordon MK & Hahn RA (2010) Collagens. *Cell Tissue Res* 339:247-257.
68. Provenzano PP, *et al.* (2006) Collagen reorganization at the tumor-stromal interface facilitates local invasion. *Bmc Med* 4.
69. Kefalides NA (1973) Structure and biosynthesis of basement membranes. *Int Rev Connect Tissue Res* 6:63-104.
70. Gullberg D, *et al.* (1992) Analysis of alpha 1 beta 1, alpha 2 beta 1 and alpha 3 beta 1 integrins in cell--collagen interactions: identification of conformation dependent alpha 1 beta 1 binding sites in collagen type I. *EMBO J* 11:3865-3873.
71. Vandenberg P, *et al.* (1991) Characterization of a type IV collagen major cell binding site with affinity to the alpha 1 beta 1 and the alpha 2 beta 1 integrins. *J Cell Biol* 113:1475-1483.
72. Liotta LA (1986) Tumor invasion and metastases--role of the extracellular matrix: Rhoads Memorial Award lecture. *Cancer Res* 46:1-7.
73. Levental KR, *et al.* (2009) Matrix crosslinking forces tumor progression by enhancing integrin signaling. *Cell* 139:891-906.
74. Shi F, Harman J, Fujiwara K, & Sottile J (2010) Collagen I matrix turnover is regulated by fibronectin polymerization. *Am J Physiol Cell Physiol* 298:C1265-1275.
75. Sottile J, *et al.* (2007) Fibronectin-dependent collagen I deposition modulates the cell response to fibronectin. *Am J Physiol Cell Physiol* 293:C1934-1946.
76. Singh P, Carraher C, & Schwarzbauer JE (2010) Assembly of fibronectin extracellular matrix. *Annu Rev Cell Dev Biol* 26:397-419.
77. Labat-Robert J (2002) Fibronectin in malignancy. *Semin Cancer Biol* 12:187-195.
78. Sethi T, *et al.* (1999) Extracellular matrix proteins protect small cell lung cancer cells against apoptosis: a mechanism for small cell lung cancer growth and drug resistance in vivo. *Nat Med* 5:662-668.
79. Frantz C, Stewart KM, & Weaver VM (2010) The extracellular matrix at a glance. *Journal of Cell Science* 123:4195-4200.
80. Sehrt B & Mangakis N (1982) Glycosaminoglycan (Gag) Content and Gag-Electropherogram-Patterns of Mammary-Tumors and Chronic Fibrous Mastopathy. *Arch Geschwulstforsc* 52:459-468.
81. Cooney CA, *et al.* (2011) Chondroitin sulfates play a major role in breast cancer metastasis: a role for CSPG4 and CHST11 gene expression in forming surface P-selectin ligands in aggressive breast cancer cells. *Breast Cancer Research* 13.
82. Hynes RO (2002) Integrins: bidirectional, allosteric signaling machines. *Cell* 110:673-687.
83. Geiger B, Spatz JP, & Bershadsky AD (2009) Environmental sensing through focal adhesions. *Nat Rev Mol Cell Biol* 10:21-33.
84. Galbraith CG, Yamada KM, & Sheetz MP (2002) The relationship between force and

focal complex development. *J Cell Biol* 159:695-705.
85. Brown MC & Turner CE (2004) Paxillin: adapting to change. *Physiol Rev* 84:1315-1339.
86. McLean GW, *et al.* (2005) The role of focal-adhesion kinase in cancer. A ew therapeutic opportunity. *Nature Reviews Cancer* 5:505-515.
87. Hinz B (2010) The myofibroblast: paradigm for a mechanically active cell. *J Biomech* 43:146-155.
88. Liotta LA & Kohn EC (2001) The microenvironment of the tumour-host interface. *Nature* 411:375-379.
89. Cornelius P, MacDougald OA, & Lane MD (1994) Regulation of adipocyte development. *Annu Rev Nutr* 14:99-129.
90. Stenman S & Vaheri A (1981) Fibronectin in human solid tumors. *Int J Cancer* 27:427-435.
91. Klotzsch E, *et al.* (2009) Fibronectin forms the most extensible biological fibers displaying switchable force-exposed cryptic binding sites. *Proc Natl Acad Sci U S A* 106:18267-18272.
92. Ignotz RA & Massague J (1986) Transforming growth factor-beta stimulates the expression of fibronectin and collagen and their incorporation into the extracellular matrix. *J Biol Chem* 261:4337-4345.
93. Chandler EM, Saunders MP, Yoon CJ, Gourdon D, & Fischbach C (2011) Adipose progenitor cells increase fibronectin matrix strain and unfolding in breast tumors. *Phys Biol* 8:015008.
94. Kumar S & Weaver VM (2009) Mechanics, malignancy, and metastasis: the force journey of a tumor cell. *Cancer Metastasis Rev* 28:113-127.
95. Levental I, Georges PC, & Janmey PA (2007) Soft biological materials and their impact on cell function. *Soft Matter* 3:299-306.
96. Provenzano PP, *et al.* (2008) Collagen density promotes mammary tumor initiation and progression. *BMC Med* 6:11.
97. Moro L, Colombi M, Molinari Tosatti MP, & Barlati S (1992) Study of fibronectin and mRNA in human laryngeal and ectocervical carcinomas by in situ hybridization and image analysis. *Int J Cancer* 51:692-697.
98. Hynes RO (1990) *Fibronectins* (Springer-Verlag, New York) pp xv, 546 p.
99. Mao Y & Schwarzbauer JE (2005) Fibronectin fibrillogenesis, a cell-mediated matrix assembly process. *Matrix Biol* 24:389-399.
100. Pankov R, *et al.* (2000) Integrin dynamics and matrix assembly: tensin-dependent translocation of alpha(5)beta(1) integrins promotes early fibronectin fibrillogenesis. *J Cell Biol* 148:1075-1090.
101. Vogel V (2006) Mechanotransduction involving multimodular proteins: converting force into biochemical signals. *Annu Rev Biophys Biomol Struct* 35:459-488.
102. Smith ML, *et al.* (2007) Force-induced unfolding of fibronectin in the extracellular matrix of living cells. *PLoS Biol* 5:e268.
103. Parker AM & Katz AJ (2006) Adipose-derived stem cells for the regeneration of damaged tissues. *Expert Opin Biol Ther* 6:567-578.
104. Iyengar P, *et al.* (2005) Adipocyte-derived collagen VI affects early mammary tumor progression in vivo, demonstrating a critical interaction in the tumor/stroma microenvironment. *J Clin Invest* 115:1163-1176.
105. Kim WS, *et al.* (2007) Wound healing effect of adipose-derived stem cells: a critical role

of secretory factors on human dermal fibroblasts. *J Dermatol Sci* 48:15-24.
106. Castello-Cros R & Cukierman E (2009) Stromagenesis during tumorigenesis: characterization of tumor-associated fibroblasts and stroma-derived 3D matrices. *Methods Mol Biol* 522:275-305.
107. Sugii S, *et al.* (2010) Human and mouse adipose-derived cells support feeder-independent induction of pluripotent stem cells. *P Natl Acad Sci USA* 107:3558-3563.
108. Schmittgen TD & Livak KJ (2008) Analyzing real-time PCR data by the comparative C(T) method. *Nat Protoc* 3:1101-1108.
109. Baneyx G, Baugh L, & Vogel V (2001) Coexisting conformations of fibronectin in cell culture imaged using fluorescence resonance energy transfer. *Proc Natl Acad Sci U S A* 98:14464-14468.
110. Johnson KJ, Sage H, Briscoe G, & Erickson HP (1999) The compact conformation of fibronectin is determined by intramolecular ionic interactions. *J Biol Chem* 274:15473-15479.
111. Little WC, Smith ML, Ebneter U, & Vogel V (2008) Assay to mechanically tune and optically probe fibrillar fibronectin conformations from fully relaxed to breakage. *Matrix Biol* 27:451-461.
112. Kubo Y, Kaidzu S, Nakajima I, Takenouchi K, & Nakamura F (2000) Organization of extracellular matrix components during differentiation of adipocytes in long-term culture. *In Vitro Cell Dev Biol Anim* 36:38-44.
113. Mann DM, McKeown-Longo PJ, & Millis AJ (1988) Binding of soluble fibronectin and its subsequent incorporation into the extracellular matrix by early and late passage human skin fibroblasts. *J Biol Chem* 263:2756-2760.
114. Dembo M & Wang YL (1999) Stresses at the cell-to-substrate interface during locomotion of fibroblasts. *Biophys J* 76:2307-2316.
115. Kostic A, Lynch CD, & Sheetz MP (2009) Differential matrix rigidity response in breast cancer cell lines correlates with the tissue tropism. *PLoS One* 4:e6361.
116. Antia M, Baneyx G, Kubow KE, & Vogel V (2008) Fibronectin in aging extracellular matrix fibrils is progressively unfolded by cells and elicits an enhanced rigidity response. *Faraday Discuss* 139:229-249; discussion 309-225, 419-220.
117. Baneyx G, Baugh L, & Vogel V (2002) Fibronectin extension and unfolding within cell matrix fibrils controlled by cytoskeletal tension. *Proc Natl Acad Sci U S A* 99:5139-5143.
118. McDonald JA, Kelley DG, & Broekelmann TJ (1982) Role of fibronectin in collagen deposition: Fab' to the gelatin-binding domain of fibronectin inhibits both fibronectin and collagen organization in fibroblast extracellular matrix. *J Cell Biol* 92:485-492.
119. Schnepel J & Tschesche H (2000) The proteolytic activity of the recombinant cryptic human fibronectin type IV collagenase from E. coli expression. *J Protein Chem* 19:685-692.
120. Armstrong T, *et al.* (2004) Type I collagen promotes the malignant phenotype of pancreatic ductal adenocarcinoma. *Clin Cancer Res* 10:7427-7437.
121. Hanahan D & Weinberg RA (2000) The hallmarks of cancer. *Cell* 100:57-70.
122. Fraser JK, *et al.* (2006) Plasticity of human adipose stem cells toward endothelial cells and cardiomyocytes. *Nat Clin Pract Cardiovasc Med* 3 Suppl 1:S33-37.
123. Muehlberg FL, *et al.* (2009) Tissue-resident stem cells promote breast cancer growth and metastasis. *Carcinogenesis* 30:589-597.
124. Padua D, *et al.* (2008) TGFbeta primes breast tumors for lung metastasis seeding through

angiopoietin-like 4. *Cell* 133:66-77.
125. Leask A & Abraham DJ (2004) TGF-beta signaling and the fibrotic response. *FASEB J* 18:816-827.
126. Clark RA, McCoy GA, Folkvord JM, & McPherson JM (1997) TGF-beta 1 stimulates cultured human fibroblasts to proliferate and produce tissue-like fibroplasia: a fibronectin matrix-dependent event. *J Cell Physiol* 170:69-80.
127. Berking C, *et al.* (2001) Transforming growth factor-beta1 increases survival of human melanoma through stroma remodeling. *Cancer Res* 61:8306-8316.
128. Cukierman E, Pankov R, Stevens DR, & Yamada KM (2001) Taking cell-matrix adhesions to the third dimension. *Science* 294:1708-1712.
129. Fraley SI, *et al.* (2010) A distinctive role for focal adhesion proteins in three-dimensional cell motility. *Nat Cell Biol* 12:598-604.
130. Schwartz MA & DeSimone DW (2008) Cell adhesion receptors in mechanotransduction. *Curr Opin Cell Biol* 20:551-556.
131. Chandler EM, *et al.* (2011) Stiffness of photocrosslinked RGD-alginate gels regulates adipose progenitor cell behavior. *Biotechnol Bioeng* 108:1683-1692.
132. Patrick CW, Jr. (2000) Adipose tissue engineering: the future of breast and soft tissue reconstruction following tumor resection. *Semin Surg Oncol* 19:302-311.
133. Lai N, Jayaraman A, & Lee K (2009) Enhanced proliferation of human umbilical vein endothelial cells and differentiation of 3T3-L1 adipocytes in coculture. *Tissue Eng Part A* 15:1053-1061.
134. Rubina K, *et al.* (2009) Adipose stromal cells stimulate angiogenesis via promoting progenitor cell differentiation, secretion of angiogenic factors, and enhancing vessel maturation. *Tissue Eng Part A* 15:2039-2050.
135. Gimeno RE & Klaman LD (2005) Adipose tissue as an active endocrine organ: recent advances. *Curr Opin Pharmacol* 5:122-128.
136. Kershaw EE & Flier JS (2004) Adipose tissue as an endocrine organ. *J Clin Endocrinol Metab* 89:2548-2556.
137. Fischbach C, *et al.* (2004) Generation of mature fat pads in vitro and in vivo utilizing 3-D long-term culture of 3T3-L1 preadipocytes. *Exp Cell Res* 300:54-64.
138. Stacey DH, Hanson SE, Lahvis G, Gutowski KA, & Masters KS (2009) In vitro Adipogenic Differentiation of Preadipocytes Varies with Differentiation Stimulus, Culture Dimensionality, and Scaffold Composition. *Tissue Eng Part A*.
139. Mariman EC & Wang P (2010) Adipocyte extracellular matrix composition, dynamics and role in obesity. *Cell Mol Life Sci*.
140. Corr DT, Gallant-Behm CL, Shrive NG, & Hart DA (2009) Biomechanical behavior of scar tissue and uninjured skin in a porcine model. *Wound Repair Regen* 17:250-259.
141. Subramanian A & Lin HY (2005) Crosslinked chitosan: its physical properties and the effects of matrix stiffness on chondrocyte cell morphology and proliferation. *J Biomed Mater Res A* 75:742-753.
142. Ulrich TA, de Juan Pardo EM, & Kumar S (2009) The mechanical rigidity of the extracellular matrix regulates the structure, motility, and proliferation of glioma cells. *Cancer Res* 69:4167-4174.
143. Zaman MH, *et al.* (2006) Migration of tumor cells in 3D matrices is governed by matrix stiffness along with cell-matrix adhesion and proteolysis. *Proc Natl Acad Sci U S A* 103:10889-10894.

144. Karamichos D, Brown RA, & Mudera V (2007) Collagen stiffness regulates cellular contraction and matrix remodeling gene expression. *Journal of Biomedical Materials Research Part A* 83A:887-894.
145. Boontheekul T, *et al.* (2008) Quantifying the relation between bond number and myoblast proliferation. *Faraday Discuss* 139:53-70; discussion 105-128, 419-120.
146. Kong HJ, *et al.* (2005) Non-viral gene delivery regulated by stiffness of cell adhesion substrates. *Nat Mater* 4:460-464.
147. Boynton AL, Whitfield JF, Isaacs RJ, & Morton HJ (1974) Control of 3T3 cell proliferation by calcium. *In Vitro* 10:12-17.
148. Jensen B, Farach-Carson MC, Kenaley E, & Akanbi KA (2004) High extracellular calcium attenuates adipogenesis in 3T3-L1 preadipocytes. *Exp Cell Res* 301:280-292.
149. Rouillard AD, *et al.* (2010) Methods for photocrosslinking alginate hydrogel scaffolds with high cell viability. *Tissue Eng Part C Methods*.
150. Chou AI & Nicoll SB (2009) Characterization of photocrosslinked alginate hydrogels for nucleus pulposus cell encapsulation. *J Biomed Mater Res A* 91:187-194.
151. Jeon O, Bouhadir KH, Mansour JM, & Alsberg E (2009) Photocrosslinked alginate hydrogels with tunable biodegradation rates and mechanical properties. *Biomaterials* 30:2724-2734.
152. Smeds KA, *et al.* (2001) Photocrosslinkable polysaccharides for in situ hydrogel formation. *J Biomed Mater Res* 54:115-121.
153. Ntambi JM & Young-Cheul K (2000) Adipocyte differentiation and gene expression. *J Nutr* 130:3122S-3126S.
154. Li Q, *et al.* (2004) Photocrosslinkable polysaccharides based on chondroitin sulfate. *J Biomed Mater Res A* 68:28-33.
155. Rouillard AD, *et al.* (2010) Control of the electromechanical properties of alginate hydrogels via ionic and covalent cross-linking and microparticle doping. *Biomacromolecules* 11:2184-2189.
156. Rowley JA, Madlambayan G, & Mooney DJ (1999) Alginate hydrogels as synthetic extracellular matrix materials. *Biomaterials* 20:45-53.
157. Niemisto A, Dunmire V, Yli-Harja O, Zhang W, & Shmulevich I (2005) Robust quantification of in vitro angiogenesis through image analysis. *IEEE Trans Med Imaging* 24:549-553.
158. Lee KY, *et al.* (2004) Nanoscale adhesion ligand organization regulates osteoblast proliferation and differentiation. *Nano Lett* 4:1501-1506.
159. Wang N, Butler JP, & Ingber DE (1993) Mechanotransduction across the cell surface and through the cytoskeleton. *Science* 260:1124-1127.
160. Winer JP, Janmey PA, McCormick ME, & Funaki M (2009) Bone marrow-derived human mesenchymal stem cells become quiescent on soft substrates but remain responsive to chemical or mechanical stimuli. *Tissue Eng Part A* 15:147-154.
161. Seib FP, Prewitz M, Werner C, & Bornhauser M (2009) Matrix elasticity regulates the secretory profile of human bone marrow-derived multipotent mesenchymal stromal cells (MSCs). *Biochem Biophys Res Commun* 389:663-667.
162. Pirone DM, *et al.* (2006) An inhibitory role for FAK in regulating proliferation: a link between limited adhesion and RhoA-ROCK signaling. *J Cell Biol* 174:277-288.
163. McBeath R, Pirone DM, Nelson CM, Bhadriraju K, & Chen CS (2004) Cell shape, cytoskeletal tension, and RhoA regulate stem cell lineage commitment. *Dev Cell* 6:483-

495.
164. Yoshida S, *et al.* (1997) Involvement of interleukin-8, vascular endothelial growth factor, and basic fibroblast growth factor in tumor necrosis factor alpha-dependent angiogenesis. *Mol Cell Biol* 17:4015-4023.
165. Taraboletti G, Roberts D, Liotta LA, & Giavazzi R (1990) Platelet thrombospondin modulates endothelial cell adhesion, motility, and growth: a potential angiogenesis regulatory factor. *J Cell Biol* 111:765-772.
166. Kang JH, Gimble JM, & Kaplan DL (2009) In vitro 3D model for human vascularized adipose tissue. *Tissue Eng Part A* 15:2227-2236.
167. Naumov GN, Akslen LA, & Folkman J (2006) Role of angiogenesis in human tumor dormancy: animal models of the angiogenic switch. *Cell Cycle* 5:1779-1787.
168. Chandler* EM, *et al.* (2012) Implanted adipose progenitor cells as physicochemical regulators of breast cancer. *In Press Proc Natl Acad Sci U S A.*
169. Cherubino M & Marra KG (2009) Adipose-derived stem cells for soft tissue reconstruction. *Regen Med* 4:109-117.
170. Surgeons ASoP (2010) Report of the 2010 Plastic Surgery Statistics: ASPS National Clearinghouse of Plastic Surgery Procedural Statistics. in *www.plasticsurgery.org*.
171. Moioli EK, *et al.* (2010) Hybrid adipogenic implants from adipose stem cells for soft tissue reconstruction in vivo. *Tissue Eng Part A* 16:3299-3307.
172. Brewster AM, *et al.* (2008) Residual risk of breast cancer recurrence 5 years after adjuvant therapy. *J Natl Cancer Inst* 100:1179-1183.
173. Janmey PA, Levental I, & Georges PC (2007) Soft biological materials and their impact on cell function. *Soft Matter* 3:299-306.
174. Nakagawa H, *et al.* (2004) Role of cancer-associated stromal fibroblasts in metastatic colon cancer to the liver and their expression profiles. *Oncogene* 23:7366-7377.
175. Kidd S, *et al.* (2012) Origins of the tumor microenvironment: quantitative assessment of adipose-derived and bone marrow-derived stroma. *PLoS One* 7:e30563.
176. Quante M, *et al.* (2011) Bone marrow-derived myofibroblasts contribute to the mesenchymal stem cell niche and promote tumor growth. *Cancer Cell* 19:257-272.
177. Cheng L, *et al.* (2010) Rb inactivation accelerates neoplastic growth and substitutes for recurrent amplification of cIAP1, cIAP2 and Yap1 in sporadic mammary carcinoma associated with p53 deficiency. *Oncogene* 29:5700-5711.
178. Santner SJ, *et al.* (2001) Malignant MCF10CA1 cell lines derived from premalignant human breast epithelial MCF10AT cells. *Breast Cancer Res Treat* 65:101-110.
179. Kraning-Rush CM, Califano JP, & Reinhart-King CA (2012) Cellular traction stresses increase with increasing metastatic potential. *PLoS One* 7:e32572.
180. Lonza (2011) Poietics™ human adipose derived stem cells (ADSC).
181. Cross VL, *et al.* (2010) Dense type I collagen matrices that support cellular remodeling and microfabrication for studies of tumor angiogenesis and vasculogenesis in vitro. *Biomaterials* 31:8596-8607.
182. Verbridge SS, *et al.* (2010) Oxygen-controlled three-dimensional cultures to analyze tumor angiogenesis. *Tissue Eng Part A* 16:2133-2141.
183. Omoto M, *et al.* (2009) The use of human mesenchymal stem cell-derived feeder cells for the cultivation of transplantable epithelial sheets. *Invest Ophthalmol Vis Sci* 50:2109-2115.
184. Buckley MR, Bergou AJ, Fouchard J, Bonassar LJ, & Cohen I (2010) High-resolution

spatial mapping of shear properties in cartilage. *J Biomech* 43:796-800.
185. Califano JP & Reinhart-King CA (2010) Substrate Stiffness and Cell Area Predict Cellular Traction Stresses in Single Cells and Cells in Contact. *Cell Mol Bioeng* 3:68-75.
186. Dembo M, Oliver T, Ishihara A, & Jacobson K (1996) Imaging the traction stresses exerted by locomoting cells with the elastic substratum method. *Biophys J* 70:2008-2022.
187. Wang YL & Pelham RJ, Jr. (1998) Preparation of a flexible, porous polyacrylamide substrate for mechanical studies of cultured cells. *Methods Enzymol* 298:489-496.
188. Williams RM, *et al.* (2010) Strategies for high-resolution imaging of epithelial ovarian cancer by laparoscopic nonlinear microscopy. *Transl Oncol* 3:181-194.
189. Cukierman E (2002) Preparation of Extracellular Matrices Produced by Cultured Fibroblasts. *Current Protocols in Cell Biology*.
190. Olaso E, *et al.* (2003) Proangiogenic role of tumor-activated hepatic stellate cells in experimental melanoma metastasis. *Hepatology* 37:674-685.
191. Hong KM, Belperio JA, Keane MP, Burdick MD, & Strieter RM (2007) Differentiation of human circulating fibrocytes as mediated by transforming growth factor-beta and peroxisome proliferator-activated receptor gamma. *J Biol Chem* 282:22910-22920.
192. De Wever O & Mareel M (2003) Role of tissue stroma in cancer cell invasion. *J Pathol* 200:429-447.
193. Guerrero J, *et al.* (2010) Soluble factors derived from tumor mammary cell lines induce a stromal mammary adipose reversion in human and mice adipose cells. Possible role of TGF-beta1 and TNF-alpha. *Breast Cancer Res Treat* 119:497-508.
194. Schauer IG, Ressler SJ, Tuxhorn JA, Dang TD, & Rowley DR (2008) Elevated epithelial expression of interleukin-8 correlates with myofibroblast reactive stroma in benign prostatic hyperplasia. *Urology* 72:205-213.
195. Yagi Y, Andoh A, Inatomi O, Tsujikawa T, & Fujiyama Y (2007) Inflammatory responses induced by interleukin-17 family members in human colonic subepithelial myofibroblasts. *J Gastroenterol* 42:746-753.
196. Peyrol S, *et al.* (1997) Lysyl oxidase gene expression in the stromal reaction to in situ and invasive ductal breast carcinoma. *Am J Pathol* 150:497-507.
197. Reinhart-King CA, Dembo M, & Hammer DA (2003) Endothelial cell traction forces on RGD-derivatized polyacrylamide substrata. *Langmuir* 19:1573-1579.
198. Shin H, Zygourakis K, Farach-Carson MC, Yaszemski MJ, & Mikos AG (2004) Modulation of differentiation and mineralization of marrow stromal cells cultured on biomimetic hydrogels modified with Arg-Gly-Asp containing peptides. *J Biomed Mater Res A* 69:535-543.
199. McLean GW, *et al.* (2005) The role of focal-adhesion kinase in cancer - a new therapeutic opportunity. *Nat Rev Cancer* 5:505-515.
200. Cho SW, *et al.* (2005) Engineering of volume-stable adipose tissues. *Biomaterials* 26:3577-3585.
201. Davidenko N, Campbell JJ, Thian ES, Watson CJ, & Cameron RE (2010) Collagen-hyaluronic acid scaffolds for adipose tissue engineering. *Acta Biomater* 6:3957-3968.
202. Storm C, Pastore JJ, MacKintosh FC, Lubensky TC, & Janmey PA (2005) Nonlinear elasticity in biological gels. *Nature* 435:191-194.
203. Prantl L, *et al.* (2010) Adipose tissue-derived stem cells promote prostate tumor growth. *Prostate* 70:1709-1715.
204. Zhang Y, *et al.* (2009) White adipose tissue cells are recruited by experimental tumors

and promote cancer progression in mouse models. *Cancer Res* 69:5259-5266.
205. Kida Y & Duffield JS (2011) Pivotal role of pericytes in kidney fibrosis. *Clin Exp Pharmacol Physiol* 38:417-423.
206. Petit JY, *et al.* (2011) Locoregional recurrence risk after lipofilling in breast cancer patients. *Ann Oncol*.
207. van Harmelen V, *et al.* (2003) Effect of BMI and age on adipose tissue cellularity and differentiation capacity in women. *Int J Obes Relat Metab Disord* 27:889-895.
208. Bianchini F, Kaaks R, & Vainio H (2002) Overweight, obesity, and cancer risk. *Lancet Oncol* 3:565-574.
209. Moutos FT & Guilak F (2010) Functional properties of cell-seeded three-dimensionally woven poly(epsilon-caprolactone) scaffolds for cartilage tissue engineering. *Tissue Eng Part A* 16:1291-1301.
210. Ochoa I, *et al.* (2011) Mechanical properties of cross-linked collagen meshes after human adipose derived stromal cells seeding. *J Biomed Mater Res A* 96:341-348.
211. Lin G, *et al.* (2010) Effects of transplantation of adipose tissue-derived stem cells on prostate tumor. *Prostate* 70:1066-1073.
212. Bellows CF, Zhang Y, Chen J, Frazier ML, & Kolonin MG (2011) Circulation of progenitor cells in obese and lean colorectal cancer patients. *Cancer Epidemiol Biomarkers Prev* 20:2461-2468.
213. Padua D & Massague J (2009) Roles of TGFbeta in metastasis. *Cell Res* 19:89-102.
214. DuFort CC, Paszek MJ, & Weaver VM (2011) Balancing forces: architectural control of mechanotransduction. *Nat Rev Mol Cell Biol* 12:308-319.
215. Chandler EM, Archer SA, Fischbach C, & Phinney-Foreman A (2012) A Inquiry-based approach to teaching fundamentals of polymers for tissue engineering. *The Science Teacher* In Prep.
216. Clohisy JC, Calvert G, Tull F, McDonald D, & Maloney WJ (2004) Reasons for revision hip surgery: a retrospective review. *Clin Orthop Relat Res*:188-192.
217. Manivasagam G, and DD, & Rajamanickam A (2010) Biomedical Implants: Corrosion and its Prevention - A Review. *Recent Patents on Corrosion Science* 2:40-54.
218. Langer R & Tirrell DA (2004) Designing materials for biology and medicine. *Nature* 428:487-492.
219. Campbell NA & Reece JB (2007) *Biology* (Pearson, Benjamin Cummings, San Francisco) 8th Ed.
220. Alberts B (2008) *Molecular biology of the cell* (Garland Science, New York) 5th Ed pp xxxiii, 1268, G 1240, I-1249 p.
221. Freshney RI (2010) *Culture of animal cells : a manual of basic technique and specialized applications* (Wiley- Blackwell, Hoboken, N.J.) 6th Ed pp xxxi, 732 p., [728] p. of plates.